(2)

THE OHIO STATE UNIVERSITY

Fundamental Studies on Erosion in MPD Thrusters

V. V. Subramaniam
Department of Mechanical Engineering

Air Force Office of Scientific Research
Bolling Air Force Base, D.C. 20332-6448

Grant No. AFOSR-87-0360
Final Report

April 1992

(U)

SECURITY CLASSIFICATION OF THIS PAGE

REPORT DOCUMENTATION PAGE

Form Approved OMB No. 0704-0188

1a. REPORT SECURITY CLASSIFICATION (U)	1b. RESTRICTIVE MARKINGS
2a. SECURITY CLASSIFICATION AUTHORITY	3. DISTRIBUTION/AVAILABILITY OF REPORT Approved for public release, distribution unlimited
2b. DECLASSIFICATION/DOWNGRADING SCHEDULE	
4. PERFORMING ORGANIZATION REPORT NUMBER(S) RF Project No. 766307/719942	5. MONITORING ORGANIZATION REPORT NUMBER(S)
6a. NAME OF PERFORMING ORGANIZATION The Ohio State University Research Foundation 6b. OFFICE SYMBOL (If applicable) OSURF	7a. NAME OF MONITORING ORGANIZATION AFOSR
6c. ADDRESS (City, State, and ZIP Code) 1960 Kenny Rd. Columbus, OH 43210	7b. ADDRESS (City, State, and ZIP Code) AFOSR/NA Bolling AFB DC 20332-6448
8a. NAME OF FUNDING/SPONSORING ORGANIZATION Air Force Office of Scientific Research 8b. OFFICE SYMBOL (If applicable) AFOSR NA	9. PROCUREMENT INSTRUMENT IDENTIFICATION NUMBER AFOSR-87-0360
8c. ADDRESS (City, State, and ZIP Code) Bldg. 410 Bolling Air Force Base, D.C. 20332-6448	10. SOURCE OF FUNDING NUMBERS PROGRAM ELEMENT NO. 61102F PROJECT NO. 2308 TASK NO. A5 WORK UNIT ACCESSION NO.
11. TITLE (Include Security Classification) Fundamental Studies on Erosion in MPD Thrusters (U)	
12. PERSONAL AUTHOR(S) V. V. Subramaniam	
13a. TYPE OF REPORT Final 13b. TIME COVERED FROM 31 Sep 87 TO 30 Sep 91	14. DATE OF REPORT (Year, Month, Day) 1992, April, 30 15. PAGE COUNT 87
16. SUPPLEMENTARY NOTATION	
17. COSATI CODES FIELD / GROUP / SUB-GROUP	18. SUBJECT TERMS (Continue on reverse if necessary and identify by block number)
19. ABSTRACT (Continue on reverse if necessary and identify by block number)	
20. DISTRIBUTION/AVAILABILITY OF ABSTRACT ☒ UNCLASSIFIED/UNLIMITED ☐ SAME AS RPT. ☒ DTIC USERS	21. ABSTRACT SECURITY CLASSIFICATION (U)
22a. NAME OF RESPONSIBLE INDIVIDUAL Dr. Mitat Birkan	22b. TELEPHONE (Include Area Code) (202) 767-4938 22c. OFFICE SYMBOL NA

DD Form 1473, JUN 86 *Previous editions are obsolete.*

SECURITY CLASSIFICATION OF THIS PAGE

(U)

THE OHIO STATE UNIVERSITY

Fundamental Studies on Erosion in MPD Thrusters

V. V. Subramaniam
Department of Mechanical Engineering

Air Force Office of Scientific Research
Bolling Air Force Base, D.C. 20332-6448

Grant No. AFOSR-87-0360
Final Report
RF Project No. 766307/719942

April 1992

TABLE OF CONTENTS

FUNDAMENTAL STUDIES ON EROSION IN MPD THRUSTERS

Grant No. AFOSR-87-0360

Final Technical Report

V. V. Subramaniam
Department of Mechanical Engineering
The Ohio State University
Columbus, Ohio 43210

1.0 INTRODUCTION

The purpose of this research is to understand and quantify the mechanisms responsible for evaporative erosion in steady state magnetoplasmadynamic (MPD) thrusters. This is necessary in order to predict thruster characteristics and lifetimes for a given design. The Back-EMF theory of Onset has been refined and expanded to enable prediction of erosion rates for steady state, self-field MPD thrusters[1]. This theory is capable of explaining both the observed oscillations as well as the increased erosion observed at Onset. This work represents the first time that the plasma discharge and electrode processes have been coupled.

Erosion processes depend on a complex coupling between plasma discharge characteristics, plasma-wall interactions, and electrode phenomena. In particular, erosion rates vary depending on whether the current conduction is through localized molten spots, or via a diffuse (distributed mode). In either case, the electron emission from the electrodes in MPD thrusters can be due to field emission (quasi-steady operation) or due to thermionic emission (steady state operation). It is important to emphasize therefore that the conditions addressed in this research are those corresponding to ***steady state*** conditions. This means that the theory and results presented herein apply more to the high power steady state experiments being conducted at the University of Stuttgart, rather than the quasi-steady experiements being conducted at Princeton University.

During the period of this work, a method has been developed for the systematic approximate determination of cathode temperatures and hence, evaporative erosion rates in steady state, self-field MPD thrusters. This theory uses the simplest level of coupling between the hot electrodes and the flowing plasma. Given the propellant mass flow rate, total current, and the geometry, all the relevant quantities are predicted for the flowing plasma as well as electrode temperatures. Once electrode temperatures are determined, evaporative erosion rates can be determined from vapor pressure data[2]:

$$\log_{10} \dot{m}'' = 7.5 - \frac{40{,}500}{T} \qquad (1)$$

where T is in degrees Kelvin, and $\dot{m}''$ is in $g/cm^2/s$. This model has been compared with steady state experiments at the University of Stuttgart on the ZT-1 and DT-2 thrusters, as well as with the quasi-steady experiments on the straight co-axial and

half scale flared anode thrusters (HSFAT) at Princeton University. It is found that the model correctly predicts thrust and electrical characteristics in the quasi-steady experiments, as well as the observed cathode damage in the steady state experiments.

This report in conjunction with three earlier annual progress reports, summarizes progress made under grant AFOSR-87-0360.

2.0 RESEARCH OBJECTIVES

The overall objective of this work was to develop the design methods and tools necessary to predict the limits of stable steady state operation of the electrodes in MPD thrusters. Given the mass flow rate, total current, and geometry, the designer must know not only the thrust and electrical characteristics, but also whether the Onset condition has been reached and whether the electrodes are operating under steady, non-molten conditions. To accomplish this goal, simple and approximate models had to be found. These include models of quasi one-dimensional ionizing MPD flow, electrode-adjacent boundary layer flow, the electrode-adjacent sheath, and the electrodes themselves.

3.0 STATUS OF RESEARCH EFFORT

The discussion below summarizes the highlights of the research efforts under this grant. A more detailed discussion can be found in the appendices and earlier references[1,3,4].

Steady state operation of MPD thrusters has been limited by the Onset phenomenon. Onset is a term that is used to denote collectively, increased erosion of thruster components and terminal voltage oscillations that are seen to occur at a critical current for a given mass flow rate and geometry. Several theories have been proposed that can predict the Onset limit[1,3,4-7]. We focus here on the back-EMF theory of Onset[1,3].

The idea of a high back-EMF being responsible for Onset phenomena was first discussed within the context of a one-dimensional, steady state, frozen, fully ionized flow. This model revealed that MPD flow was parametrized by the Magnetic Force Number $S^*=B^{*2}/\mu_0 Fa^*$, where the superscript * refers to quantities evaluated at the magnetogasdynamic sonic point. S^* was also related to the Onset parameter $J_c^2/\dot{m}$, utilized by experimentalists to describe Onset. In this theory, S^* was found to have an upper limit for supersonic flow in the MPD thruster, thus yielding a quantitative limit for the Onset parameter derived from first principles by theory to be:

$$\frac{J_c^2}{\dot{m}} \leq 8.52 \frac{W}{H} \frac{a^*}{\mu_0 \kappa^2} \tag{2}$$

where J_c is the critical current at Onset, $\dot{m}$ is the total propellant mass flow rate, W is the effective channel width, H is the effective channel height, a^* is the frozen speed of sound at the sonic point, μ_0 is the permeability of free space, and $\kappa=B_i/B^*$ is the ratio of magnetic induction at the inlet to the magnetic induction at the sonic point. Equation (2) was found to give excellent agrrement with the experimental results of Malliaris et.

al.[8]. Incorporation of finite rate ionization and recombination did not alter these results qualitatively, but an explicit closed form expression for the Onset limit could not be found[3].

The back-EMF theory has also been compared with measurements on the straight co-axial thruster[3], and the half-scale flared anode thruster (HSFAT)[9] at Princeton for quasi-steady operation. We have shown previously that the quasi one-dimensional model predicts the electrical characteristics for the straight co-axial geometry fairly well. Fig. 1 shows the thrust versus total current for the HSFAT operating under quasi-steady conditions. It can be seen that the quasi one-dimensional model compares extremely well with experiemental measurements. In fact, the agreement is even better than the two-dimensional, fully ionized, frozen, axi-symmetric model of ref[10]. The transition from electrothermal to electromagnetic acceleration is evident in the slight change in slope visible in the figure at a current level near 14 kA. The 2-D model does not appear to reproduce this fact.

Although this back-EMF theory quite satisfactorily predicts the limits of steady state operation, electrode phenomena had to be included to study the erosion processes in select regions of the thruster. This is because electrode processes together with the plasma-electrode interactions influence erosion. Further, no existing theory was able to explain the observed increase in erosion at Onset. In order to resolve this issue, the aforementioned quasi one-dimensional model was coupled via a two-temperature boundary layer theory to the electrode-adjacent sheath. Analyses of the sheaths via simple models revealed some new phenomena:

- Stable, diffuse mode behavior transitions into the spot mode at a critical value of the sheath voltage drop.

- This diffuse to spot transition is caused by a ***thermal runaway*** due to ***excessive electron bombardment***..

- The thermal runaway occurs in the ***low current density regions of the cathode, and the high current density regions of the anode***.

The increased erosion at Onset can thus be explained as follows. As the total current is increased for a given mass flow rate and geometry, the back-EMF climbs from a small value at the inlet, reaches a maximum somewhere in the middle of the channel, and then decreases toward the exit. This causes the net current density to reach a minimum in the middle of the channel, while being large in the exit region. From current conservation, it can be shown that the sheath voltage drop follows the same trend as the net current density[11]. Thus, the theory predicts that the middle portion of the cathode (i.e. away from the inlet and exit regions) is prone to damage because of thermal runaway. Simultaneously, when the sheath voltage drop reaches values comparable with the energy of the first excited state of the propellant atoms, the electron distribution function is modified near the electrode, due to two principal groups of electrons. The first are "low" energy plasma electrons, and the second are beam electrons emitted by the electrode and accelerated through the sheath. Interaction between these two groups of electrons can lead to longitudinal voltage

oscillations arising from the well known beam instability[12].

Experiments confirm these theoretical predictions. Barnett reported that for uniform flow to the benchmark thruster operating quasi-steady, at Onset, voltage oscillations were observed in the exit regions of the flow[13]. Recent experiments at the University of Stuttgart on high power steady state MPD thrusters showed severe damage in the ***middle*** of the cathode consistently[14]. A schematic of the damage is shown for these DT-2 and ZT-1 thrusters in Fig. 2 and Fig. 3. Both cathodes appear to have exploded from within, at 6500 A and 8000 A respectively. The back-EMF theory not only correctly predicted these current limits, but also the temperature profiles shown in Fig. 4. As expected, the centerline temperature far exceeds the cathode surface temperature. Further, at Onset, the interior temperature exceeds the melting temperature. When this occurs, pressure builds up inside the cathode driving crack propagation and promoting fissures. Although the back-EMF theory correctly predicts this Onset and damage limit, it cannot describe the events after the damage and melting have begun to occur.

The theory that has been developed and discussed extensively in the appendices, enable the designer to use quick tools for performance studies and design evaluations. Further work is however needed to accurately determine the level of ionization in the electrode pre-sheath regions, which can affect the accuracy of the predicted erosion rates using the present theory.

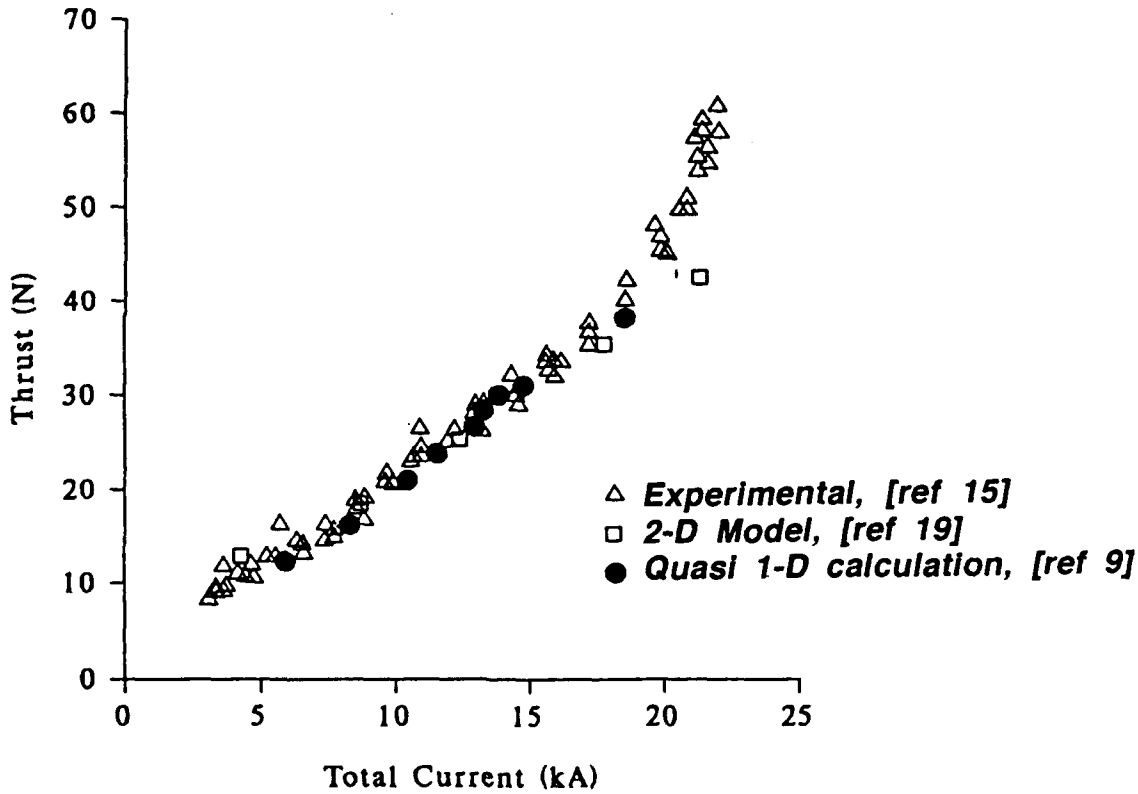

Fig. 1: Comparisons of total thrust versus total current between simulations and experiment are shown here for Princeton's Half-Scale Flared Anode Thruster (HSFAT).

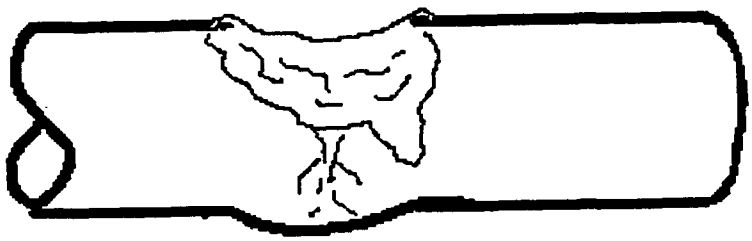

Fig. 2: Schematic of damage sustained by the Stuttgart DT-2 thruster after steady state operation up to 6.5 KA.

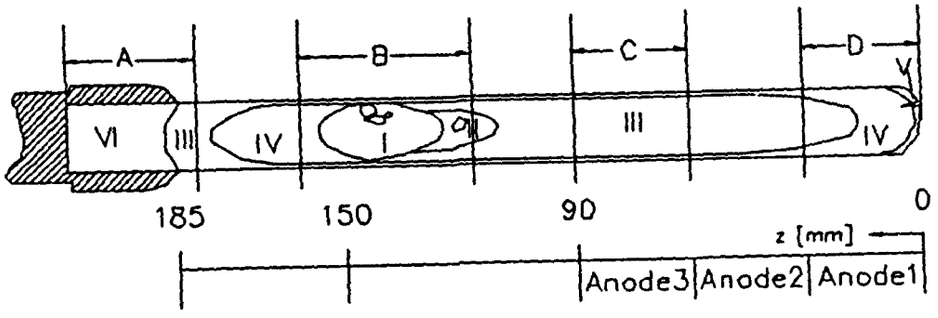

Fig. 3: Schematic of damage sustained by the Stuttgart ZT-1 thruster after steady state operation up to 8 KA.

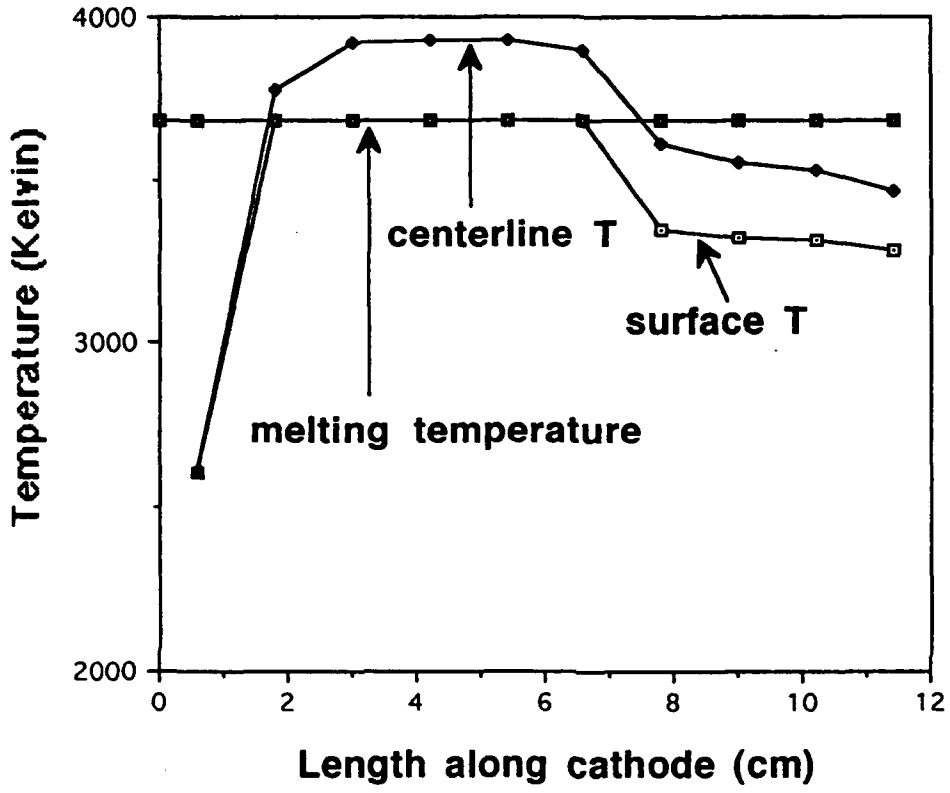

Fig. 4: Shown here are calculated surface and centerline temperature profiles versus distance along the cathode for the Stuttgart ZT-1 thruster. The horizontal line at 3680 K denotes the melting temperature of tungsten. Temperatures above this value cannot be taken seriously from the theoretical predictions, since the theory does not account for phenomena once melting has occurred. However, as the model suggests and as shown in this figure, the centerline temperature has exceeded the surface temperature in the select region thereby explaining the exploded cathode observed in the Stuttgart test.

4.0 REFERENCES

(1) J. L. Lawless, and V. V. Subramaniam, "Theory of Onset in Magnetoplasmadynamic Thrusters", **J. Propulsion & Power**, Vol. 3, No. 2, pp. 121-127, March-April 1987.

(2) G. D. Rieck, ***Tungsten and its compounds***, Pergamon Press Ltd., London, 1967.

(3) V. V. Subramaniam, and J. L. Lawless, "Onset in Magnetoplasmadynamic Thrusters with Finite Rate Ionization", **J. Propulsion & Power**, Vol. 4, No. 6, pp. 526-532, November-December 1988.

(4) V. V. Subramaniam, and J. L. Lawless, "Electrode-Adjacent Boundary Layer Flow in MAgnetoplasmadynamic Thrusters", **Phys. Fluids (31)** (1), pp. 201-209, January 1988.

(5) F. G. Baksht, B. Ya. Moizhes, and A. B. Rybakov, "Critical Regime of a Plasma Accelerator, **Sov. Phys. Tech. Phys.**, Vol. 18, No. 12, pp. 1613-1616, 1974.

(6) H. O. Schrade, M. Auweter-Kurtz, and H. L. Kurtz, "Stability Problems in Magnetoplasmadynamic Arc Thrusters", AIAA 18th Fluid Dynamics and Plasmadynamics and Lasers Conference, Cincinnati, Ohio, 1985.

(7) H. Hugel, "Effect of Self-Magnetic Forces on the Anode Mechanism of a High Current Discharge", **IEEE Trans. Plasma Sci.**, Vol. PS-8, No. 4, pp. 437-442, 1980.

(8) A. C. Malliaris, R. R. John, R. L. Garrison, and D. R. Libby, "Performance of Quasi-Steady MPD Thrusters at High Powers", **AIAA J.**, Vol. 10, No. 2, February 1972.

(9) G. Lefever-Button, and V. V. Subramaniam, "Quasi One-Dimensional Ionizing MPD Flows", submitted to **J. Propulsion & Power** (under review). See also Appendix A.

(10) M. R. Lapointe, "Numerical Simulation of Self-Field MPD Thrusters", paper AIAA-91-2341, presented at the AIAA/SAE/ASME/ASEE 27th Joint Propulsion Conference, Sacramento, California, June 24-27 1991.

(11) V. V. Subramaniam, K. S. Hoyer, and J. L. Lawless, "Limits on Steady Diffuse Mode Operation of the Cathode in MPD Thrusters", **J. Propulsion & Power**, Vol. 7, No. 4, pp. 565-572, July-August 1991.

(12) A. F. Alexandrov, L. S. Bogdankevich, and A. A. Rukhadse, ***Principles of Plasma Electrodynamics***, Springer-Verlag, New York, 1984.

(13) J. D. Barnett, *Operation of the MPD Thruster with Stepped Current Input*, Ph.D. Dissertation, Princeton University, 1985.

(14) M. Auweter-Kurtz, B. Glocker, H. L. Kurtz, O. Loesener, H. O. Schrade, N. Tubanos, T. Wegmann, D. Willer, and J. Polk, "Cathode Phenomena in Plasma Thrusters", paper AIAA-90-2662 presented at the 21st International Electric Propulsion Conference, Orlando, July 1990.

4.0 PERSONNEL

V. V. Subramaniam, Principal Investigator

Kevin S. Hoyer, Graduate Student

G. Lefever-Button, Graduate Student

V. Babu, Graduate Student

Appendix A

Quasi One-Dimensional Ionizing MPD Flow

G. Lefever-Button and V. V. Subramaniam
Department of Mechanical Engineering
The Ohio State University
Columbus, Ohio 43210
U.S.A.

Abstract

Quasi one-dimensional models can serve as useful testbeds for testing various numerical algorithms for integrating the types of stiff differential equations that result from including finite rate kinetics (i.e. ionization and recombination). They are an important prelude to more complicated multi-dimensional simulations. In this paper, an earlier quasi one-dimensional model is extended to study the effects of varying area on *ionizing* MPD flow. Three popular numerical integrators of chemical rate equations (Runge-Kutta, Gear, and Bulirsch-Stoer) are compared for speed and accuracy. Based on the tests reported here, the Bulirsch-Stoer algorithm appears far superior. Results are also presented for MPD channel flow with area variation and finite rate kinetics. Comparisons of the thrust computed using the present quasi one-dimensional model with the recent experimentally measured values for the HSFAT (Half-Scale Flared Anode Thruster) are excellent. An important outcome of this work is the finding that channel divergence has significant effects not only on the thrust, but also on ionization and current density profiles.

Nomenclature

a	Frozen speed of sound
A	Area
B	Magnetic induction
e	Electronic charge
E	Electric field
h	Enthalpy per unit mass
j	Current density
J	Total current
k	Boltzmann's constant
k_f	Ionization rate constant
k_r	Recombination rate constant
l	Computed channel length
L	Given channel length
m_A	Atomic mass

$\dot{m}$	Mass flow rate
M	Mach number
P	Pressure
T	Temperature
u	Velocity
x	Coordinate along channel
α	Ionization fraction
ε_i	Ionization potential of gas
μ_o	Permeability of free space
ρ	Mass density
σ	Electrical conductivity

*	superscript for quantities evaluated at the sonic point
e	subscript denoting exit values
i	superscript denoting i^{th} iteration
i	subscript denoting inlet values

I. Introduction

Earlier theoretical works have considered one-dimensional and quasi one-dimensional models of MPD flows (see for instance refs.[1]-[8]). The main motivation for such drastic simplifications has been to study the influence of individual phenomena on MPD flow, either as a prelude to studies of complicated multi-dimensional plasma flows or to arrive at a basic understanding of operating limits and Onset phenomena. However, there exists another important use for these models. Quasi one-dimensional models that include finite rate kinetics can act as test beds for numerical algorithms that may be used in multi-dimensional simulations. Alternatively, simple models are often very effective design tools. It is with these goals in mind that we extend a previous one-dimensional flow model with finite rate kinetics[5], to include varying-area channels.

Finite rate kinetics introduce numerical stiffness that often overwhelms the speed and even stability of the best algorithms[9]. Further, quasi 1-D models, unlike multi-dimensional simulations, are complicated by the existence of singular points such as saddle points, nodes, and spirals (foci)[10]. In this paper, the back-EMF theory[4,5] is extended to include the effects of area variation. Also, the best presently available numerical techniques for handling stiff systems are compared.

This paper is organized as follows. The model assumptions and governing equations

are discussed next, followed by a discussion of the numerical procedures used to integrate these equations. The results for select cases are then discussed, followed finally by the summary and conclusions.

II. Governing Equations

We consider here the equations of quasi 1-D, steady flow with the electric field perpendicular to the flow direction. The self-generated magnetic induction is taken to be perpendicular to both this electric field and the flow direction. This is tantamount to the assumption of negligible Hall effect. Further, we assume the MPD plasma to be composed of electrons, neutrals, and singly charged ions. Finite rate kinetics are included in the overall collisional reactions of electron-impact ionization and three-body recombination:

$$e^- + A \rightleftharpoons e^- + A^+ + e^- \tag{1}$$

The ionization rate k_f and recombination rate k_r for argon are[5]:

$$\begin{aligned} k_f &= \frac{48 \times 10^{-9} \exp(-\varepsilon_i / kT)}{T^3 (5.556 \times 10^{-11})^{3/2}} \quad (cm^3/s) \\ k_r &= 4 \times 10^{-9}\, T^{-9/2} \qquad\qquad (cm^6/s) \end{aligned} \tag{2}$$

where ε_i is the ionization potential of the propellant. The conservation equations are:

mass:

$$\frac{d}{dx}(\rho u A) = 0 \tag{3}$$

momentum:

$$\frac{dP}{dx} + \rho u \frac{du}{dx} + \frac{d}{dx}(B^2/2\mu_o) = 0 \tag{4}$$

energy:

$$\rho u \frac{dh}{dx} + \rho u^2 \frac{du}{dx} - Ej = 0 \tag{5}$$

state:

$$h = \frac{5P}{2\rho} + \frac{\varepsilon_i \alpha}{m_A} \tag{6}$$

rate:

$$\frac{d\alpha}{dx} = \frac{k_f \rho \alpha (1-\alpha)}{m_A u} - \frac{k_r \rho^2 \alpha^3}{m_A^2 u} \tag{7}$$

Gauss' law:

$$\frac{d}{dx}(EA) = 0 \tag{8}$$

Ampere's law:

$$\frac{dB}{dx} = -\mu_o j \tag{9}$$

Ohm's law:

$$j = \sigma(E - uB) \tag{10}$$

Although viscous and two-temperature effects are known to be important[11], they are neglected here. The existence of two distinct flow regimes, one dominated by ohmic heating and the other by the electromagnetic body force, leads to the magnetogasdynamic sonic or choking condition [5]. This choking condition determines the electric field at the sonic point:

$$E^* = \frac{7}{4} a^* B^* + \{\beta_1 + \beta_2 + \beta_3\}^{1/2} \tag{11}$$

where $\beta_1 = \frac{9}{16} a^{*2} B^{*2}$,

$$\beta_2 = \frac{5}{2} \frac{P^* a^*}{\sigma^* A^*} \frac{dA}{dx}\bigg|_{x=x^*}, \text{ and}$$

$$\beta_3 = \frac{\rho^* a^*}{\sigma^*} \frac{e_i}{m_A} \frac{d\alpha}{dx}\bigg|_{x=x^*},$$

and * denotes quantities evaluated at the sonic point, i.e. where the flow speed equals the local frozen speed of sound[5]. This sonic or choking condition has been the subject of much confusion [12,13], but a rigorous treatment including proofs can be found in ref.[10].

III. Numerical Procedure

Before proceeding with a discussion of the solution procedure of the system (3) through (10), we briefly describe three integrators of systems of ordinary differential equations. These integrators are (1) 4th order Runge-Kutta with variable step size, (2) Gear's predictor-corrector method[14], and (3) Bulirsch-Stoer technique with Richardson extrapolation[15].

In the 4th order Runge-Kutta method, functional values at the initial point, two intermediate points, and a trial endpoint are used. Derivatives are then evaluated at each of these four points, and a weighted average of these values is used to calculate the end point value.

The Bulirsch-Stoer method uses rational function extrapolation (Richardson extrapolation) in order to extrapolate interim solutions to that corresponding to a zero step size. This is achieved by successively bisecting the original interval and subsequent subintervals, and integrating using the midpoint method (2nd order Runge-Kutta)[16]. In contrast to these two, Gear's method uses many initial and/or previous points to predict the functional value at the next point. A corrector equation specially formulated for stiff equations is then used to iterate on the functional value at the next point.

Although all three numerical methods are capable of handling stiff equations, they vary considerably in the handling of the sonic singularity. Consequently, these techniques were first tested on the quasi 1-D isentropic flow equations of classical gas dynamics. This test isentropic flow problem consisted of an area variation given by $A(x)=1.98x^2-3.96x+2$ (m^2), channel length of 2 meters, upstream stagnation pressure of 1.01×10^5 N/m^2, upstream stagnation temperature of 273 K, and ρ_o=1.7798759259 Kg/m^3. A comparison of the three numerical methods in terms of the number of right hand side evaluations, number of bisections to evaluate the correct inlet velocity, and total elapsed CPU time (run on a VAX 8500), is shown in Fig. 1. In Fig. 2, the

overall accuracy of the three methods is compared. It can be seen that the best compromise between speed, efficiency, and accuracy, is the Bulirsch-Stoer algorithm. This is evident when all three methods are compared for speed while holding the total error constant to within the same order of magnitude. In this case, the Bulirsch-Stoer algorithm is seen to be most efficient, followed by the Gear method, and then by the 4^{th} order Runge-Kutta method with variable step size.

The system (3) through (10) may be simplified since the density, electric field, and enthalpy may be computed directly from:

$$\rho u A = constant \tag{12}$$

$$EA = constant \tag{13}$$

$$h = \frac{5}{2}\frac{P}{\rho} + \alpha\frac{\varepsilon_i}{m_A} \tag{14}$$

This leaves the following four equations to be integrated:

$$\frac{dB}{dx} = -\mu_o\sigma(E - uB) \tag{15}$$

$$\frac{d\alpha}{dx} = \frac{k_f\rho\alpha(1-\alpha)}{m_A u} - \frac{k_r\rho^2\alpha^3}{m_A^2 u} \tag{16}$$

$$\frac{du}{dx} = \frac{\left\{\frac{5}{3}\frac{Pu}{\rho A}\frac{dA}{dx} + \frac{2}{3}u\frac{\varepsilon_i}{m_A}\frac{d\alpha}{dx} + \frac{5}{3}\frac{u}{\rho}Bj - \frac{2}{3\rho}Ej\right\}}{u^2 - a^2} \tag{17}$$

$$\frac{dP}{dx} = B\sigma(E - uB) - \rho u\frac{du}{dx} \tag{18}$$

The above system, along with the associated boundary conditions, constitutes a two-point boundary value problem. At the nozzle inlet, the mass flow rate, magnetic induction, and ionization fraction are specified. The nozzle area variation as a function of position x is given, as is the total thruster length. The velocity and

electric field at the inlet must be solved for, such that the downstream flow exiting the thruster is supersonic and the computed length matches the specified thruster length. The temperature at the inlet is constrained by the value of the electric field, which is itself bound by the sonic point choking condition. However, the location of the sonic point and hence the value of the electric field at that point are not known a priori. The correct inlet values can only be determined after the sonic point is successfully crossed. The algorithm developed thus entails integrating through the channel repeatedly, each time refining the inlet conditions using bisections. Since the sonic point is a mathematical singularity, a "jump" algorithm is needed to cross it. This is discussed next.

An iterative procedure is used to cross the sonic point. This proceeds as follows. Let the adjacent point on the subsonic side of the sonic point be denoted the subscript 1, and the adjacent point on the supersonic side by the subscript 2. Let M_2=2-M_1. The temperature at the pre-sonic point T_1 is used as an initial approximation for T_2. Then u_2 is computed iteratively from:

$$u_2^{(i)} = M_2\left[\frac{5}{3}\frac{k_B}{m_A}T_2^{(i-1)}\left(1+\alpha_2^{(i-1)}\right)\right]^{1/2} \tag{19}$$

where the superscript i refers to the i^{th} iteration. The jump distance is then:

$$\Delta x^{(i)} = (u_2^{(i)} - u_1)\Big/\left(\frac{du}{dx}\right)_{x=x_1} \tag{20}$$

the new temperature is computed from:

$$T_2^{(i)} = T_1 + \left.\frac{dT}{dx}\right|_{x=x_1}\Delta x^{(i)} \tag{21}$$

and the new ionization fraction is:

$$\alpha_2^{(i)} = \alpha_1 + \left.\frac{d\alpha}{dx}\right|_{x=x_1}\Delta x^{(i)} \tag{22}$$

Equations (19) through (22) are placed in a loop where they are repeatedly evaluated until the differences in temperature and ionization fraction between two successive iterations is smaller than some specified tolerance. In the present calculation a tolerance of 10^{-6} was specified. Thus the Mach number, velocity, temperature, and

ionization fraction on the supersonic side of the sonic point are all calculated, along with its coordinate:

$$x_2^{(i)} = x_1 + \Delta x^{(i)} \tag{23}$$

The other properties across the sonic point are then determined using the conservation equations.

The integration of the system (15) through (18) is achieved starting from the subsonic inlet. Since not all initial conditions are known, usually a manual shooting method is used in which guessed initial estimates are refined after integration past the sonic point. Rather than relying on such an ad-hoc shooting method, an automatic algorithm for integrating the governing equations has been developed. To accomplish this, a sequence of tests have been designed which determine which inlet variable to modify and in what direction to modify it. Some of these tests are performed after a complete integration through the channel, while others are done in a specific region, such as within the jump routine. Still others are performed after every integration step. These diagnostic tests are summarized in Table I.

As mentioned previously, the inlet temperature is constrained somewhat by the electric field. It was found empirically that this constraint was much weaker for lower values of total current. It was also found, however, that the solution was not sensitive to the inlet temperature. Figure 3 shows a comparison of the resulting temperature distributions for total current J = 8.276 kA, and inlet temperatures ranging $5500 \le T_i \le 11{,}500$ K for the flared geometry of the HSFAT thruster, which will be discussed in the following section. For the case of $T_i < 5500$ K convergence could not be obtained, and at $T_i > 11{,}500$ K the flow is already supersonic at the inlet. It can be seen that, beyond the sonic point, the results do not change for different inlet temperatures. The computed thrust varied up to a maximum of 7%.

The numerical algorithm presented here has been applied to the solution of the governing equations for a constant area channel. These results have been compared to existing solutions for constant area channels[5]. The agreement is found to be good to at least the third decimal place in all the variables. In the next section, results are presented for the simplest of geometries, i.e. linearly varying channel height.

IV. Results

Before discussing the varying area cases, we will briefly revisit the constant area geometry. The effect of different mass flow rates on the profiles of ionization fraction

along the length of the channel is shown in Fig. 4, for mass flow rates ranging from 0.003 kg/s to 0.006 kg/s. The magnetic induction at the inlet (x=0) is 0.159, the cross sectional area is 0.001 m^2, the length is 20 cm., and the inlet ionization fraction is 0.05. It can be seen from Fig. 4 that the density has a profound effect on the rate of ionization. From equation (7), it can be seen that the recombination term in the rate equation for α varies as ρ^2 in contrast to the ionization term which varies as ρ. Thus, for higher mass flow rates, and hence higher densities, α actually decreases along the channel until near the exit, where the temperature increases. This effect of density on the ionization fraction has not been previously reported[5-8,12].

Let us now consider a channel with an area variation given by $A(x)=0.001+x(\delta A)$, where x is in meters and A(x) is in m^2. The total channel length is taken to be 20 cm. so that $x\varepsilon[0.0,0.2]$. The four cases reported here are $\delta A=0$ (constant area), $\delta A=0.0175$, $\delta A=0.04$, and $\delta A=0.07$. The fixed quantities are inlet area $A_i=10$ cm^2, mass flow rate=0.006 kg/s, $B_i=0.159$, $\alpha_i=0.05$, and length=20 cm. The profiles of u, T, j, α, B, and M are shown in Figs. 5-10. Qualitatively, each profile is similar to those discussed previously[5]. However, the flared varying area geometry is seen to be very different in several ways when compared to the constant area geometry. First, the most obvious effect of varying area is apparent in the velocity distributions. The exit speeds and hence specific impulses are 1.7, 2.0, and 2.2 times larger than the constant area case for area ratios of 4.5, 9, and 15 respectively. Second, the ionization fraction shows the same behavior seen in Fig. 4 for a constant area channel with the higher mass flows. The flared geometry has a dramatic effect on the ionization fraction. As the flare angle is increased, the value of α is seen to increase. This is due to the aforementioned decrease in density for the same mass flow rate but different flare angles. Third, the magnetic induction shows the effects of increasing back-EMF as the flare angle is increased for a fixed mass flow rate and total current. Finally, the current density rise at the exit usually seen in the constant area channels[5] is diminished greatly by the flared geometry.

We now turn our attention to a modified version of the original King anode[17]. Thrust measurements have recently been made on the Half-Scale Flared Anode Thruster (HSFAT)[18]. Comparisons between these HSFAT measurements and two-dimensional axi-symmetric frozen, fully ionized flow modelling results have also recently been performed[19]. The HSFAT is essentially the same shape as the original King anode[17], but much shorter in axial length (10 cm. versus 20 cm.). Figures 11 and 12 show comparisons of thrust and thrust-to-total current squared, between the present work, experimental measurements of ref.[18], and the numerical results of ref.[19]. As can be seen, the agreement is excellent. Furthermore, there is a subtle inflection point around 11 kA in the experimental results shown in Fig.

11 that is correctly reproduced in the present results. This inflection point is due to the transition from electrothermal to electromagnetic acceleration. Taking the electrothermal contribution to the thrust to be proportional to

$$\int_0^L j(E-uB)A\,dx \tag{24}$$

and the electromagnetic contribution as

$$\int_0^L [u\cdot(j\times B)]A\,dx \tag{25}$$

and comparing the ratio of electromagnetic to electrothermal contributions gives the graph of Figure 13.

In addition, there is a dramatic increase in thrust beyond approximately 21 kA. The present quasi one-dimensional predictions end around 16 kA because the flow is nearly fully ionized over a significant length inside the thruster (see Fig. 14). We conclude therefore that the dramatic increase in thrust at currents above 20 kA is due to the presence of doubly charged ions, which we have not considered here. It is also interesting to note the typical current density and back-EMF profiles shown in Figs. 15 and 16. Also plotted in these figures for reference are the corresponding curves for a linear flared anode (i.e. area varying linearly from inlet to exit). The back-EMF is highest in the region where the electric field is highest, and lower where the electric field is lower. This is in contrast to the straight coaxial thruster where the electric field is constant and the back-EMF reaches a maximum in the region approximately midway between inlet and exit. Such nozzle contouring can therefore help control Onset due to an excessive back-EMF[4,5].

V. Summary & Conclusions

An efficient algorithm utilizing the Bulirsch-Stoer method for integration of quasi one-dimensional ionizing MPD flow has been presented. Solutions have been compared with previous solutions for constant area channels, and have revealed features not reported in previous studies[5-8,12]. This work has revealed that for a constant channel area and total current, the exit ionization fraction increases with decreasing mass flow rate. Furthermore, for a fixed mass flow rate and total current, substantial increases in ionization fraction and specific impulse may be achieved by using a flared geometry. Too much of a flare or abrupt expansion, however, can lead to Onset by the back-EMF mechanism[5]. Comparison of the present model with

measurements on the HSFAT show excellent agreement. This suggests that thruster geometries can be optimized for specific operating points (i.e. total current and mass flow rate) to maximize thrust and specific impulse, using the present model.

Acknowledgements

The authors acknowledge helpful discussions with Dr. J. L. Lawless, Space Power, Inc. This work was supported in part by AFOSR-87-0360 and by the College of Engineering Undergraduate Honors Research Scholarship program at The Ohio State University.

References

(1) R. K. Seals, and H. A. Hassan, "Analysis of MPD Arcs with Nonequilibrium Ionization", *AIAA J.*, Vol. 6, pp. 2273-2278, December 1968.

(2) F. G. Baksht, B. Ya. Moizhes, and A. B. Rybakov, "Critical Regime of a Plasma Accelerator", *Sov. Phys.-Tech. Phys.*, Vol. 18, No. 12, pp 1613-1616.

(3) D. Q. King, K. E. Clark, and R. G. Jahn, "Effect of Choked Flow on Terminal Characteristics of MPD Thrusters", paper AIAA-81-0686, presented at the 15th International Electric Propulsion Conference, Las Vegas, Nevada, April 1981.

(4) J. L. Lawless, and V. V. Subramaniam, "Theory of Onset in Magnetoplasmadynamic Thrusters", *J. Propulsion & Power*, Vol. 3, pp. 121-127, March-April 1987.

(5) V. V. Subramaniam, and J. L. Lawless, "Onset in Magnetoplasmadynamic Thrusters with Finite Rate Ionization", *J. Propulsion & Power*, Vol. 4, No. 6, pp. 526-532, November-December 1988.

(6) M. Martinez-Sanchez, "Structure of Self-Field Accelerated Plasma Flows", *J. Propulsion & Power*, Vol. 7 (1), pp. 56-64, Jan.-Feb. 1991.

(7) T. Shoji, and I. Kimura, "Analytical Study on the Influence of Non-equilibrium Ionization for Current Flow Pattern and Flow Field of MPD Arcjets", paper AIAA-90-2609, presented at the 21st International Electric Propulsion Conference, Orlando, Florida, July 1990.

(8) E. Niewood, and M. Martinez-Sanchez, "Quasi One-Dimensional Numerical Simulation of Magnetoplasmadynamic Thrusters", paper AIAA-90-2604, presented at the 21st International Electric Propulsion Conference, Orlando, Florida, July 1990.

(9) E. S. Oran, and J. R. Boris, *Numerical Simulation of Reactive Flows*, Science Publishing Company, Elsevier, New York, 1987.

(10) Z. Bilicki, C. Dafermos, J. Kestin, G. Majda, and D. L. Zeng, "Trajectories and Singular Points in Steady State Models of Two-Phase Flows", *Int. J. Multiphase Flow*", Vol. 13, No. 4, pp. 511-533, 1987.

(11) V. V. Subramaniam, and J. L. Lawless, "Electrode -Adjacent Boundary Layer

Flow in Magnetoplasmadynamic Thrusters", *Phys. Fluids* 31 (1), pp. 201-209, January 1988.

(12) M. Martinez-Sanchez, "The Structure of Self-Field Accelerated Plasma Flows", paper AIAA-87-1065, presented at the 19th International Electric Propulsion Conference, Colorado Springs, Colorado, May 1987.

(13) K. Kuriki, and T. Nakayama, "Magnetosonic Condition in Magnetoplasmadynamic Flow", paper AIAA-90-2605, presented at the 21st International Electric Propulsion Conference, Orlando, Florida, May 1987.

(14) C. W. Gear, "The Automatic Integration of Ordinary Differential Equations", *Numerical Mathematics, Communications of the ACM*, Vol. 14, No. 3, March 1991.

(15) R. Bulirsch, and J. Stoer, "Numerical Treatment of Ordinary Differential Equations by Extrapolation Methods", *Numerische Mathematik*, Vol. 8, pp. 1-13, 1966.

(16) G. Lefever-Button, "Quasi One-Dimensional Ionizing Supersonic Flow in a Magnetoplasmadynamic Thruster", *Undergraduate Honors Thesis*, College of Engineering, The Ohio State University, July 1990.

(17) D. Q. King, *Magnetoplasmadynamic Channel Flow for Design of Coaxial MPD Thrusters*, Ph.D. Dissertation, Department of Mechanical and Aerospace Engineering, Princeton University, December 1981.

(18) J. H. Gilland, *The Effect of Geometrical Scale Upon MPD Thruster Behavior*, M.S. Thesis No. 1811-T, Department of Mechanical and Aerospace Engineering, Princeton University, March 1988.

(19) M. R. LaPointe, "Numerical Simulation of Self-Field MPD Thrusters", paper AIAA-91-2341, presented at the AIAA/SAE/ASME/ASEE 27th Joint Propulsion Conference, Sacramento, California, June 24-27 1991.

Figure and Table Captions

Figure 1: Comparison of integrator performance characteristics for isentropic test case.

Figure 2: Comparison of overall integration errors for isentropic test case.

Figure 3: Plot of temperature profiles for varying inlet temperatures in the flared channel of the HSFAT thruster (see section IV for details).

Figure 4: Ionization fraction profiles for a constant area channel, A=0.001 m^2, B_i=0.159, L=20 cm., at various mass flow rates.

Figure 5: Velocity profiles for exit/inlet area ratios of 1 (constant area), 4.5, 9, and 15, with A_i=0.001 m^2 and 20 cm. length.

Figure 6: Temperature profiles for linearly-varying areas, A_i=0.001 m^2 and 20 cm. length.

Figure 7: Current density profiles for linearly-varying areas, A_i=0.001 m^2 and 20 cm. length.

Figure 8: Ionization fraction profiles for linearly-varying areas, A_i=0.001 m^2 and 20 cm. length.

Figure 9: Magnetic field profiles for linearly-varying areas, A_i=0.001 m^2 and 20 cm. length.

Figure 10: Mach number profiles for linearly-varying areas, A_i=0.001 m^2 and 20 cm. length.

Figure 11: Comparison of experimentally measured and calculated values of thrust for 10 cm. HSFAT channel.

Figure 12: Comparison of experimentally measured and calculated values of thrust/J^2 for 10 cm. HSFAT channel.

Figure 13: Comparison of the ratio of electromagnetic/electrothermal contributions for various total currents.

Figure 14: Comparison of ionization fraction profiles in 10 cm. HSFAT channel.

Figure 15: Comparison of HSFAT current density profile with that of a linearly-varying channel with the same A_i and A_e.

Figure 16: Comparison of back-EMF of HSFAT with that of a linearly-varying channel with the same A_i and A_e.

Table I: Tests performed and actions taken for automatic integration of MPD channels. Variables subscripted 1 are previous points, those subscripted 2 are evaluated at the present location, and the subscript T denotes the throat, or minimum area location.

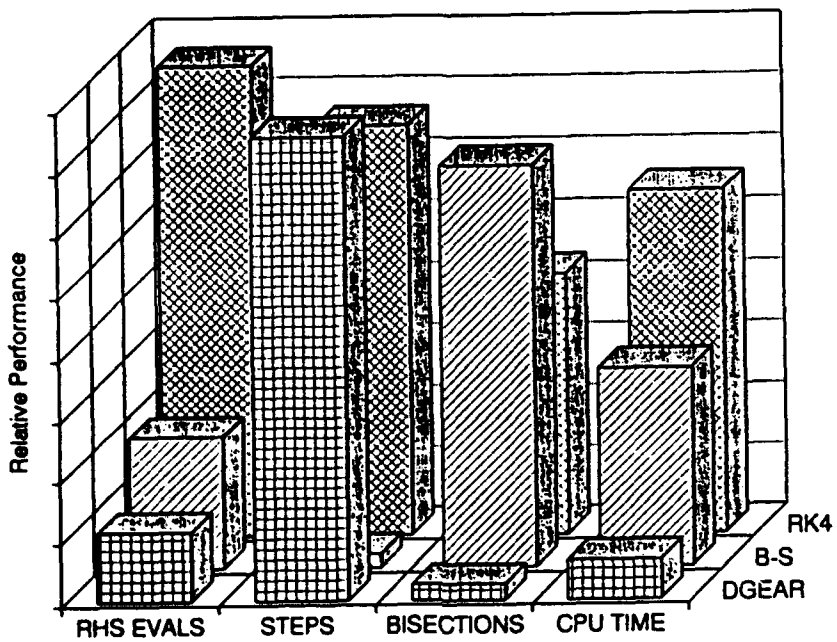

Integrator	RHS Evals	Integrator Steps	Number of Bisections	CPU Time (sec)
Runge-Kutta	15262	1328	17	11.13
Bulirsch-Stoer	4269	44	26	6.42
IMSL DGEAR	2200	1499	1	1.24

Fig. 1

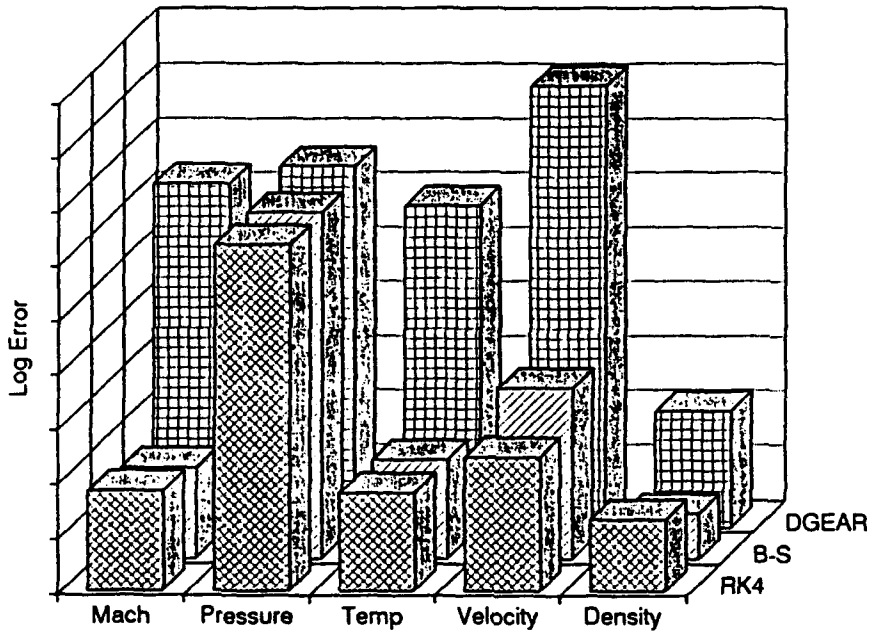

Integrator	Mach Number	Pressure	Temperature	Velocity	Density
Runge-Kutta	6.60E-07	2.20E-02	6.10E-07	2.80E-06	2.00E-07
Bulirsch-Stoer	4.50E-07	2.20E-02	6.40E-07	1.30E-05	6.80E-06
IMSL DGEAR	1.90E-02	4.00E-02	7.50E-03	1.20E+00	7.70E-03

Fig. 2

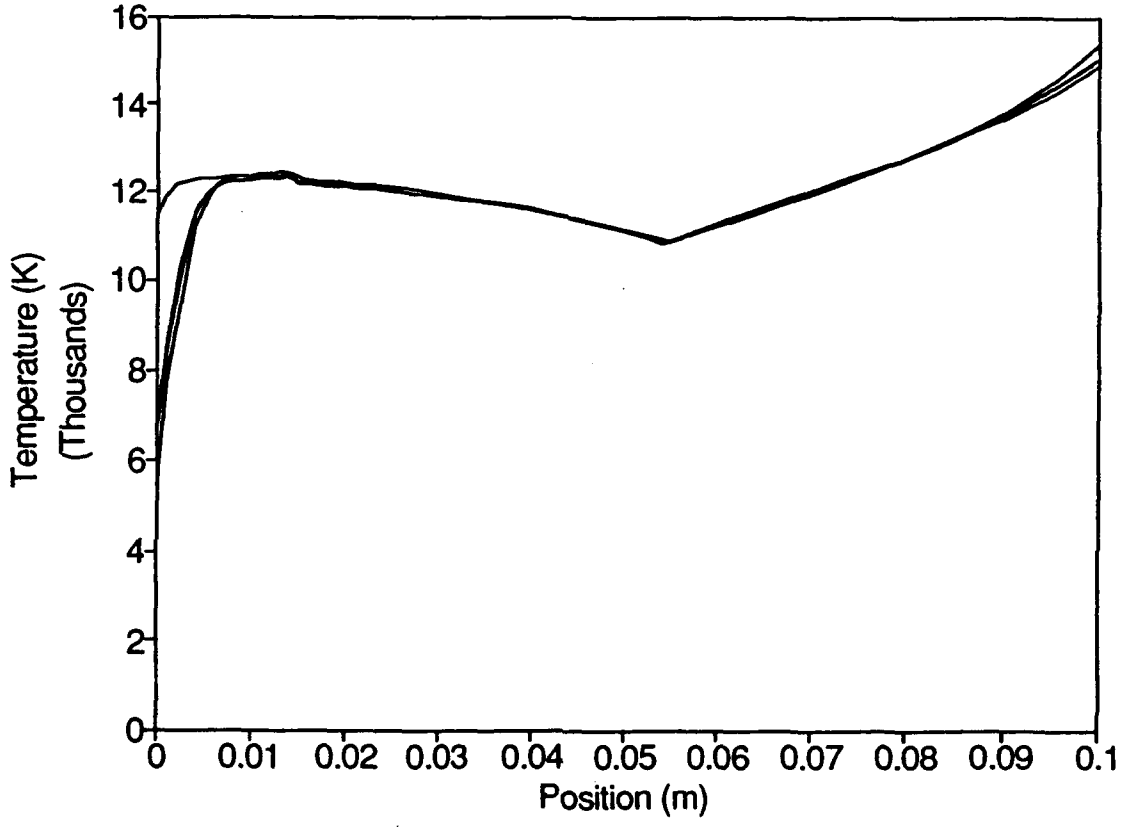
16
14
12
10
8
6
4
2
0
Temperature (K)
(Thousands)
0
0.01
0.02
0.03
0.04
0.05
0.06
0.07
0.08
0.09
0.1
Position (m)

Fig. 3

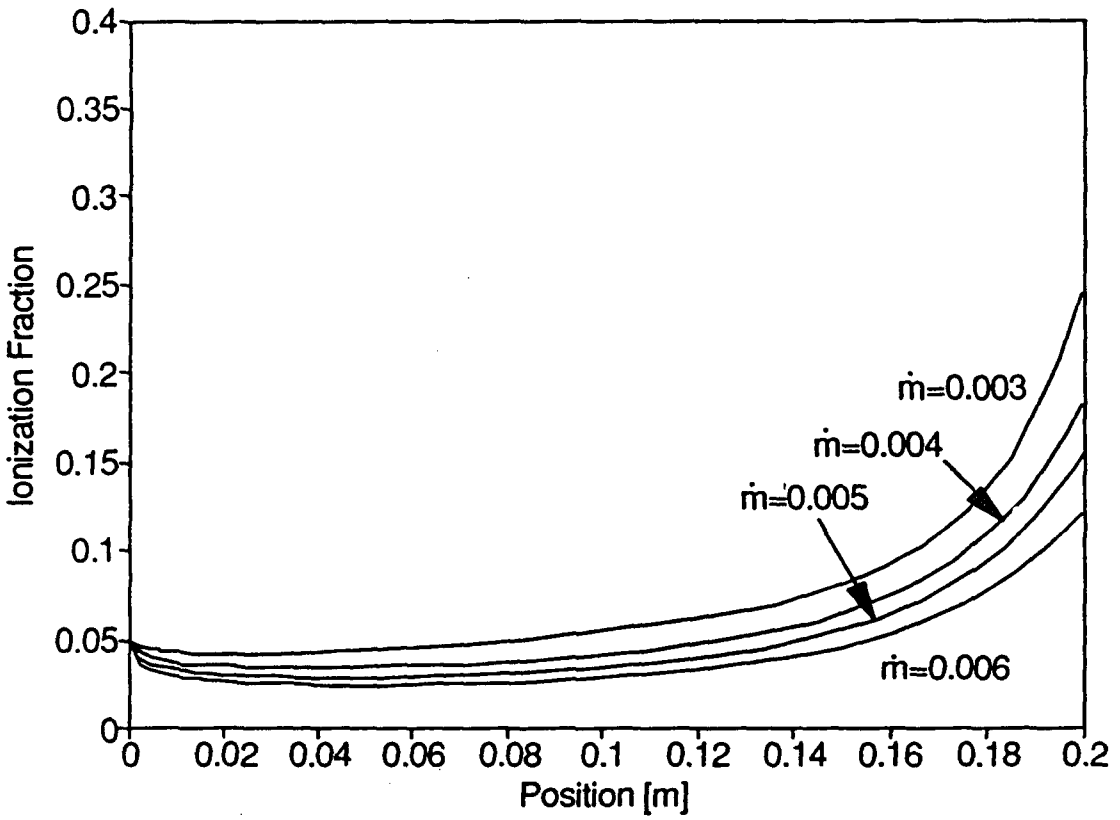
0.4
0.35
0.3
0.25
0.2
0.15
0.1
0.05
0
Ionization Fraction
0
0.02
0.04
0.06
0.08
0.1
0.12
0.14
0.16
0.18
0.2
Position [m]
ṁ=0.003
ṁ=0.004
ṁ=0.005
ṁ=0.006

Fig. 4

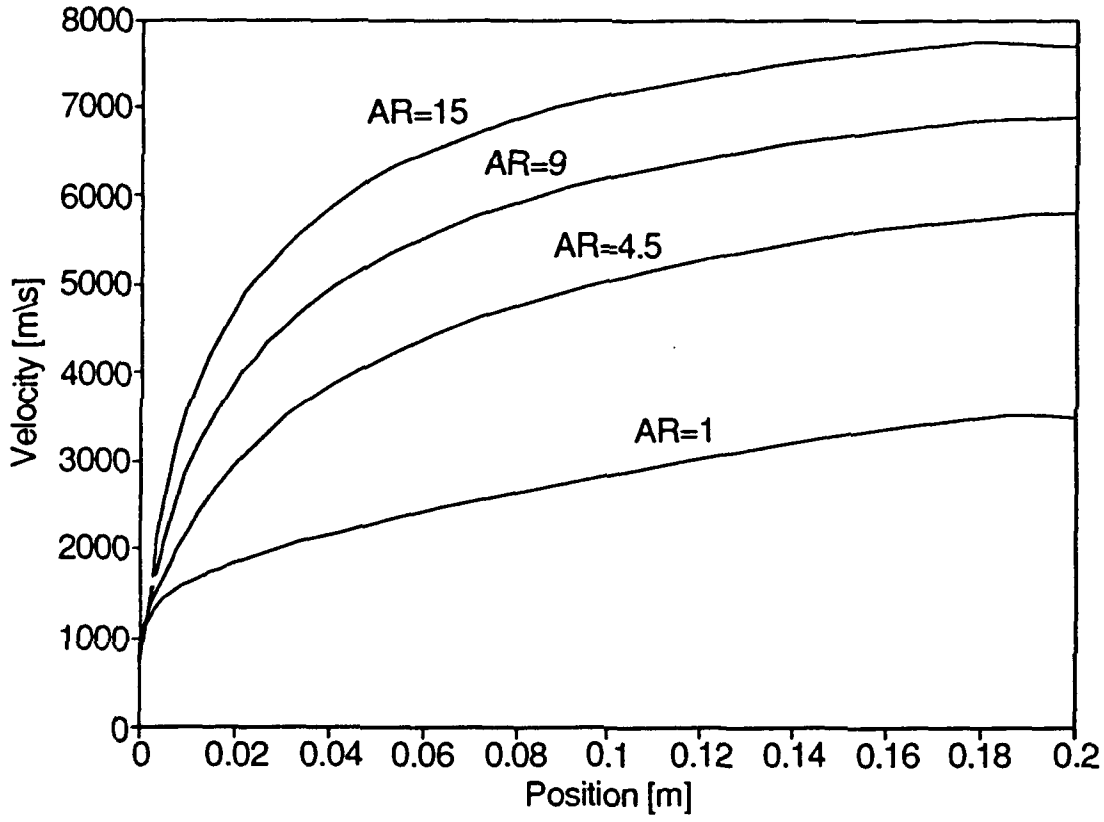
8000
7000
6000
5000
4000
3000
2000
1000
0
Velocity [m\s]
AR=15
AR=9
AR=4.5
AR=1
0
0.02
0.04
0.06
0.08
0.1
0.12
0.14
0.16
0.18
0.2
Position [m]

Fig. 5

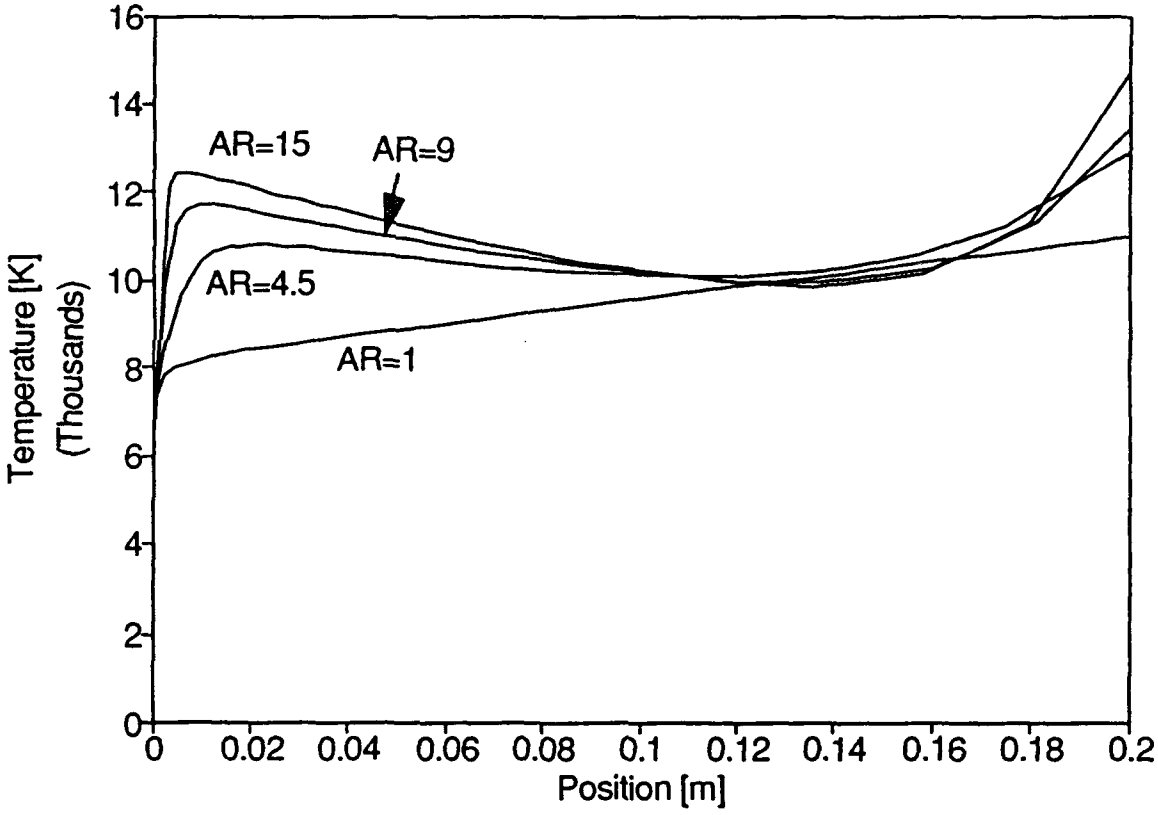
16
14
12
10
8
6
4
2
0
Temperature [K]
(Thousands)
AR=15
AR=9
AR=4.5
AR=1
0
0.02
0.04
0.06
0.08
0.1
0.12
0.14
0.16
0.18
0.2
Position [m]

Fig. 6

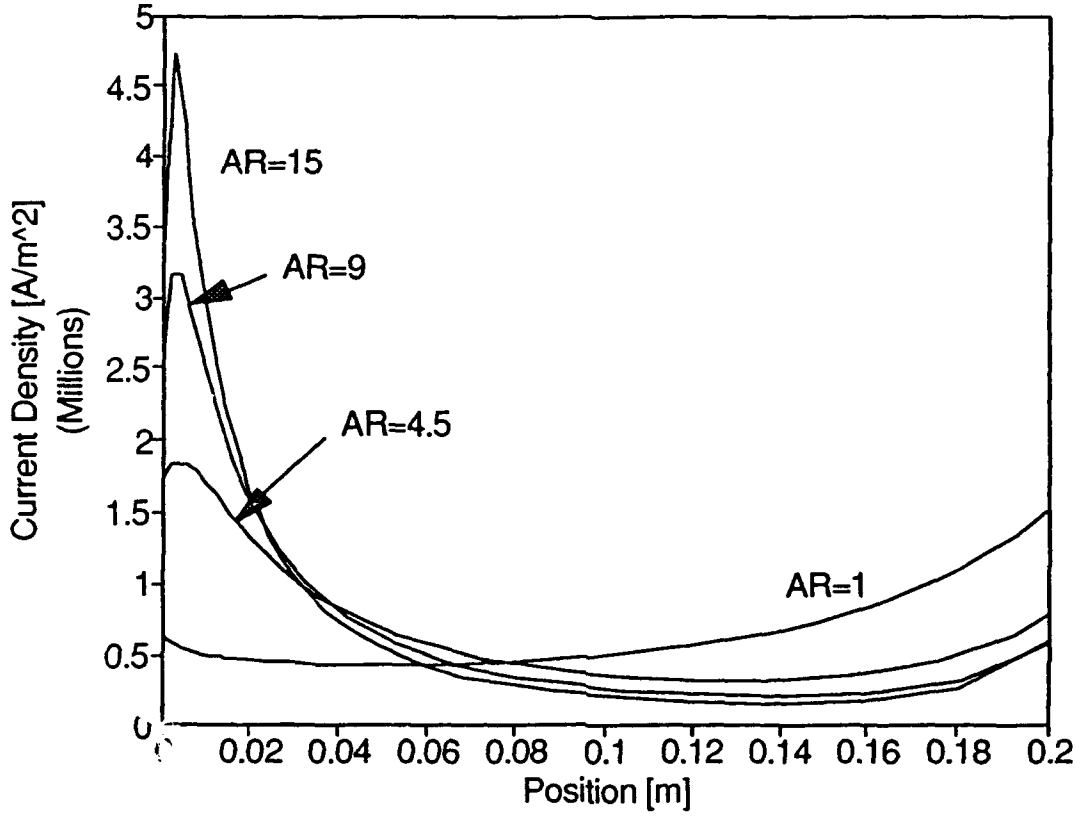
Current Density [A/m^2]
(Millions)
5
4.5
4
3.5
3
2.5
2
1.5
1
0.5
0
AR=15
AR=9
AR=4.5
AR=1
0.02
0.04
0.06
0.08
0.1
0.12
0.14
0.16
0.18
0.2
Position [m]

Fig. 7

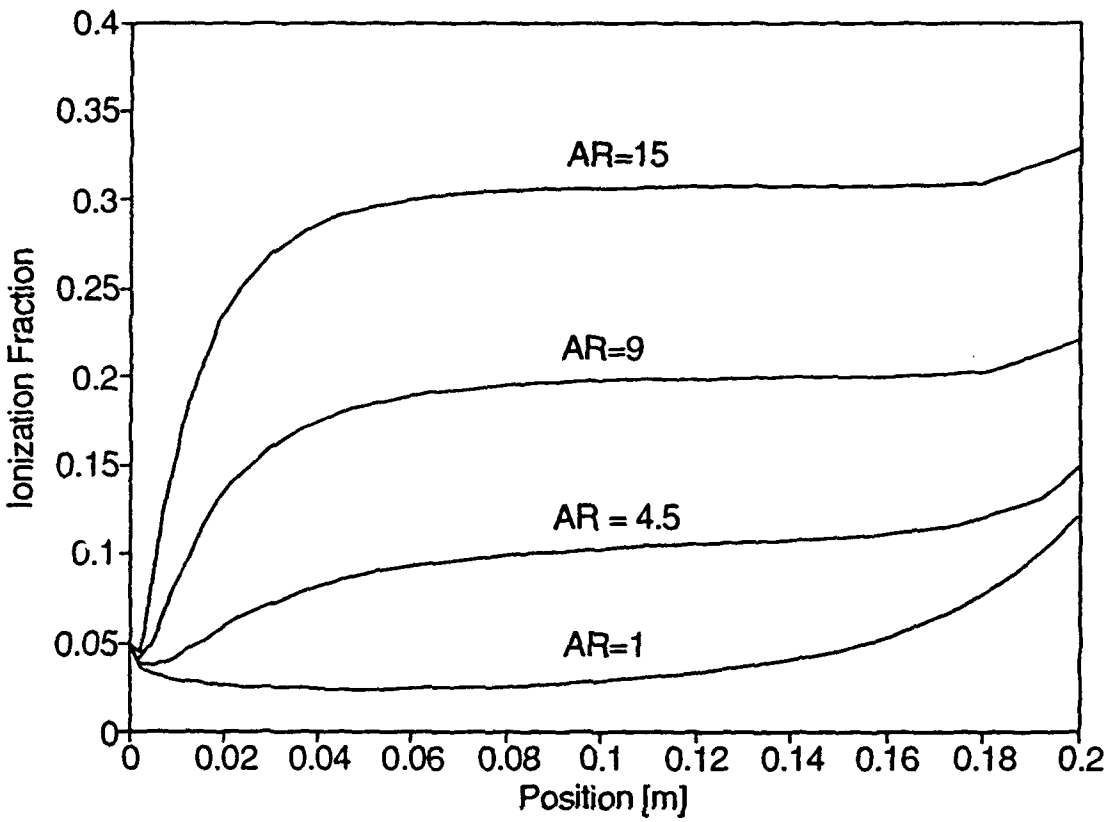
0.4
0.35
0.3
0.25
0.2
0.15
0.1
0.05
0
Ionization Fraction
AR=15
AR=9
AR = 4.5
AR=1
0
0.02
0.04
0.06
0.08
0.1
0.12
0.14
0.16
0.18
0.2
Position [m]

Fig. 8

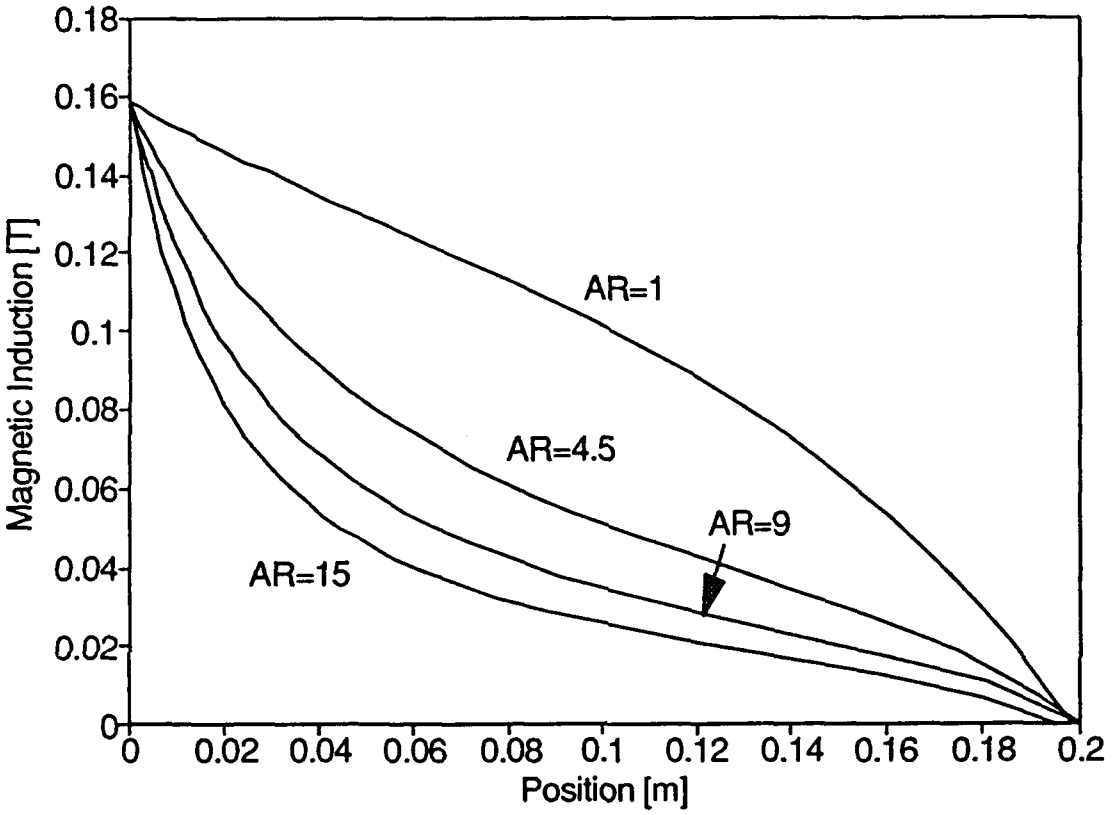
0.18
0.16
0.14
0.12
0.1
0.08
0.06
0.04
0.02
0
Magnetic Induction [T]
AR=1
AR=4.5
AR=9
AR=15
0
0.02
0.04
0.06
0.08
0.1
0.12
0.14
0.16
0.18
0.2
Position [m]

Fig. 9

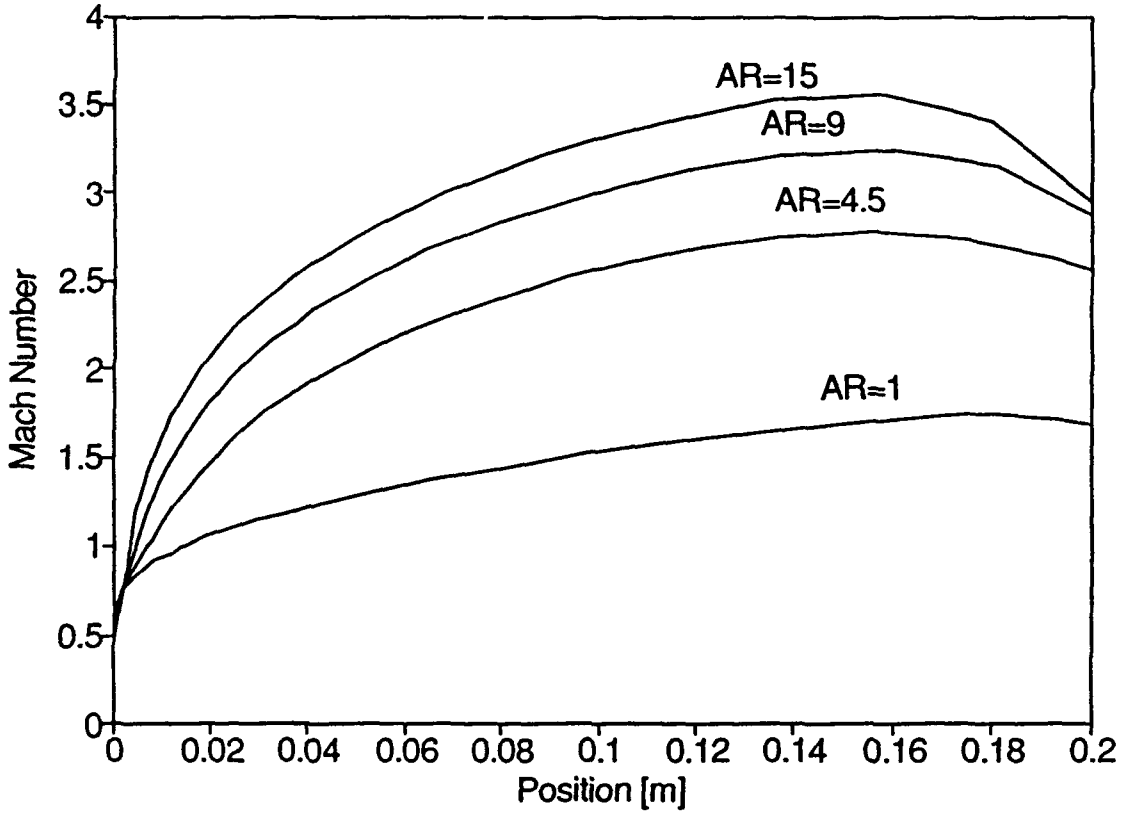
AR=15
AR=9
AR=4.5
AR=1
Mach Number
Position [m]
0
0.5
1
1.5
2
2.5
3
3.5
4
0
0.02
0.04
0.06
0.08
0.1
0.12
0.14
0.16
0.18
0.2

Fig. 10

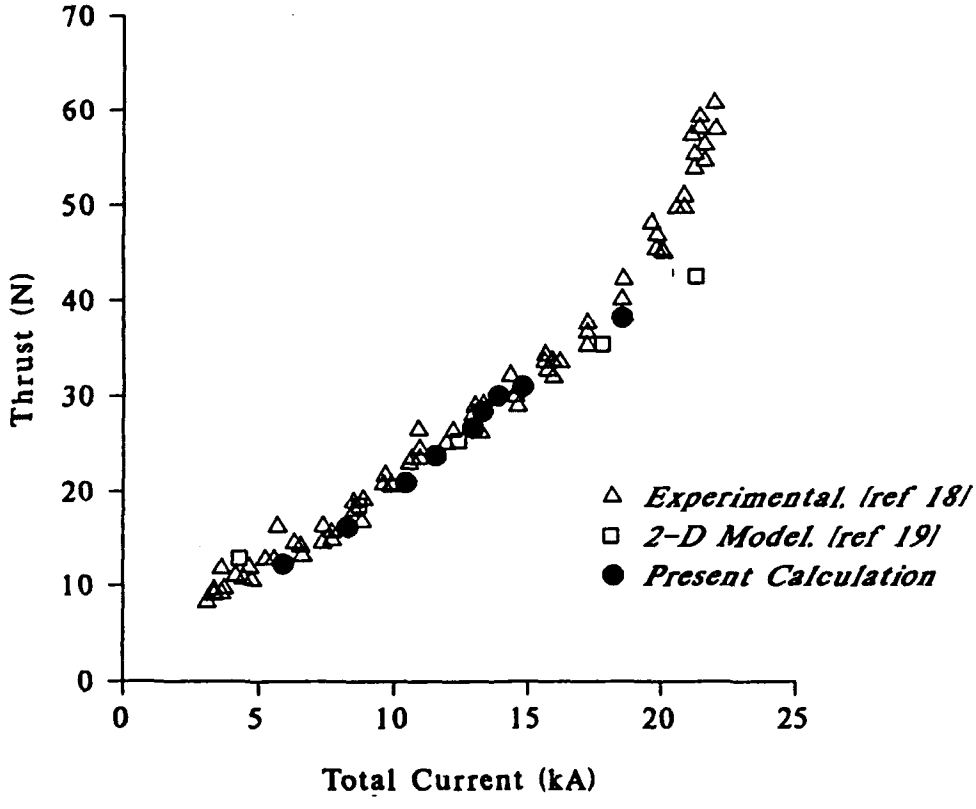
70
60
50
40
30
20
10
0
Thrust (N)
0
5
10
15
20
25
Total Current (kA)
Experimental. [ref 18]
2-D Model. [ref 19]
Present Calculation

Fig. 11

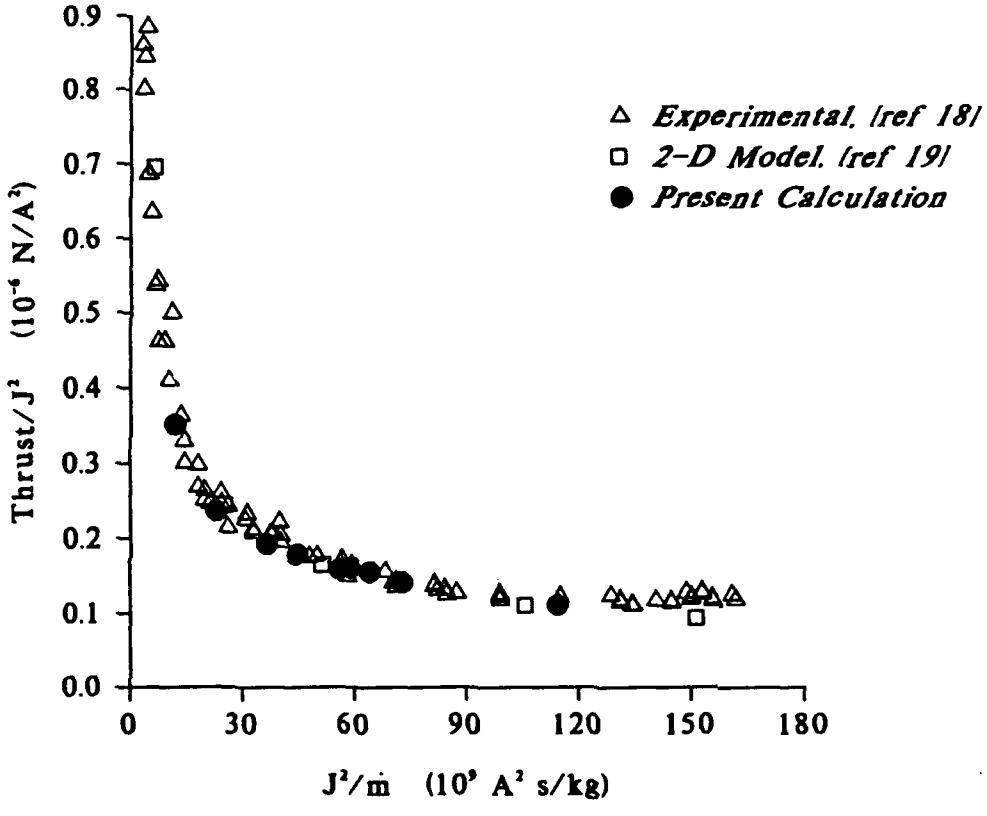
0.9
0.8
0.7
0.6
0.5
0.4
0.3
0.2
0.1
0.0
Thrust/J² (10⁻⁶ N/A²)
0
30
60
90
120
150
180
J²/ṁ (10⁹ A² s/kg)
Experimental, [ref 18]
2-D Model, [ref 19]
Present Calculation

Fig. 12

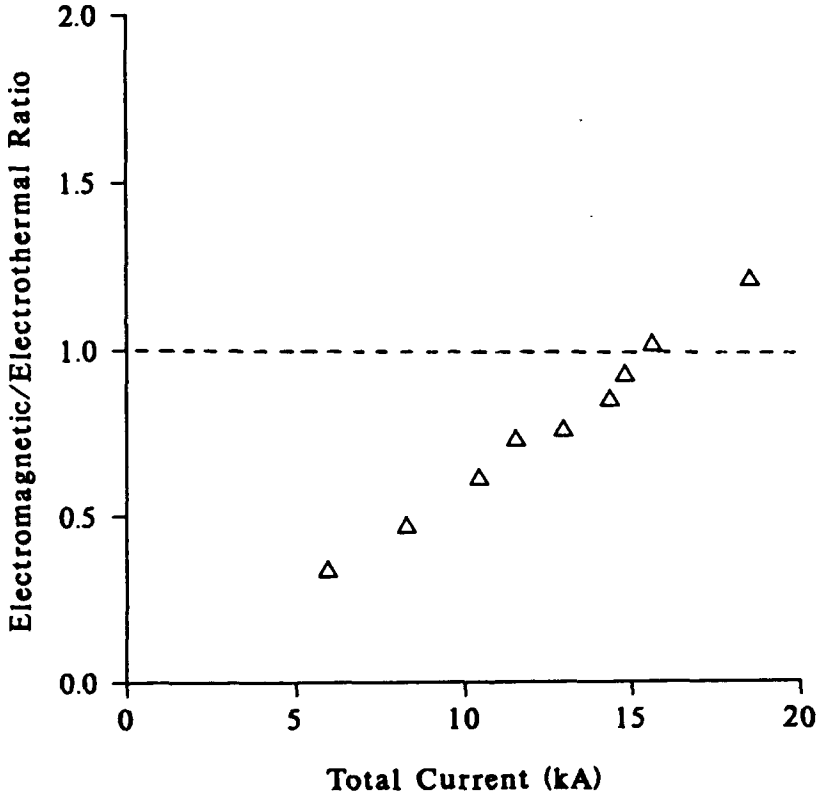
Electromagnetic/Electrothermal Ratio
2.0
1.5
1.0
0.5
0.0
0
5
10
15
20
Total Current (kA)

Fig. 13

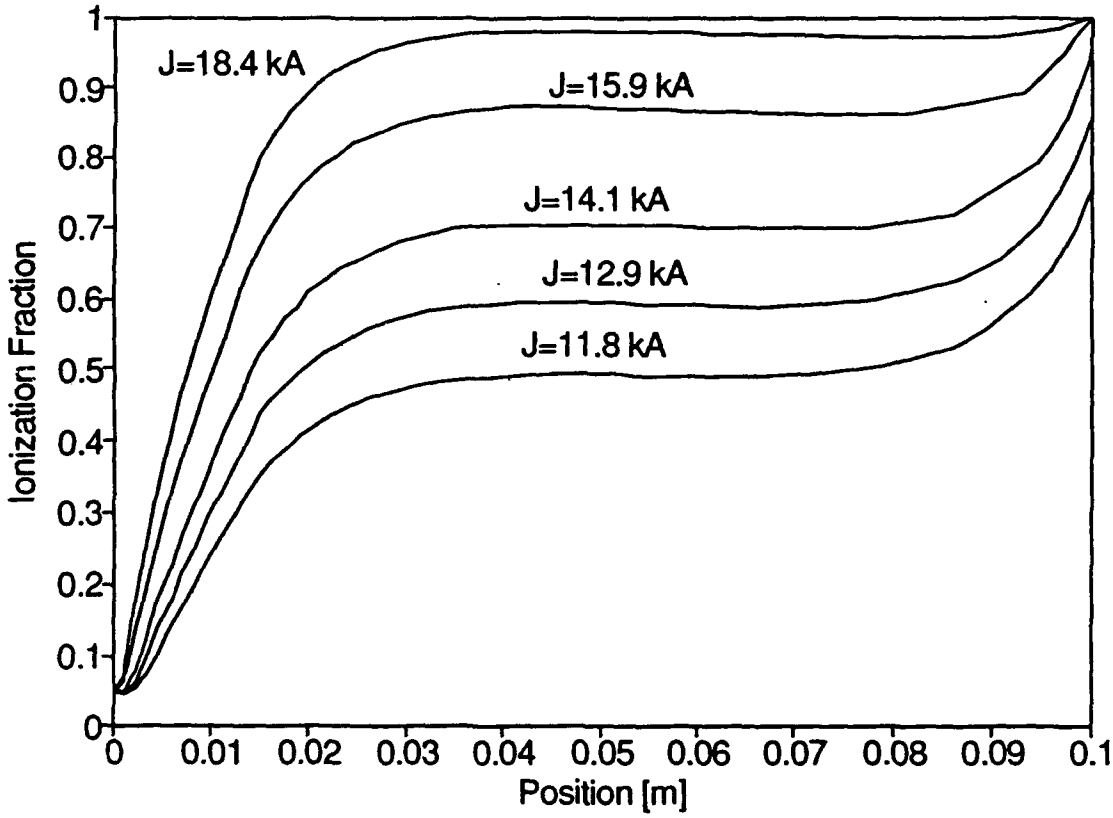
J=18.4 kA
J=15.9 kA
J=14.1 kA
J=12.9 kA
J=11.8 kA
Ionization Fraction
Position [m]
0
0.1
0.2
0.3
0.4
0.5
0.6
0.7
0.8
0.9
1
0.01
0.02
0.03
0.04
0.05
0.06
0.07
0.08
0.09
0.1

Fig. 14

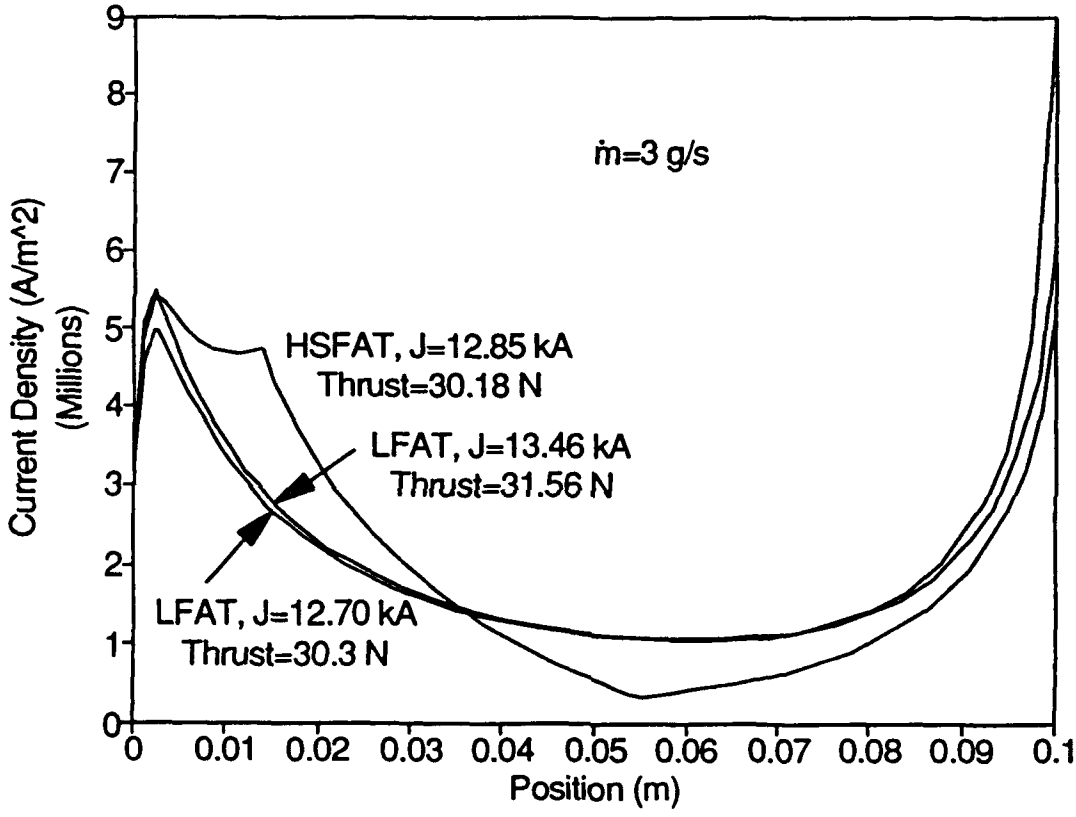
ṁ=3 g/s
HSFAT, J=12.85 kA
Thrust=30.18 N
LFAT, J=13.46 kA
Thrust=31.56 N
LFAT, J=12.70 kA
Thrust=30.3 N
Current Density (A/m^2)
(Millions)
Position (m)
0
1
2
3
4
5
6
7
8
9
0
0.01
0.02
0.03
0.04
0.05
0.06
0.07
0.08
0.09
0.1

Fig. 15

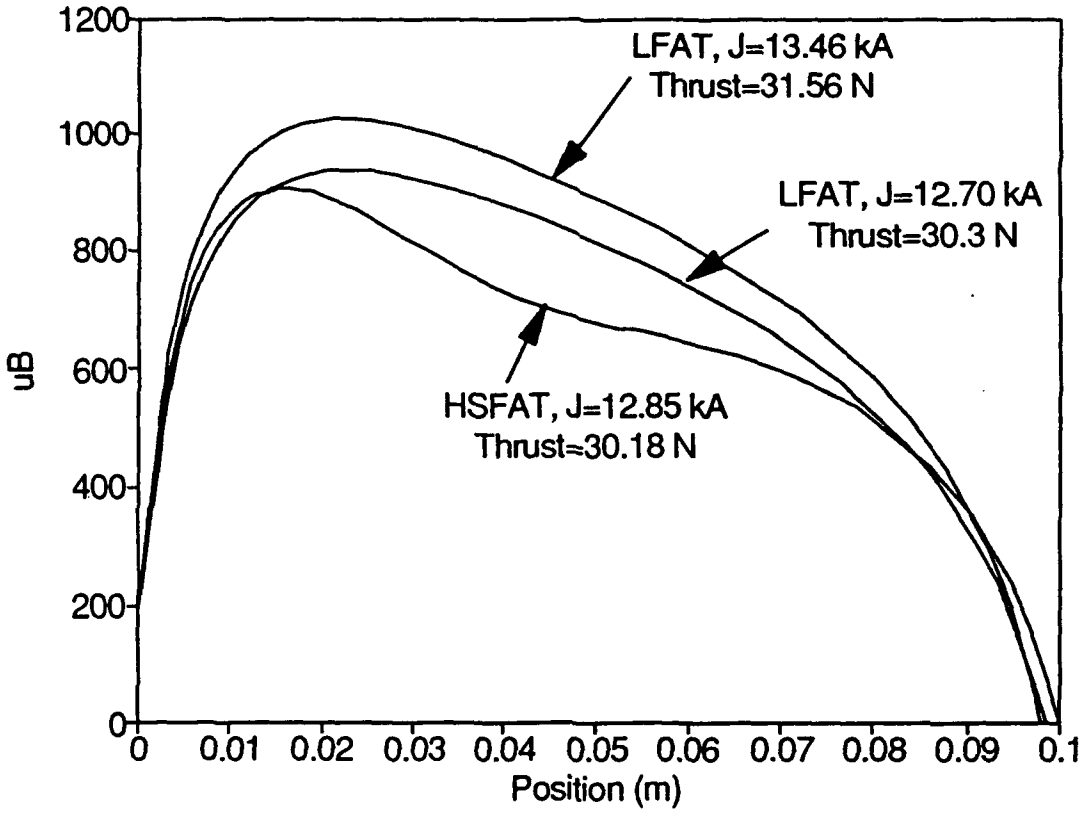
LFAT, J=13.46 kA
Thrust=31.56 N
LFAT, J=12.70 kA
Thrust=30.3 N
HSFAT, J=12.85 kA
Thrust=30.18 N
uB
Position (m)
1200
1000
800
600
400
200
0
0
0.01
0.02
0.03
0.04
0.05
0.06
0.07
0.08
0.09
0.1

Fig. 16

TEST	PLACE	TRUE	FALSE
$M_2 > M_1$ ($x < x_T$)	every step before x_T	no action	restart at inlet with higher u_o
$M_2 > M_1$ ($x > x_T$)	every step after x_T	no action	if #successive failures > 25 restart with lower u_o
$T_2 > T_1$	every step before x_T	no action	restart with lower u_o
$P > 0, \alpha > 0$	every step	no action	restart with lower u_o
$B < 0$	every step	nozzle end; check length	no action
$\lvert l\text{-}L \rvert > \varepsilon_L$	after completed integration	Done!	correct E_o and restart
$l < L$	after completed integration	decrease E_o and restart	no action
$l > L$	after completed integration	increase E_o and restart	no action
$x > 1.5L$	every step	increase E_o and restart	no action
$x = L$ and no jump	every step	increase u_o and restart	no action

TABLE 1

Appendix B

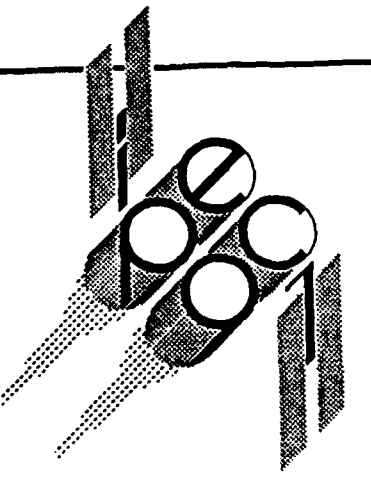

IEPC-91-019

A Review of the Theory of Self-Field MPD Thrusters

J. L. Lawless
Space Power, Inc.
San Jose, CA 94134
U.S.A.
and
V. V. Subramaniam
Department of Mechanical Engineering
The Ohio State University
Columbus, Ohio 43210
U.S.A.

AIDAA/AIAA/DGLR/JSASS 22nd International Electric Propulsion Conference

October 14-17, 1991 / Viareggio, Italy

A Review of the Theory of Self-Field MPD Thrusters

J. L. Lawless[1]
Space Power Inc.
San Jose, Ca 94134
and
V. V. Subramaniam[2]
Department of Mechanical Engineering
The Ohio State University
Columbus, Ohio 43210-1107

Abstract

A great amount of research has been performed in self-field Magnetoplasmadynamic (MPD) thruster research during the past decade. In contrast to previous years, activity in the theoretical and modelling areas have increased. This paper will review the developments in the theory of self-field MPD thrusters, concentrating mainly on one-dimensional and quasi one-dimensional theories, for which exact or approximate solutions can be obtained.

Nomenclature

a	Frozen speed of sound
B	Magnetic induction
C_e	Mean thermal speed of electrons
C_H	Mean thermal speed of heavy particles
E	Electric field
h	Enthalpy per unit mass
H	Channel height
j	Current density
J	Total current
k	Boltzmann's constant
L	Channel length
$\dot{m}$	Mass flow rate
m_A	Atomic mass
m_e	Electron mass
n_e	Electron or charged particle number density
P	Pressure
Q_{AA}	Total momentum transfer cross section for atom-atom collisions
Q_{iA}	Total momentum transfer cross section for ion-atom collisions
Q_{ii}	Total momentum transfer cross section for ion-ion collisions
T	Temperature
T_e	Electron temperature
T_h	Thrust
T_H	Heacy particle temperature
u	Axial component of velocity
W	Channel width
x	Coordinate along channel
α	Ionization fraction
ϵ_i	Ionization potential
η_H	Heavy particle viscosity
κ	Ratio of magnetic induction at inlet to the magnetic induction at the choking point
μ_0	permeability of free space
ρ	Mass density
σ	Electrical conductivity
i	Subscript denoting inlet quantity
e	Subscript denoting exit quantity
*	Superscript denoting quantity evaluated at the sonic or choking point

I. Introduction

During the past ten years, there has been a great deal of activity in self-field magnetoplasmadynamic (MPD) thruster research. This paper will attempt to summarize the developments in the theory of these thrusters and compare theory to available experiments. Models are now capable of predicting I-V curves from first principles. The conditions under which electrodes erode are beginning to be understood. Quantitative prediction of the destructive "onset" phenomenon also appears to be possible now.

Early work in the field of MPD thrusters has been summarized by Jahn[1]. The technology of MPD thrusters has been

[1] Member AIAA
[2] Member AIAA

recently reviewed by Myers et al[2]. This review will concentrate on developments in the theory of MPD thrusters. As two dimensional models are still in their early stages of development, emphasis will be given to quasi-one-dimensional models and their implications for thruster performance and future thruster design.

Magnetoplasmadynamic (MPD) thrusters use electric and magnetic fields to accelerate a plasma to high speeds, commonly 20 to 45 km/s. This acceleration is achieved by the action of jxB forces in a steady flow. The magnetic field may be generated by the current itself, "self-field." Alternatively, the magnetic induction, B, may be externally applied. Self-field thrusters generally require instantaneous input powers of the order of 1 MW. Applied field thrusters can operate with powers as low as 100 kW. Over the past ten years, research has concentrated on self-field thrusters and this review will concentrate on this type.

A sample configuration for a self-field thruster is shown in Figure 1. The geometry is axisymmetric. The propellant, typically a rare gas and most often argon, is injected through holes in the back plate. A current is drawn between the center cathode and outer anode. The current induces an azimuthal magnetic field. The resulting jxB force is largely axial, accelerating the propellant out of the thruster.

Self-field thrusters tend to have higher efficiencies as the current driving them increases. Specific impulse also increases with current. This increase in performance has a well-know limit: above a certain current level, instabilities and erosion set in. This is collectively called "onset" and the current at which this happens is called the critical current or Onset current. Much theoretical effort has been devoted towards explaining this phenomenon, and hence will also be discussed in this review.

This paper is organized as follows. Early flow models are discussed in the next section, followed by a discussion of theories of Onset. Electrode and boundary layer models are then discussed, followed by the current status of analyses of electrode behavior under steady-state MPD operation.

II. Flow Models

While the flow in an MPD thruster may be complex, there is one simple feature: the magnetic body force is the strongest force operating on the fluid. From this starting point, useful information can be derived. The magnitude of the magnetic body force depends only on the current distribution and not directly on the fluid properties. By assuming current profiles and integrating the body force over the flow volume, the thrust, T_h, can be derived. If the current lines are radial between a cylindrical cathode of radius r_c and an anode of radius r_a, as shown in Figure 2a, the resulting thrust is:

$$T_h = \frac{\mu_0 J^2}{4\pi} \ln\left(\frac{r_a}{r_c}\right) \qquad (1)$$

where J is the total current and μ_0 is the permeability of free space. If the current is carried by the conical section of the cathode as shown in Figure 2b, the thrust is determined from:

$$T_h = \frac{\mu_0 J^2}{4\pi}\left[\frac{3}{4} + \ln\left(\frac{r_a}{r_c}\right)\right] \qquad (2)$$

A remarkable feature of these equations is that they do not depend on the path that the current follows between the electrodes[1].

Notice that the geometry in Figure 2b produces a larger thrust for the same current J than the geometry of Figure 2a. This does not, however, mean that one geometry is more efficient than the other. This level of theory cannot tell us the voltage required to drive the current J or hence the electrical input power used to generate the thrust T_h.

The next level of theory considers one-dimensional (or quasi one-dimensional) flow through the thruster. A thruster geometry which can be analyzed as one-dimensional is shown in Figure 3. This plane-parallel geometry avoids radial variations in fields that occur when $r_a >> r_c$. The behavior is otherwise analogous. For example, by conservation of momentum, the thrust for this geometry can be found to be:

$$T_h = \frac{\mu_0 J^2}{2}\frac{H}{W} \qquad (3)$$

This equation is very similar in form to those above. In fact, equation (3) can by derived from equation (1) by identifying $H = r_a - r_c$ and $W = 2\pi r_c$ and considering H small. Since the

thrust T_h is the product of the mass flow rate, $\dot{m}$, and the exhaust speed, u_e, the above equation also determines exhaust speed:

$$u_e = \frac{\mu_0 J^2}{2\dot{m}} \frac{H}{W} \qquad (4)$$

For the case of an applied field thruster, the gas dynamics of the channel flow were first studied in 1958 by Sears and Resler[3,4]. Their study mapped the various regions of operation including such important effects as MPD choking. Further discussion of this theory can be found textbooks[5,6].

In the 1970's, attention shifted to self-field thrusters. Self-field thrusters offered engineering simplicity by not requiring large magnets. Inspired by a Ph.D. thesis by Martinache[7], King[8,9], developed a model of self-field thrusters that could successfully compare to experiment. In King's model, the thruster is modeled as a one-dimensional flow subjected to ohmic heating and the magnetic body force (See Table I).

To understand the flow, it is necessary to know how the various phenomena affect the flow's Mach number. This is summarized in Table II and is not always intuitive[10]. At the inlet of a MPD thruster, ohmic heating is dominant and this drives the flow towards the sonic point (M=1). As the flow speed increases, the magnetic body force becomes increasingly important. Under exactly the right condition, ohmic heating lifts the Mach number to 1 and the magnetic body force then drives the Mach number still higher. The condition under which this happens is called the choking condition, and a rigorous mathematical discussion of this condition can be found in Ref.[11]. For an ideal monatomic gas, the choking condition is:

$$E = \frac{5}{2} a^* B^* \qquad (5)$$

where a is the speed of sound, E is the electric field, B is the magnetic induction and the superscript * indicates that these are evaluated at the choking point. This condition must be satisfied or the flow cannot accelerate from subsonic to supersonic speeds. This generally happens far upstream in the thruster as shown in Figure 1.

One might naively assume that, if the flow is introduced into the thruster supersonically, then the choking condition would be irrelevant. This is generally not the case. Immediately after the flow is injected, it is still subjected to strong ohmic heating. From Table II, ohmic heating lowers the Mach number of supersonic flow. Since the magnitude of the ohmic heating generally greatly exceeds the stagnation enthalpy of the injected propellant, the flow is quickly driven to Mach 1. In order to accelerate again to supersonic speeds, the choking condition must still be met. The case of supersonic propellant injection was extensively studied by King[9].

King recognized that this model had important implications for thruster design. This led to the development of the King anode[8].

To clarify the relationship between this theory and earlier work, the equations (1)-(3), (4) for thrust can be derived from the momentum equation given in Table I by neglecting pressure.

There is another restriction on the electric field. From consideration of Ohm's law under usual MPD thruster conditions, it is found that the back-EMF must never exceed the applied, electric field, E:

$$uB \le E \qquad (6)$$

This restriction does not replace the choking condition. Rather, it must be obeyed in addition to the choking condition, equation (5). This presents an interesting and important issue. Let us combine the inequality (6) with the choking condition:

$$uB \le \frac{5}{2} a^* B^* \qquad (7)$$

Somewhere in the middle region of the thruster, the product uB reaches a maximum. This region is observed experimentally as a region of low current density. Let us call the values of u and B at this point u_m, and B_m, respectively. Now, rewrite inequality (7) as:

$$u_m \le \frac{5}{2} a^* \frac{B^*}{B_m} \qquad (8)$$

The magnetic induction at the choking point, B^*, is within 10% of the magnetic induction at the thruster inlet. The magnetic induction, B_m, where the back-EMF is a maximum is usually 0.6 to 0.7 times the value at the inlet. Thus, their ratio can be approximated as 1.5. Substituting in this value:

$$u_m \le 3.75 a^* \qquad (9)$$

The right-hand side above is fairly constant. a^* is determined by the temperature at the choking point and plasma temperatures are known to vary little. The left-hand side varies strongly with current. From equation (4), the exhaust speed scales as $J^2/\dot{m}$. Thus, equation (9) appears to place a limit on $J^2/\dot{m}$. Let us estimate u_m as 2/3 of u_e. Then

combining equation (4) with equation (9) gives:

$$\frac{2}{3}\frac{\mu_0 J^2}{\dot{m}}\frac{H}{W} \le 3.75a^* \qquad (10)$$

Rearranging this gives:

$$\frac{J^2}{\dot{m}} \le 11.25\frac{Wa^*}{H\mu_0} \qquad (11)$$

This equation expresses the restriction on $J^2/\dot{m}$ that comes from combining the choking condition, equation (5), with the limit on back-EMF, uB≤E. The above derivations included several approximations. If the equations on Table I are solved exactly, the result is:

$$\frac{J^2}{\dot{m}} \le 8.52\frac{W}{H}\frac{a^*}{\mu_0\kappa^2} \qquad (12)$$

where κ is the ratio of the magnetic induction at the inlet to the magnetic induction at the choking point. This typically has a value of about 1.1[9]. This explanation of onset first appeared in Ref[12].

It should be mentioned that the role of inlet flow conditions in altering the occurrence of back-EMF onset is contained entirely in the κ factor. This quantity is restricted to a small range about 1.1. Inlet conditions are extensively discussed in Ref. [9].

The above discussion was based on the ideal gas choking condition, equation (5). For quantitative results, non-ideal effects must be considered, principally ionization. If one considers equilibrium flow, the choking condition becomes:

$$E^* = \left[\rho^* \left.\frac{\partial h}{\partial P}\right|_{s^*}\right] a^* B^* \qquad (13)$$

The quantity in square brackets is 5/2 for an ideal monatomic gas. For equilibrium argon, its value is shown in Fig. 4. It is seen that the equilibrium theory and ideal monatomic gas theory agree only at low temperatures, <5000K. For higher temperatures, the equilibrium theory predicts much higher electric fields. These higher electric fields would have the effect of delaying back-EMF onset to larger values of $J^2/\dot{m}$. The magnitude of the increase in $J^2/\dot{m}$ can be estimated by replacing 5/2 in equation (7) with the values given in Fig. 4 and then continuing the derivation as before.

Unfortunately, the equilibrium assumption is not accurate. Real gases have finite ionization rates and this reduces the electric field below the peak values that the equilibrium theory would allow. For a monatomic gas with finite rate ionization, the choking condition is:

$$E^* = \frac{5}{2}a^* B^* + \frac{\rho^* a^* \epsilon_i}{j^* m_A}\left.\frac{d\alpha}{dx}\right|_{x=x^*} \qquad (14)$$

where α is the ionization fraction, ϵ_i is the ionization potential, m_A is the atomic mass, and j^* is the current density evaluated at the choking point. It is apparent that the ionization rate at the choking point raises the electric field above the value it would have for an ideal monatomic gas. This allows the thruster to operate at higher $J^2/\dot{m}$ than the ideal gas theory would permit. How much higher depends on the ionization fraction and temperature at the choking point. To determine this currently requires a full numerical model. With such a model, it has been possible to quantitatively predict onset currents, as shown in Figure 5 and Figure 6[13].

For simplicity, most of the models above have assumed a one-temperature plasma. The plasmas in MPD thrusters are more accurately described by two-temperatures. A fairly complete simulation of a two-temperature MPD thruster with ionizing argon has been performed by Richley[14]. The simulation was capable of modeling fully unsteady flow. A sample temperature profile is shown in Figure 7.

Shoji and Kimura have developed a theory of two-temperature flow in MPD thrusters[15]. They also extended the model to include dissociating molecular gases and performed calculations on hydrogen. As for ionization, nonequilibrium dissociation alters the choking condition, raising the allowed electric field. They restricted their study to the region between choking and exit regions and parametrically varied the conditions at choking. For fixed thermodynamic conditions at the choking point and for fixed total current, they varied the mass flow. They numerically found a minimum mass flow, i.e. maximum $J^2/\dot{m}$, for which the thruster had a finite length. This is exactly the behavior expected from the above discussion of back-EMF Onset and choking conditions. This is the first calculation of this effect in a two-temperature model.

Models of self-field MPD thrusters have greatly advanced over the past ten years. Beginning with simple estimates for thrust,

models are now able to predict detailed temperature and speed distributions. The models described in this section have, however, been restricted to quasi one-dimensional flows. This limits, for example, their ability to describe flow in the Princeton "benchmark" thrusters which have an anode lip protruding into the flow. They have, however, quantitatively described flows in straight channel coaxial thrusters as well as thrusters with the diverging King anode[8,9, 13]. More recent comparisons between this quasi one-dimensional model and experimental results at Princeton on the Half-Scale Flared Anode Thruster (HSFAT) show excellent agreement as can be seen from Fig. 8[16]. This suggests that quasi on-dimensional models may serve as very useful tools for design and optimization.

III. More Theories of Onset

The phenomenon of "onset" has attracted a great deal of experimental and theoretical interest. Several theoretical explanations of onset have been advanced and more than one have experimental evidence to support them. It may be possible that onset does not represent a single phenomenon but several phenomena which all occur at high current levels. The back-EMF theory of onset was discussed above because it is an integral part of quasi-one-dimensional MPD flow theory. Some of the other theories of onset will be discussed here.

Several theories focus on plasma conditions near the anode. Specifically, consider a plasma with electron density n_e and mean thermal speed $C_e=(8kT_e/m_e\pi)^{1/2}$. The random thermal current density is $j_{thermal}=en_eC_e/4$. If the net current density between the plasma and the anode is less than $j_{thermal}$, an anode sheath forms with a potential that discourages the flow of electrons to the anode. This potential is a negative voltage drop and is observed most of the time during low current operation of MPD thrusters. For high current operation, several effects combine to change this condition. First, for high current operation the current density is simply higher. Secondly, at high current, the flow is accelerated to higher speeds and hence lower densities. Thirdly, at higher currents, the Hall effect becomes stronger and this tends to drive the plasma from the anode towards the thruster centerline. These latter two effects tend to reduce the random thermal current density, $j_{thermal}$. At sufficiently high current, the required net current density may exceed the random thermal current. Under this condition, the anode sheath voltage drop is expected to change signs and become positive in order to help draw more current. This effect is sometimes called anode mass starvation.

This change in sign of the anode sheath voltage drop was analyzed by Bakshi, Moizhes, and Rybakov in 1974 using a simple quasi-one-dimensional model[17]. They took this change in sign as their onset criterion. Several refinements to this model have been made by Heimerdinger[18]. Korsun considered a similar mass starvation effect in a two dimensional model[19]. Hugel measured the anode sheath voltage drop in a thruster and found that onset was associated with the change in sign[20].

The reason why a change in sign of the anode sheath should cause onset was not clear because many discharges operate in a stable steady state with anode sheaths of both signs. Two hypotheses exist to explain this. Kuriki and Onishi suggest that when the anode fall is positive, ions accelerated in the sheath may produce sputtering[21]. Alternatively, Shubin found that anode mass starvation is associated not just with anode sheath reversal but also with plasma instabilities[22]. He suggested that these instabilities may cause onset.

If onset were solely due to anode mass starvation, the experimental remedy would be clear: inject more mass near the anode. This in fact was done as part of a very detailed set of onset experiments performed by Barnett[23]. He found that, under some conditions, onset was associated with instabilities near the anode. However, he also found that injecting mass near the anode did not prevent the occurrence of onset. Rather, onset still occurred but was associated with instabilities in other regions of the thruster. He found that, by controlling mass injection, he could cause the region of instability to move around the thruster from anode to cathode. This appears to indicate that, while anode mass starvation may be one onset mechanism, it is certainly not the only onset mechanism.

IV. Electrode and Boundary Layer Models

A key issue in MPD thruster research has been the electrode erosion rates and mechanisms. Between the bulk plasma flow and the wall, there is a fluid mechanical boundary layer and an electrostatic boundary layer (sheath). These layers govern the plasma-electrode interactions.

Between the bulk plasma flow and the electrodes, there are thermal, viscous, and electrostatic boundary layers. Modeling of these layers is very important to both thruster performance and life. They affect performance because they determine the viscous drag. They affect life because they determine plasma conditions adjacent to the electrodes and hence influence electrode operating temperatures and heat fluxes.

In the boundary layer, the flow speed changes from the free stream value to a small value just above the electrode surface. Several other plasma properties also change, including ionization fraction, heavy particle temperature, and plasma density. Not all these properties change monotonically. Compressible boundary layer theory for single-temperature fluids has been summarized by Schlichting[24].

It is only recently that a quantitative model of the MPD boundary layer has become available[25]. This boundary layer analysis, the first such for an MPD thruster showed the important effects of ionization fraction on viscosity, and hence on boundary layer growth. The following expression for viscosity can be derived from kinetic theory[25]:

$$\eta_H = m_A C_H \left(\frac{\alpha}{\alpha Q_i + (1-\alpha) Q_A} + \frac{1-\alpha}{(1-\alpha) Q_{AA} + \alpha Q_A} \right) \qquad (16)$$

where C_H is the mean thermal speed of the heavy particles, α is the ionization fraction, Q_A is the total momentum transfer cross section for ion-neutral collisions, Q_{AA} is the total momentum transfer cross section for neutral-neutral collisions, and Q_{ii} is the total momentum transfer cross section for ion-ion collisions. In the core flow, i.e. away from the walls, the plasma is nearly fully ionized so that α is near 1. In this region, the momentum transfer is determined primarily the ion-ion collisions, as can be seen from equation (16) by setting $\alpha \sim 1$. However, as one moves radially toward the walls and away from the core flow, the gas becomes less ionized. This is because of wall-driven recombination reducing the number density of charged particles. In these wall-adjacent regions, the electron temperature tends to remain fairly constant, while the heavy particle (ions and neutrals) temperature decreases from the core flow value down to very nearly the wall or electrode temperature. The decrease in ionization fraction as one approaches the walls causes the viscosity to be determined by the ion-neutral total momentum transfer cross section (which is typically several orders of magnitude smaller than Q_{ii}. Thus, the viscosity changes by orders of magnitude going from the core to the walls. If the ionization fraction in the near-wall regions drops much below ~0.05, then Q_{AA} dominates the viscosity. Since MPD flows are less than fully ionized over much of the channel length, they are also viscous.

V. Steady-State MPD Operation

It is important to understand erosion and lifetime issues in MPD thrusters. Because of the high power required, most laboratory experiments on MPD thrusters have involved operation for only a few milliseconds. In space, by contrast, it is likely that MPD thrusters will be operated in steady-state. The erosion and lifetime issues are very different between these two modes.

When operated for a few milliseconds, the plasma flow has time to reach steady-state. The electrodes, however, do not have time to reach thermal steady-state. As a consequence, the erosion mechanism in pulsed ("quasi-steady") operation and steady-state operation are very different.

For the cold electrodes of quasi-steady operation, it is experimentally observed that, at high current levels, visible hot spots form on the electrode surfaces. These hot spots can be explained as thermal instabilities of the plasma-electrode interaction. Theories have recently been developed to describe these effects[26-28]. The nature of these instabilities differs between the cathode and anode.

For the long life demanded of space-worthy equipment, the erosion rates of spot-mode current conduction, >1μg/C, are generally unacceptable. On hot cathodes, current can be emitted thermionically. This enables erosion rates to drop down to the order of 1 ng/C[29].

An important issue is the stability of diffuse (thermionically) emitting cathodes. Two recent papers have analyzed thermal stability limits of diffuse mode operation of cathodes and anodes[26,27]. The limits have been found to be very different for the two. Both stability limits involve thermionic emission and sheath theory.

On anodes, it is found that areas of low current density are generally stable. In regions of high current density, a runaway heating of the electrode can occur. The runaway is driven by thermionic emission. While thermionic emission is undesirable on an anode, it happens unavoidably at the high temperatures (e.g. 3000K) of steady-state operation. While thermionic emission cools the anode, it has another indirect effect. The more thermionic emission that there is, the more plasma current that must be drawn to the electrode. The net effect is heating since the plasma electrons are much hotter (e.g. 10,000K) than the anode. The result of heating the anode is still more thermionic emission and then still more heating. The anode spots observed in the high current regions of steady-state thrusters may be evidence for this mechanism.

On cathodes, thermionic emission is essential for diffuse mode operation. This emission must be adequate to conduct the electricty in the high current density regions, such as the tip of the cathode. Since the mid-section of the cathode is usually nearly as hot as the tip (or possibly more so), it also has thermionic emission. Its emission, however, becomes excessive as onset is approached. Near onset, the current density in the middle of the thruster drops rapidly due to an increasing back-EMF. The result is that plasma electrons must enter the cathode to replace the electrons emitted thermionically. This again leads to a thermal runaway effect.

The recent theories that have been developed for cathodes and anodes operating at steady state predict several effects that may be observable in constant cross sectional area geometries. First, at high total currents, current densities are highest near the inlet and exit regions while being smallest in the middle region due to high back-EMF. Second, thermal runaway destabilizes the diffuse mode operation at high current densities at the anode. The same mechanism destabilizes the diffuse mode at the cathode at low current densities. This means that portions of the anode near the exit, and portions of the cathode near the middle are particularly susceptible to melting. Recent steady state experiments on straight coaxial thrusters at Stuttgart appear to corroborate this prediction[28].

VI. Summary

This review article has discussed recent developments in the theoretical understanding of self-field MPD thrusters. The focus has been primarily on one-dimensional, quasi one-dimensional, and partially two-dimensional models. Ongoing efforts in two and three dimensional simulations of steady MPD flow[30-32] are likely to extend our present understanding of MPD flow dynamics and behavior. Electrode processes are also begining to be understood, and when fully coupled with flow models, should provide valuable insight in the design of experiments and interpretation of experimental results.

References

(1) R. G. Jahn, *Physics of Electric Propulsion*, McGraw-Hill Book Company, New York, 1968.

(2) R. M. Myers, M. A. Mantenieks, M. L. LaPointe, "MPD Thruster Technology", paper AIAA-91-3568, September 1991.

(3) E. L. Resler, Jr., and W. R. Sears, "The Prospects for Magneto-Aerodynamics", *Journal of the Aeronautical Sciences*, pp. 235-245, April 1958.

(4) E. L. Resler, Jr., and W. R. Sears, "Magneto-Gasdynamic Channel FLow", *ZAMP*, Vol. IXb, pp. 509-519, 1958.

(5) G. W. Sutton, and A. Sherman, *Engineering Magnetohydrodynamics*, McGraw-Hill, New York, 1965.

(6) W. F. Hughes, and F. J. Young, *The Electrodynamics of Fluids*, John Wiley & Sons, Inc., New York, 1966.

(7) G. H. C. Martinache, "A Theory on a Parallel Plate Accelerator", Ph.D. Dissertation, Princeton University, Princeton, New Jersey, 1971.

(8) D. Q. King, K. E. Clark, and R. G. Jahn, "Effect of Choked Flow on Terminal Characteristics of MPD Thrusters", paper AIAA-81-0686, April 1981.

(9) D. Q. King, *Magnetoplasmadynamic Channel Flow for Design of Coaxial MPD Thrusters*, Ph.D. Dissertation, Princeton University, Princeton, New Jersey, December 1981.

(10) A. H. Shapiro, *The Dynamics and Thermodynamics of Compressible Fluid Flow*, Ronald Press, New York, 1953.

(11) Z. Bilicki, C. Dafermos, J. Kestin, G. Majda, and D. L. Zeng, "Trajectories and Singular Points in Steady State Models of Two-Phase Flows", *Int. J. Multiphase Flow*, Vol. 13, No. 4, pp. 511-533, 1987.

(12) J. L. Lawless, and V. V. Subramaniam, "Theory of Onset in Magnetoplasmadynamic Thrusters", *J. Propulsion & Power*, Vol. 3, pp. 121-127, March-April 1987.

(13) V. V. Subramaniam, and J. L. Lawless, "Onset in Magnetoplasmadynamic Thrusters with Finite Rate Ionization", *J. Propulsion & Power*, Vol. 4, No. 6, pp. 526-532, November-December 1988.

(14) E. Richley, *A Computational Methodology for Modelling Non-Equilibrium Phenomena in High Pressure Electric Arcs*, Ph.D. Dissertation, Carnegie-Mellon University, Pittsburgh, May 1984.

(15) T. Shoji, and I. Kimura, "Analytical Study on the Influence of Nonequilibrium Ionization for Current Flow Pattern and Flow Field of MPD Arcjets", paper AIAA-90-2609, July 1990.

(16) G. Lefever-Button, and V. V. Subramaniam, "Quasi One-Dimensional MPD Flows", paper IEPC-91-061, October 1991.

(17) F. G. Baksht, B. Ya. Moizhes, and A. B. Rybakov, "Critical Regime of a Plasma Accelerator", *Sov. Phys. Tech. Phys.*, Vol. 18, No. 12, pp. 1613-1616, 1974.

(18) D. J. Heimerdinger, "An Approximate Two-Dimensional Analysis of an MPD Thruster", M.S. Thesis, Massachusetts Institute of Technology, June 1984.

(19) A. G. Korsun, "Current Limiting by Self-Magnetic Field in a Plasma Accelerator", *Sov. Phys. Tech. Phys.*, Vol. 19, No. 1, pp. 124-126, 1974.

(20) H. Hugel, "Effect of Self-Magnetic Forces on the Anode Mechanism of a High Current Discharge", *IEEE Trans. Plasma Sci.*, Vol. PS-8, No. 4, pp. 437-442, 1980.

(21) K. Kuriki, and M. Onishi, "Thrust Measurement of KIII MPD Arcjet", *AIAA J.*, Vol. 20, pp. 1414-1419, 1982.

(22) A. P. Shubin, "Dynamic Nature of Critical Regimes in Steady-State High-Current Plasma Accelerators", *Sov. J. Plasma Phys.*, Vol. 2, No. 1, pp. 18-21, 1976.

(23) J. Barnett, *Operation of the MPD Thruster with Stepped Current Input*, Ph. D. Dissertation, Princeton University, Princeton, New Jersey, 1985.

(24) H. Schlichting, *Boundary-Layer Theory*, McGraw-Hill, New York, 1968.

(25) V. V. Subramaniam, and J. L. Lawless, "Electrode-Adjacent Boundary Layer Flow in Magnetoplasmadynamic Thrusters", *Phys. Fluids*, 3 1 (1), pp. 201-209, January 1988.

(26) V. V. Subramaniam, and J. L. Lawless, "Thermal Instabilities of the Anode in an MPD Thruster", *J. Propulsion & Power*, Vol. 6, No. 2, pp. 221-224, March-April 1990.

(27) V. V. Subramaniam, K. S. Hoyer, and J. L. Lawless, "Limits on Steady Diffuse Mode Operation of the Cathode in MPD Thrusters", *J. Propulsion & Power*, Vol. 7, No. 4, July-August 1991.

(28) V. V. Subramaniam, "Onset and Erosion in Self-Field MPD Thrusters", paper IEPC-91-021, October 1991.

(29) M. Auweter-Kurtz, B. Glocker, H. L. Kurtz, O. Loesener, H. O. Schrade, N. Tubanos, T. Wegmann, D. Willer, and J. E. Polk, "Cathode Phenomena in Plasma Thrusters", paper AIAAA-90-2662, July 1990.

(30) M. Auweter-Kurtz, H. L. Kurtz, H. O Schrade, and P. C. Sleziona, "Numerical Modeling of the Flow Discharge In MPD Thrusters", paper AIAA-87-1091, May 1987.

(31) M. R. LaPointe, "Numerical Simulation of Self-Field MPD Thrusters", paper AIAA-91-2341, August1991.

(32) V. Babu, Department of Mechanical Engineering, The Ohio State University, Columbus, Ohio, private communication, September 18, 1991.

Mass: $\rho u = F = constant$

Momentum: $P+Fu+\frac{B^2}{2\mu_0} = constant$

Energy: $Fh+\frac{Fu^2}{2}+\frac{EB}{\mu_0} = constant$

State: $h = h(P,\rho)$

Ohm's Law: $j = \sigma(E-uB)$

Ampere's Law: $\frac{dB}{dx} = \mu_0 j$

Table I. Equations of motion for a *self-field one-temperature* quasi-one-dimensional MPD flow.

Phenomena	Effect on Mach number in subsonic flow	Effect on Mach number in supersonic flow
Ohmic heating	increases	decreases
Accelerating body force	decreases	increases
Friction	increases	decreases
Wall cooling	decreases	increases
Endothermic reactions	decreases	increases

Table II: Various phenomena cause the flow Mach number to change toward or away from 1.

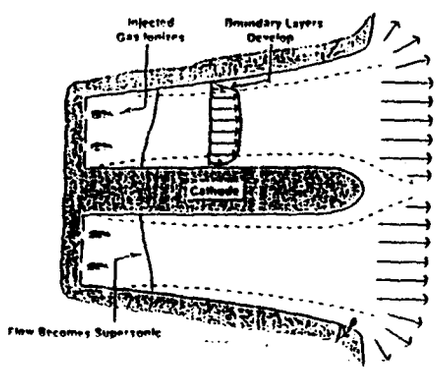

Fig. 1: Sample configuration for a self-field MPD thruster.

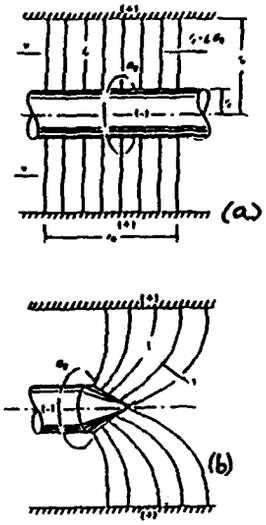

Fig. 2: Idealized models with (a) uniform radial current, and (b) current into conical section, from ref.[1].

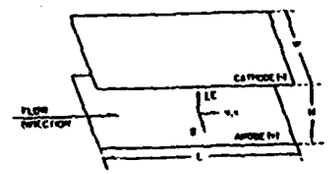

Fig. 3: One-dimensional thruster geometry.

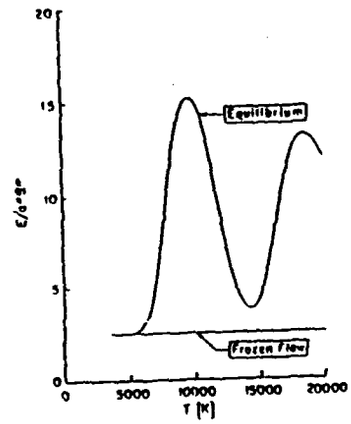

Fig. 4: The electric field determined by the magnetogasdynamic choking condition, *is plotted here against* the temperature at the choking point, for the two cases of equilibrium and frozen flow (from ref.[12]).

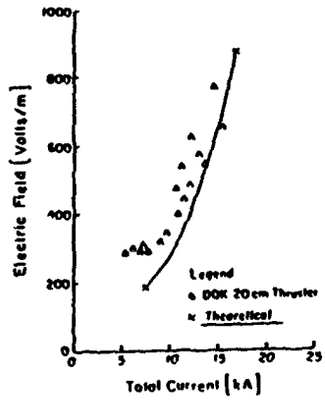

Fig. 5: Electric field versus total current, for a total mass flow of 3 g/s. The uppermost point on the solid curve is the theoretical Onset limit (from ref.[13]).

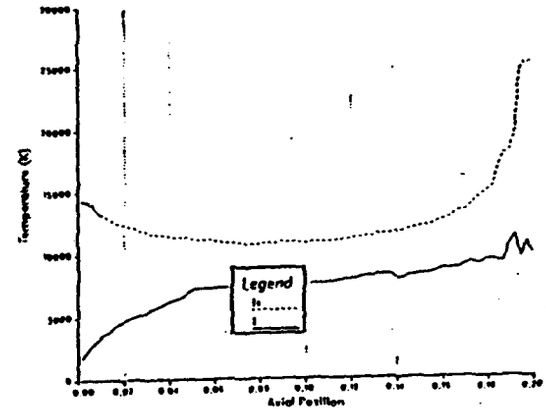

Fig. 7: Heavy particle and electron temperatures in a 20 cm. long MPD thruster, from ref.[14].

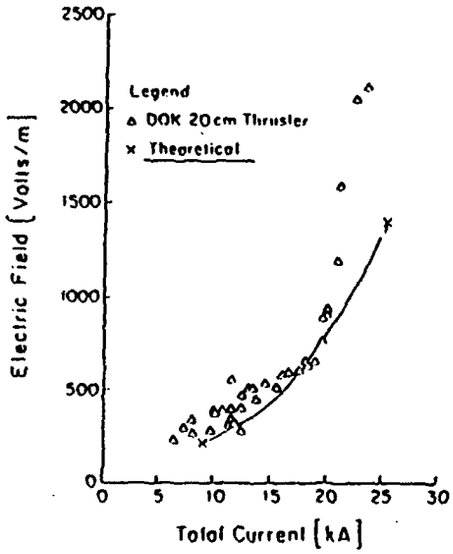

Fig. 6: Electric field versus total current, for a total mass flow of 6 g/s. The uppermost point on the solid curve is the theoretical Onset limit (from ref.[13]).

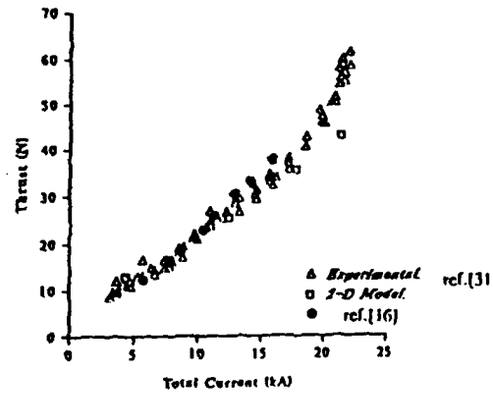

Fig. 8: Comparison of thrust versus total current between quasi one-dimensional model, two-dimensional axisymmetric model, and experimental measurements for the HSFAT thruster (from ref.[16]).

Appendix C

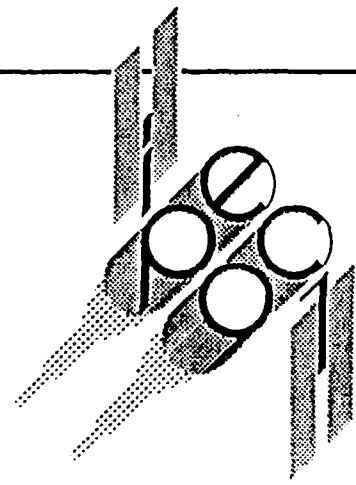

IEPC-91-021

Onset and Erosion in Self-Field MPD Thrusters

V. V. Subramaniam
Department of Mechanical Engineering
The Ohio State University
Columbus, Ohio 43210
U.S.A.

AIDAA/AIAA/DGLR/JSASS 22nd International Electric Propulsion Conference

October 14-17, 1991 / Viareggio, Italy

Onset and Erosion in Self-Field MPD Thrusters

V. V. Subramaniam'
Department of Mechanical Engineering
The Ohio State University
Columbus, Ohio 43210
U.S.A.

Abstract

A method is outlined for the determination of cathode temperatures and hence, evaporative erosion rates using the simplest level of coupling between the electrode and flowing MPD plasma. Given the mass flow rate, total current, and geometry, a previously developed quasi one-dimensional model is used to generate profiles of all relevant quantities in the axial direction. These are then used as boundary conditions for a boundary layer model, which in turn generates the necessary boundary conditions for the electrode-adjacent sheath and electrode thermal analysis. The steady state heat conduction equation is then solved numerically to estimate cathode temperatures. The coupling between the flowing plasma and the electrode is modelled via the boundary conditions so that solutions are tractable. A simple version of this technique is then used to compare model predictions with experimental observations of cathodes in steady state MPD thrusters operating at high current levels. The model correctly predicts the observed damage to the ZT-1 and DT-2 thrusters, and shows the inter-relations between back-EMF onset, erosion, and terminal voltage oscillations.

Nomenclature

a	Speed of sound
B	Magnetic induction
C	Mean thermal speed
e	electronic charge
H	Channel height
j	Net current density
J	Total current
k	Boltzmann's constant
k_c	Thermal conductivity of cathode material
L	Thruster length
m_A	Atomic mass
q	Heat flux
q_{end}	Heat flux at cathode tip
q_{base}	Heat flux at base
$q_{surface}$	Heat flux at the cathode surface
S	Magnetic force number
T	Temperature
u	Velocity
W	Channel width
x	Coordinate along cathode length
α	Ionization fraction
η	Viscosity of heavy particles
μ	Permeability of free space
ρ	Mass density
σ	Electrical Conductivity
*	Superscript indicating evaluation at the sonic point
i	Subscript denoting inlet value

I. Introduction:

The behavior of self-field MPD thrusters at high values of total current for a given propellant mass flow rate and thruster geometry, has been a subject of considerable interest. Particularly, the phenomenon encountered at high currents known as Onset has received much attention due to its significant influence on the performance of these devices. Onset is a term used to denote collectively, increased erosion of thruster components and terminal voltage oscillations that are seen to occur during operation at high current levels[1,2]. The focus of this paper is to show that the conditions leading to voltage oscillations and electrode erosion are indeed linked, and to provide

'Assistant Professor; Member, AIAA.

a basis for quantitative prediction of erosion rates at and below the Onset limit.

Several theories have been successful at predicting an Onset limit[3-6]. Schrade et. al. have attempted further to explain the increased erosion observed at Onset[4]. They have analyzed the behavior and stability limits of a single current carrying channel, and have predicted the critical current at which such a channel becomes unstable subsequently forming other neighboring spots (molten, concentrated regions of high current density on an electrode). Although the erosion rate from a single spot can be predicted with such a model, generalization to an overall erosion rate from an electrode surface is an insurmountable task.

Recently, it has been shown that cathode and anode behavior are strongly controlled by a combination of variables, notably the local current and number densities[7,8]. A thermal runaway mechanism triggered by bombardment of energetic plasma *electrons* shown to operate at the cathode in regions where the local current density was low and the local number density was high[8]. The same mechanism was shown to be operative at the anode as well, but in regions of high current density and low number density[7]. In this paper, it is shown that these conditions are consistent with the Back-EMF theory of Onset, and that this theory is capable of explaining oscillations as well as increased erosion at Onset. Also, a methodology is outlined whereby evaporative erosion rates can be predicted purely as a function of the global parameters such as total mass flow rate, total thruster current, and thruster geometry. Such an approach is deemed a useful tool to the designer.

This paper is organized as follows. The Back-EMF Onset theory is reviewed first in the following section, followed by a detailed discussion of a simple model that couples the MPD plasma flow and electrode processes. The numerical results from this model are presented, followed by a discussion of the relationship between Back-EMF Onset and erosion, and Back-EMF Onset and oscillations, respectively. Finally, the findings of the present study are summarized and conclusions drawn.

II. Back-EMF Onset Revisited:

The idea of a high Back-EMF being responsible for Onset phenomena was first discussed within the context of a one-dimensional, steady state, frozen, fully ionized flow[6]. Although restrictive in its assumptions, this simple model revealed several important facts. First, MPD flow was parametrized by the Magnetic Force Number $S^* = B^{*2}/\mu_0 F a^*$, where the superscript * denotes quantities evaluated at the magnetogasdynamic sonic or choking point. Second, there was shown to be an upper limit on S^* for sustaining supersonic flow in the thruster. Finally, S^* was shown to be related to the Onset parameter J_c^2/m, utilized by experimentalists to describe Onset. A limit on S^* thus translated to a limit on J_c^2/m, and this limit was derived to be:

$$\frac{J_c^2}{\dot{m}} \leq 8.52 \frac{W}{H} \frac{a^*}{\mu_0 \kappa^2} \qquad (1)$$

Equation (1) showed excellent agreement with the data of Malliaris et. al. on quasi-steady MPD thrusters[1]. The measured dependence of J_c^2/m on the propellant atomic mass as well as on the thruster geometry are correctly predicted by (1)[6]. Subsequently, the assumption of frozen, fully ionized flow was removed[9]. This meant that closed form analytical solutions could not be obtained for MPD channel flow. However, numerical solutions of the governing equations showed an upper limit on S^* analogous to that given by equation (1). This upper limit was interpreted to be the Onset limit, and showed agreement with the experimentally measured Onset limits in quasi-steady, straight coaxial thrusters[10]. Physically, Back-EMF Onset is caused by a conflict between the electric field necessary to draw all the applied current (as per Ohm's law)

and that amount of the electric field necessary to sustain supersonic flow in the thruster (as dictated by the magnetogasdynamic sonic or choking condition). Both constraints on E could be met at low currents, but beyond a critical value of the current (or S*), both requirements could not be simultaneously satisfied at steady state. For a more recent discussion of this theory, see ref.[11].

Although this Back-EMF theory can quite satisfactorily predict the limits of steady operation of self-field thrusters, electrode phenomena must be included to study erosion processes in select regions of the thruster. This is because electrode processes together with the plasma-electrode interactions influence erosion. It is to these that we now focus our attention.

III. A Simple Model:

The structure of MPD flow has been examined previously within the context of a one-temperature core flow, with a two-temperature boundary layer, including finite-rate ionization and recombination[12]. These models have revealed that the MPD flow is highly viscous with entry lengths on the order of a few centimeters[12]. The primary reason for this high viscosity is due to the effects of decreasing ionization fraction on the viscosity[12]:

As one proceeds from the flow centerline toward the electrodes (walls), the ionization fraction and charged particle number density drop due to wall-driven recombination. The consequences of this can be seen from equation (2) when α varies from a number near 1 towards a value near 0. The dominant cross section for momentum transfer changes from that due to Coulomb interactions in the core flow, to that due to ion-neutral collisions in the boundary layer. Since these two cross sections typically differ by orders of magnitude, the viscosity gains increasing importance in the near-wall regions of the flow[12]. It must be pointed out that several authors have earlier[13,14] and more recently[15] included two-temperature effects, but primarily in the axial direction. This has an effect on the boundary layer but is relatively weak when compared to the effect of changing α, since η_H varies as the square root of T_H and thus the boundary layer thickness then only varies as $T_H^{1/4}$.

With electrode phenomena in mind, let us now consider the following model. Under the assumption of axisymmetry, the steady state temperature distribution in the cathode satisfies the heat conduction equation, which in polar coordinates is:

$$\frac{1}{r}\frac{\partial}{\partial r}\left(r k_c \frac{\partial T}{\partial r}\right) + \frac{\partial^2}{\partial x^2}(k_c T) + \frac{j^2}{\sigma} = 0 \qquad (3)$$

where j is the current density through the cathode, σ is the electrical conductivity, and k_c is the thermal conductivity. The boundary conditions are:

$$\left.\frac{\partial T}{\partial r}\right|_{r=0} = 0 \qquad (4)$$

$$-k_c \left.\frac{\partial T}{\partial r}\right|_{r=r_c} = -q_{surface} \qquad (5)$$

$$-k_c \left.\frac{\partial T}{\partial x}\right|_{x=0} = -q_{base} \quad \text{or} \quad T(x=0,r) = T_{base} \qquad (6)$$

$$-k_c \left.\frac{\partial T}{\partial x}\right|_{x=L} = q_{end} \qquad (7)$$

where $q_{surface}$ is taken to be positive when flowing <u>into</u> the surface at $r=r_c$, q_{base} is positive when flowing <u>out</u> of the surface at x=0, and q_{end} is positive when flowing <u>out</u> of the surface at x=L. The condition (4) is a symmetry condition valid only for a solid cathode. Since the centerline, r=0, is a line of symmetry, it is an adiabat. With these considerations, **the maximum temperature should be expected to occur somewhere along the centerline, i.e along r=0.** Because of the Neumann boundary conditions (4) through (7), there is a constraint that must be met in order for a steady state to exist:

$$\int_0^L q_{surface}\, r_c\, dx + \int_0^L \int_0^{r_c} \frac{j^2}{\sigma}\, r\, dr\, dx = \int_0^{r_c} q_{base}\, r\, dr + \int_0^{r_c} q_{end}\, r\, dr \qquad (8)$$

Equation (8) is an overall energy balance on the cathode and states that the heat removed from the cathode base, q_{base}, must satisfy it in order to maintain a steady state.

The surface boundary at $r=r_c$ couples the solid cathode to the adjacent plasma. The surface energy flux consists of ion and electron bombardment, surface electron emission, and radiative energy exchange with the anode. This surface and sheath model has been discussed in a previous paper[8]. $q_{surface}$ is given by:

$$q_{surface}(r=r_c,x,T) = j_i(\epsilon_i + V_c - \phi) + j_e\left(\phi + \frac{2kT_\infty}{e}\right) - j_E\left(\phi + \frac{2kT}{e}\right) - \sigma_{SB}F_{12}\left(T^4 - T_{anode}^4\right) \quad (9)$$

where the cathode sheath voltage drop V_c is determined from overall current conservation[8]. The plasma electron current density j_e is also dependent on V_c and can be a dominant source of heating under MPD conditions[7,8]. As V_c decreases, j_e increases exponentially leading to increased surface heating. The cathode tip is assumed to radiate to cold space, so that:

$$q_{end}(r) = \epsilon\sigma_{SB}T^4(r,x=L) \quad (10)$$

A method can now be outlined to determine cathode surface temperatures. A similar approach can be used to determine anode temperatures as well. As in any design or experimental situation, the total current, propellant mass flow rate, and geometry are assumed to be specified. Given these quantities, a suitable flow model may be used to provide axial profiles of the plasma temperature, ionization fraction, current density, and velocity along the length of the thruster[9,16]. Next, a two-temperature boundary layer model can be used to predict charged particle number densities, current densities, electron and heavy particle temperatures outside the sheath edge[12]. An appropriate sheath model can then be utilized to calculate the ion number densities, electron number densitites, sheath voltage drop, electron temperatures, and heavy particle temperatures along the electrode surface[8]. These provide the necessary information to determine the right hand side of equation (9). The system (3) through (10) is then solved numerically to calculate the temperature profiles within the electrodes as well as on the surface. Knowing the electrode surface temperature, evaporative erosion rates can be determined from vapor pressure data. In this manner, plasma discharge and electrode processes are coupled. It must be pointed out at the outset, that the method just outlined is only and approximate solution procedurefor considering the fully coupled plasma flow and electrode processes. The fully coupled problem is extremely trdious to solve, even numerically.

In the following section, the approximate method just outlined is applied to study the ZT-1 steady state thruster at the University of Stuttgart[17].

IV. Numerical Results

Recently, there have been reports of tests conducted at the University of Stuttgart on steady-state, straight, coaxial, self-field MPD thrusters[17]. The results of these tests showed severe cathode damage in the middle as opposed to the tip (see Figures 1 and 2). It appears that the cathodes melted and exploded from within suggesting that the internal temperatures far exceeded the surface temperatures at this location. The authors of ref. [17] report that they believe the damage to be caused by ohmic heating in selected regions of the thoriated tungsten cathode. However, this phenomenon can and will occur at Onset according to our theory, and is intimately linked to the recently reported thermal runaway mechanism[7,8].

The method discussed in the previous section can be applied to the ZT-1 and DT-2 thrusters used in the Stuttgart experiments. Since specific details were not reported for the DT-2 thruster, we focus on the ZT-1 thruster. This thruster had a cathode approximately 18 cm. long and 1.8 cm diameter. The thruster consisted of a straight constant area channel 15 cm. long, with three segmented anode sections accounting for the latter 9 cm. of the channel length. The argon propellant was introduced at an axial location of 15 cm. before the exit, at a

rate of 2g/s. This thruster according to ref.[17], was operated at steady state up to about 8000 A. This information regarding the geometry, propellant mass flow rate, and total current, provides enough information to obtain electrode temperature distributions using the method of section III. An additional simplification is made here. The boundary layer analysis is omitted so that the core flow quasi one-dimensional axial profiles are directly applied as boundary conditions to the electrode thermal analysis.

Given the total current, channel geometry, and propellant mass flow rate, the governing equations of quasi one-dimensional MPD flow including ionization and recombination, are solved using a method previously reported[9]. This analysis yields profiles of all the relevant quantities. Figures 3 - 8 show the profiles of B, u, T, α, the back-EMF uB, and j as a function of distance for the supersonic section (approximately latter 12 cm.) of the channel. These have been computed for a total current of 8030 A, and mass flow of 2 g/s. These profiles then provide the necessary boundary conditions for solving the system of equations (3) through (10), for the cathode temperature distributions. Computations using the method outlined in section III were carried out on a 10x10 uniform grid. Finer grids (50x50 and 100x100) resulted in quantitatively different temperatures, but trends were identical. Furthermore, the significant results obtained (see Fig. 9) were independent of the grid size. As can be seen from Fig. 9, the maximum temperature occurs in the middle of the thruster and not at the cathode tip. Also, the internal temperatures are higher than the surface temperatures, due to significant Joule heating. The surface, once molten due to the thermal runaway caused by excessive electron bombardment[7,8], evaporates. The interior of the cathode, on the other hand once molten continues to change phase and build up pressure within the material. This explains the observed damage to the ZT-1 and DT-2 Stuttgart thrusters.

V. Back-EMF Onset and Erosion

Let us review the phenomena occuring as the total current is increased for a fixed mass flow rate, and a given geometry:

(1) The back-EMF climbs from a small value at the inlet, reaches a maximum somewhere in the middle of the channel, and then decreases toward the exit (see Fig. 7).

(2) This causes the net current density to reach a minimum in the middle of the channel, while being large near exit region (see Fig. 8).

(3) Earlier cathode and anode sheath theories [7,8] have shown that the diffuse mode behavior becomes unstable (possibly transitioning into the spot mode) at the *cathode* at *low current densities* , and at the *anode* at *high current densities.*

Thus, the center of the cathode and the exit regions of the anode are prime candidates for regions of significant erosion.

VI. Back-EMF Onset and Voltage Oscillations

It can be shown from current conservation, that the sheath voltage drop follows the same trend as the net current density[8]. The regions of low current density at the cathode then have small sheath voltage drops, thereby making the thermal runaway more likely. However, the exit region of the cathode has higher sheath voltage drops. It is therefore clear, that as the total current is increased, the sheath voltage drop in the middle of the cathode continuously decreases, while the sheath voltage drops near the exit region increases. When the sheath voltage drop reaches a value comparable with the energy of the first excited state of the propellant atoms, the electron energy distribution function is modified near the electrode. Two principal groups of electrons then result. These are the "low" energy plasma electrons, and the energetic

electrons emitted by the electrode and which are accelerated through the cathode sheath. Interaction between these two groups of electrons can then lead electric field or voltage oscillations arising from the well known beam instability[18].

VII. Summary

A method has been outlined that allows determination of the MPD flow structure and electrode temperature distributions, given the global parameters, mass flow rate, Total current, and geometry. This theory extends previous work on back-EMF Onset, to include erosion. The general predictions of this theory appear to be in agreement with experimental onservations at Stuttgart[17].

Acknowledgements

This work was supported by AFOSR-87-0360.

References

[1] A. C. Malliaris, R. R. John, R. L. Garrison, and D. R. Libby, "Performance of Quasi-Steady MPD Thrusters at High Powers", *AIAA J.*, Vol. 10, No. 2, February 1972.

[2] J. D. Barnett, *Operation of the MPD Thruster with Stepped Current Input*, Ph.D. Dissertation, Princeton University, 1985.

[3] F. G. Baksht, B. Ya. Moizhes, and A. B. Rybakov, "Critical Regime of a Plasma Accelerator", *Sov. Phys. Tech. Phys.*, Vol. 18, No. 12, pp. 1613-1616, 1974.

[4] H. O. Schrade, M. Auweter-Kurtz, and H. L. Kurtz, "Stability Problems in Magnetoplasmadynamic Arc Thrusters", AIAA 18th Fluid Dynamics and Plasmadynamics and Lasers Conference, Cincinnati, Ohio, 1985.

[5] H. Hugel, "Effect of Self-Magnetic Forces on the Anode Mechanism of a High Current Discharge", *IEEE Trans. Plasma Sci.*, Vol. PS-8, No. 4, pp. 437-442, 1980.

[6] J. L. Lawless, and V. V. Subramaniam, "Theory of Onset in Magnetoplasmadynamic Thrusters", *J. Propulsion & Power*, Vol. 3, pp.121-127, March-April 1987.

[7] V. V. Subramaniam, and J. L. Lawless, "Thermal Instabilities of the Anode in an MPD Thruster", *J. Propulsion & Power*, Vol. 6, No. 2, pp. 221-224, March-April 1990.

[8] V. V. Subramaniam, K. S. Hoyer, and J. L. Lawless, "Limits on Steady Diffuse Mode Operation of the Cathode in MPD Thrusters", *J. Propulsion & Power*, Vol. 7, No. 4, July-August 1991.

[9] V. V. Subramaniam, and J. L. Lawless, "Onset in Magnetoplasmadynamic Thrusters with Finite Rate Ionization", *J. Propulsion & Power*, Vol. 4, No. 6, pp. 526-532, November-December 1988.

[10] D. Q. King, *Magnetoplasmadynamic Channel Flow for Design of Coaxial MPD Thrusters*, Ph. D. Dissertation, Princeton University, December 1981.

[11] J. L. Lawless, and V. V. *Subramaniam*, "Review of the Theory of Self-Field MPD Thrusters", paper IEPC-91-019, 22nd International Electric Propulsion Conference, Viareggio, Italy, October 14-17, 1991.

[12] V. V. Subramaniam, and J. L. Lawless, "Electrode-Adjacent Boundary Layer Flow in Magnetoplasmadynamic Thrusters", *Phys. Fluids*, 31 (1), pp. 201-209, January 1988.

[13] T. Shoji, and I. Kimura, "Analytical Study on the Influence of Non-equilibrium Ionization for Current Flow Pattern and Flow Field of MPD Arcjets", paper AIAA-90-2609, Orlando, 1990.

[14] E. Richley, *A Computational Methodology for Modelling Non-Equilibrium Phenomena in High Pressure Electric Arcs*, Ph.D. Dissertation, Carnegie-Mellon University, Pittsburgh, May 1984.

[15] E. Niewood, and M. Martinez-Sanchez, "Quasi One-Dimensional Numerical Simulation of Magnetoplasmadynamic Thrusters", paper AIAA-90-2604, 21st International Electric Propulsion Conference, Orlando, July 1990.

[16]G.Lefever-Button,and V. V. Subramaniam,
"Quasi One-Dimensional MPD Flows", paper IEPC-91-061, 22nd International Electric Propulsion Conference, Viareggio, Italy, October 14-17, 1991.

[17] M. Auweter-Kurtz, B. Glocker, H. L. Kurtz, O. Loesener, H. Schrade, N. Tubanos, T. Wegmann, D. Willer, and J. Polk, "CAthode Phenomena in Plasma Thrusters", paper AIAA-90-2662, 21st International Electric Propulsion Conference, Orlando, July 1990.

[18] A. F. Alexandrov, L. S. Bogdankevich, and A. A. Rukhadse, *Principles of Plasma Electrodynamics*, Springer-Verlag, New York, 1984.

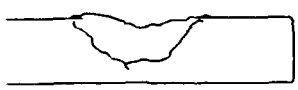

Fig. 1: Schematic of blown cathode from DT-2 thruster. For photograph, see ref.[17].

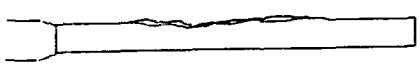

Fig. 2: Schematic of blown cathode from ZT-1 thruster. For photograph, see ref.[17].

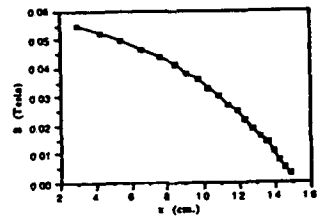

Fig. 3: The calculated values of magnetic induction are shown here versus distance along the cathode, for the ZT-1 thruster.

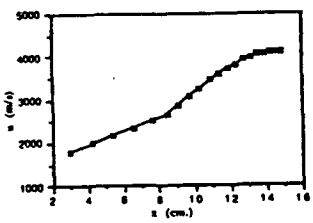

Fig. 4: The calculated values of velocity are shown here versus distance along the cathode, for the ZT-1 thruster.

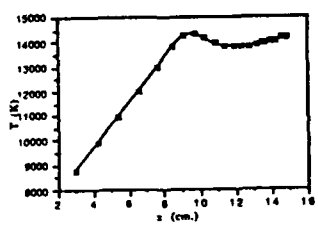

Fig. 5: The calculated values of Temperature are shown here versus distance along the cathode, for the ZT-1 thruster.

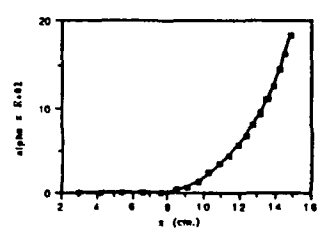

Fig. 6: The calculated values of ionization fraction are shown here versus distance along the cathode, for the ZT-1 thruster.

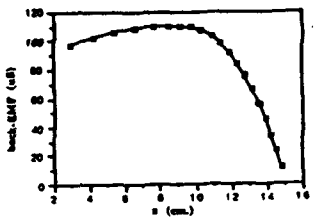

Fig. 7: The calculated values of the back-EMF (uB) are shown here versus distance along the cathode, for the ZT-1 thruster.

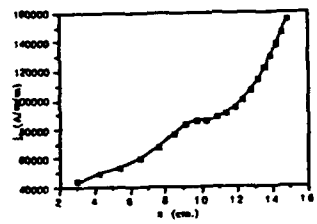

Fig. 8: The calculated values of net current density are shown here versus distance along the cathode, for the ZT-1 thruster.

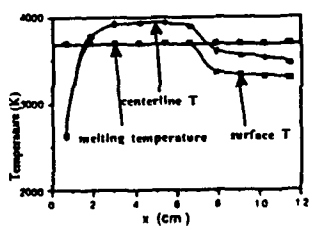

Fig. 9: The calculated centerline and surface temperatures are shown here for the ZT-1 thruster. For reference, the melting temperature of tungsten (3680 K) has been plotted as a horizontal line. Note that the temperatures in the middle region are in excess of the melting temperature, and that centerline temperatures are always larger than the surface temperature.

Appendix D

Limits on Steady Diffuse Mode Operation of the Cathode in Magnetoplasmadynamic Thrusters

V. V. Subramaniam† and K. S. Hoyer*
Ohio State University, Columbus, Ohio 43210
and
J. L. Lawless‡
Space Power, Inc., San Jose, California 95134

Electrode erosion in magnetoplasmadynamic thrusters is significantly dependent on whether the mode of operation is diffuse (i.e., the net current density is distributed over the electrode surface) or via spots. Since spot mode erosion rates are typically much higher than the diffuse mode erosion rates, the latter is more desirable from the standpoint of sustained steady-state operation. In this paper, the steady-state thermal response of the cathode in a magnetoplasmadynamic thruster is analyzed in order to determine the limits of diffuse mode operation. An energy balance at the cathode surface along with current conservation serve to simultaneously determine the surface temperature and the total sheath voltage drop at a given location on the electrode. It is found that two different limits to steady-state diffuse mode operation exist. One limit corresponds to an unsteady thermal runaway caused by excessive *electron bombardment*, in which regenerative heating leads to local melting of the electrode surface. The other limit corresponds to an operating regime where a steady state cannot exist because of increased ion bombardment. In this regime, a small increase in the net plasma current density results in a large sheath voltage drop. This causes an increase in local surface heating through ion bombardment, until a new state is reached, which is inherently unsteady and accompanied by plasma oscillations. These two limits found here may correspond to transitions from diffuse to prespot modes of electrode operation. These operating limits are also found to be influenced strongly by electrode and discharge parameters, as well as by external cooling.

Nomenclature

A = thermionic emission constant
C_e = absolute velocity of an electron
C_{ey} = component of the absolute velocity of an electron in the y direction, i.e., in the direction normal to the surface
E = electric field
E_c = magnitude of the x component of the electric field at the cathode surface
E_w = y component of the electric field at the sheath edge
e = electronic charge
f_e = electron velocity distribution function
h = heat transfer coefficient roughly representing overall heat transfer to an external coolant that is at a temperature T_{cool}
j_E = surface electron emission current density
j_e = current density of plasma electrons
j_i = current density of plasma ions
j_w = net plasma current density at a given axial location
K_t = thermal conductivity of cathode material
k = Boltzmann's constant
L = cathode length
m_e = mass of an electron
m_i = mass of an ion
n_e = electron number density
n_i = ion number density
n_x = charged particle number density at the edge of the collisionless sheath, at a given axial location
Q = net heat per unit area per unit time into the cathode surface, at a given axial location
T = local cathode surface temperature
T_{cool} = temperature of an external coolant
T_x = plasma electron temperature at a given axial location
V = voltage or potential
V_c = value of the voltage at the cathode surface at a given axial location, or the total voltage drop across the sheath
y = coordinate in the direction normal to the cathode surface
ϵ_i = ionization potential of the propellant gas
ϕ = electrode work function

I. Introduction

ELECTRODE erosion is of primary importance for the prediction of lifetimes of magnetoplasmadynamic (MPD) thrusters. Erosion processes depend on a complex coupling between plasma discharge characteristics, plasma-wall interactions, and electrode phenomena. In particular, erosion rates depend on whether the current conduction is through spots, or via a diffuse (distributed) mode. The diffuse mode is characterized by distributed current emission over the electrode surface, surface temperatures well below the material's melting temperature, and non-negligible plasma ion current. By contrast, spots are characterized by locally constricted or filamentary current conduction, surface temperatures at or above the material's melting temperature, and strong temperature-field emission. Spots are detrimental to the electrode material because of their high erosion rates.[1] Therefore, it is important to understand how and under what conditions they may be formed and exactly when diffuse mode behavior ends. Current understanding of this transition from diffuse to spot behavior is, at best, rather poor. In this paper, the steady-state diffuse

Received Oct. 9, 1989; revision received July 9, 1990; accepted for publication July 15, 1990.

*Graduate Student, Department of Mechanical Engineering.
†DuPont Assistant Professor, Department of Mechanical Engineering. Member AIAA.
‡Senior Scientist and Manager of Advanced Concepts. Member AIAA.

mode at the cathode is examined theoretically. Limits on thruster operation in this mode are found, and an explanation for a possible transition to spot formation is given. Additionally, the analysis yields a means of estimating cathode surface temperature, which can be used to predict evaporative erosion rates for the cathode.

Earlier research on cathode processes has focused mainly on spot behavior and spot characteristics.[2-10] Although these works reveal the intricate and complex phenomena occurring in a cathode spot, little or no information is provided as to how spots are formed in the first place. Some authors have attempted to describe transition from diffuse to spot modes. Moizhes and Rybakov[11] have found a negative-slope region in the emission current voltage characteristic, which they attribute to transition to a spot mode. These authors attribute the transition to a thermal instability, whose physical meaning or origin is totally unclear. A thermal runaway mechanism in spots due to a positive feedback between Joule heating and a temperature dependent electrical conductivity has been proposed by Hantzsche.[12] In the same paper, however, the author shows that thermionic emission cools the surface and prevents this thermal runaway. It is important to note that Hantzsche assumes the sheath voltage drop to be constant and given.

By contrast to the cathode, transition at the anode appears to have been studied more extensively.[13-19] These works attribute spot formation to an initial local surface meltdown arising primarily from Joule heating at high current densities. However, another thermal runaway mechanism involving the much ignored sheath exists.[20] In this theory, electron emission from the electrode surface decreases the sheath potential drop, resulting in increased electron bombardment from the plasma. This results in a positive feedback between increased emission and heating due to electron bombardment, causing a thermal runaway. This may occur when the anode sheath voltage difference (defined here as anode potential minus the adjacent plasma potential) is negative and increasing. This thermal runaway mechanism arises before the well-known anode sheath reversal[21] and may explain formation of anode spots. In this paper, the same mechanism is shown to be also operative at the cathode.

A simple model of the cathode surface and its adjacent sheath is discussed in Sec. II. Results for a purely thermionically emitting cathode under a range of conditions corresponding to MPD thruster operation, are given in Sec. III. The physical meanings of the limits on steady-state diffuse mode operation are discussed in Sec. IV, and the effects of field-enhanced and temperature-field emission are discussed in Sec. V. Finally, a summary of this work along with its conclusions are presented in Sec. VI.

II. Simple Model

This section will focus on a thermal model of the cathode surface at steady state. The cathode surface is subjected to both heating and cooling (Fig. 1). Charged particles (i.e., electrons and ions) from the plasma bombard the surface and consequently heat it. The ions (which we will assume to be singly charged) also recombine with electrons at the electrode,

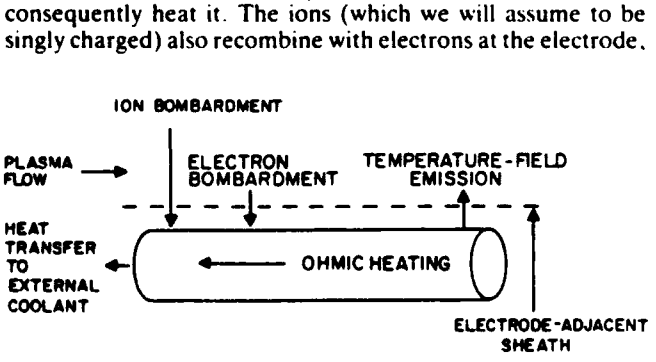

Fig. 1 Cathode along with the various heating and cooling mechanisms.

thereby heating the surface even further. Additional heating due to radiation from the plasma is also present and expected to be important,[22] but will be neglected here. The electrode may also emit electrons, which can result in heating (during field emission) or in cooling (during thermionic emission). During steady-state operation, it is likely that the electrode is cooled externally.[1,23] This is usually done by cooling the cathode at its base. Finally, the cathode surface may radiate away its heat. With these considerations, we may proceed to write the following for the net heat area per unit and per unit time entering the cathode surface:

$$Q = j_e\left[\phi + \frac{2kT_e}{e}\right] + j_i(V_c + \varepsilon_i - \phi) - j_E\left[\phi + \frac{2kT}{e}\right] - h(T - T_{cool}) \tag{1}$$

The quantity $h(T - T_{cool})$ represents a very rough model of the overall cooling, and h can be considered as equivalent to the electrode material thermal conductivity per unit length (i.e., K_t/L). At steady state, Q must be 0 and Eq. (1) determines the surface temperature T. Radiative heat transfer to the anode can be shown to be negligible and is, therefore, ignored here.

Consider next the sheath region immediately adjacent to the electrode surface. This region is typically of the order of tens of Debye lengths. The electron mean free path, however, is orders of magnitude larger.[22] Consequently, the sheath may be treated as a collisionless sheath. The electrons entering the sheath from the plasma are then described by the collisionless steady Boltzmann equation, which in one dimension is

$$C_{e_y}\frac{\partial f_e}{\partial_y} + \frac{eE}{m_e}\frac{\partial f_e}{\partial C_{e_y}} = 0 \tag{2}$$

Using the following transformations,

$$\xi = \frac{m_e C_e^2}{2kT_e} + \frac{eV}{kT_e}, \qquad \eta = y \tag{3}$$

along with $E = -\partial V/\partial y$, yields

$$\frac{\partial f_e}{\partial \eta} = 0, \quad \text{or that} \quad f_e = f_e(\xi) \quad \text{only} \tag{4}$$

With the condition that the electron distribution function be Maxwellian at the sheath edge (where V is taken to be 0), we obtain the following exact solution for the electron distribution function in the sheath:

$$f_e = n_e(m_e/2\pi kT_e)^{1.2}\exp[-m_e C_e^2/2kT_e]. \tag{5}$$

where

$$n_e = n_s \exp[-eV/kT_e] \tag{6}$$

with n_s being the electron number density at the edge of the sheath where V is taken to be 0. The average flux of electrons may then be calculated easily from Eqs. (5) and (6) by integrating f_e over dC_{e_x} and dC_{e_z} from $-\infty$ to ∞, and over dC_{e_y} from 0 to ∞. This flux when evaluated at the wall and multiplied by e gives the electron current density at the wall:

$$j_e = en_s(kT_e/2m_e\pi)^{1.2}\exp[-eV_c/kT_e] \tag{7}$$

where $-V_c$ is the potential of the cathode with respect to the sheath edge (where $V = 0$), and j_e is taken to be positive in the direction away from the cathode.

The ions entering the sheath are assumed to be monoenergetic. The Bohm criterion for a stable monotonic sheath

is, therefore, satisfied.[24] This condition is only slightly altered in the presence of electron emission from the surface.[25] More exact theories that provide the velocity distribution function of the ions entering the sheath from the collisional presheath exist.[26–28] However, for present purposes, the frequently employed monoenergetic assumption simplifies the problem a great deal. We may then write the ion current density at the surface as

$$j_i = en_\infty(kT_\infty/m_i)^{1/2} \tag{8}$$

where j_i is taken to be positive toward the cathode and quasineutrality ($n_i \approx n_e = n_\infty$) is assumed as the sheath edge. The sheath edge is a rather arbitrary definition since no such rigid demarcation exists in reality. When the ions are monoenergetic, the sheath edge has a clear meaning. However, even when the ion distribution function is not monoenergetic, the sheath edge can be defined as the location where the velocity of the ions reaches the value of the Bohm velocity $(kT\infty/m_i)^{1/2}$. In this paper, we will adopt this definition and take the data for the sheath potential at this location (i.e., $V = 0$ at the sheath edge). Now, if the surface emission current density denoted by j_E is taken to be positive toward the surface and the net plasma current density denoted by j_∞ is taken to be positive toward the cathode, we may write overall current conservation at steady state as

$$j_\infty = j_E + j_i - j_e \tag{9}$$

where, in general, j_E is a function of the local surface temperature T and the local electric field at the cathode surface E_c. Determination of E_c is discussed in Sec. V. Equation (9) determines the total cathode sheath voltage drop V_c. Given the parameters n_∞, j_∞, T_∞, ϕ, h, T_{cool} and the surface electric field E_c, Eqs. (1) and (9) represent two simultaneous equations in the two unknowns T and V_c. It must be pointed out that Crawford and Cannara mention overall current conservation in their work.[29] However, their regime of interest was at very low densities (10^{14} m^{-3}), and, hence, ion and electron currents from the plasma were negligible in comparison with the emission current. This is an important difference between their work and the present work.

A simple solution may be found for the case of pure thermionic emission (which is likely for refractory materials), where the surface emission current density depends only on T. For this case, the total sheath voltage drop may be explicitly obtained from Eq. (9):

$$V_c = -\frac{kT_\infty}{e}\ln\left(\frac{j_i + j_E - j_\infty}{j_r}\right) \tag{10}$$

where $j_r = en_\infty(kT_\infty/2\pi m_r)^{1/2}$. Substituting Eq. (10) into Eq. (1) yields the following:

$$Q = \frac{2kj_E}{e}(T_\infty - T) + j_i\left(V_c + \varepsilon_i + \frac{2kT_\infty}{e}\right) - j_\infty\left(\phi + \frac{2kT_\infty}{e}\right) - h(T - T_{cool}) \tag{11}$$

Since at steady state Q must be zero, Eq. (11) represents an implicit equation for the local surface temperature T, where V_c is given by Eq. (10).

An interesting phenomenon is revealed by Eq. (11). The emission current density, which under thermionic conditions results in energy transport away from the cathode, appears as an input heating source. This can be understood upon close examination of Eq. (9) or (10). When the emission current density increases for a fixed plasma number density and plasma current density, the sheath voltage drop must decrease in order to conserve total current. This results in an increase in electron bombardment, which contributes to heating the surface. Thus, although thermionic emission cools the surface, its overall effect is to *heat* the surface via increased electron bombardment. It is, therefore, important to include the effects of the sheath when attempting to determine the surface temperature.

A simple model has been developed in this section, which considers a thermal balance of the cathode surface along with overall current conservation. The local surface temperature and overall sheath voltage drop can be determined from this. Results for a purely thermionically emitting cathode under typical MPD conditions are presented next.

III. Results for Pure Thermionic Emission

The governing equations presented in the preceding section are solved in this section for the case of pure thermionic emission (i.e., no field-enhanced or temperature-field emission). Temperatures and sheath voltage drops are calculated for typical MPD conditions.

For pure thermionic emission, the emission current density is given by

$$j_E = AT^2\exp[-e\phi/kT] \tag{12}$$

The sheath voltage drop V_c can then be written in terms of T using Eq. (10). Given the parameters n_∞, j_∞, T_∞, ϕ, h, and T_{cool}, Eqs. (10–12) may be combined and solved for T. The sheath voltage drop can then be determined from Eq. (10). The emission coefficient may vary considerably for materials with oxide layers. Both A and ϕ may vary locally on a given surface, so that it is important to consider the sensitivity of final results to variations in these parameters. This is addressed later in this section.

A typical variation of the net heat into the cathode Q vs the surface temperature is displayed in Fig. 2. Two intersections with the horizontal axis are found, representing two possible steady-state solutions. The first (lower temperature) is a stable attractor and the second (higher temperature) is an unstable repeller. This can be seen quite easily by perturbing the solutions to either side and determining if the initial state is restored. The physical meaning of the stable point is clear. The incoming energy on the surface is exactly balanced by the outgoing energy. Furthermore, the surface

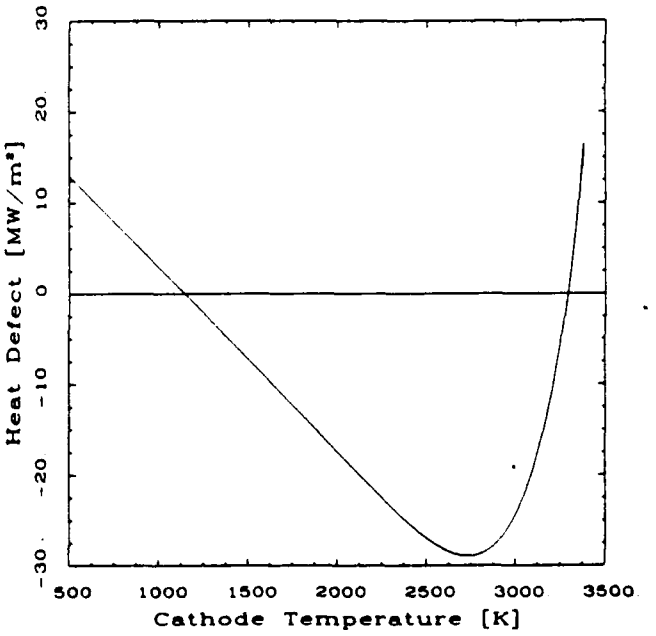

Fig. 2 Typical variation of the net heat per unit area per unit time into the cathode surface vs surface temperature. Variation predicted by Eqs. (10) and (11) in Sec. II.

can maintain this temperature for an indefinite period of time, even for small fluctuations in the discharge. The unstable point requires some explanation. Although an exact balance between incoming and outgoing energy is possible at this point, the surface cannot remain in this state indefinitely and is susceptible to change due to infinitesimal fluctuations. Physically, this state represents an operating regime where the temperature and, hence, the emission current density is high enough to lower the sheath voltage drop below a critical value. This causes excessive heating due to increased electron bombardment, resulting in a temperature rise. The subsequent increase in temperature causes an increase in current emission, which lowers the sheath voltage drop further. This positive feedback process then repeats itself until the surface is regeneratively heated up to the melting temperature. This effect is quantitatively described in Sec. IV.

Results from the present calculation are shown in Figs. 3–6. In these figures, the steady-state surface temperatures calculated from Eq. (11) are shown vs the net plasma current density j_∞, the charged particle number density at the sheath edge n_∞, the electrode work function ϕ, and the temperature of the external coolant T_{cool}. The heat transfer coefficient h is fixed at 20 kW/m²/K, the plasma electron temperature is taken to be 12,000 K, and $A = 3 \times 10^4$ A/m²/K². The value of h is obtained from an estimate of the thermal conductance through a tungsten cathode. All four plots display both the stable (lower temperature) and unstable (higher temperature) regimes. Figures 3 and 4 display the variation of T with j_∞ and n_∞, respectively, for $\phi = 2.63$ V and $T_{cool} = 500$ K. From Fig. 3, it can be seen that, for a given number density, the stable diffuse mode is limited both at low as well as high values of the current density. Similarly, for a given current density, there are lower and upper limits on the range of allowable number densities. At low current densities (n_∞ fixed) and at high number densities (j_∞ fixed), the stable and unstable solutions are seen to merge and disappear. Also, at the higher current densities (n_∞ fixed) and the lower number densities (j_∞ fixed), the stable diffuse operation is limited and only the unstable mode exists. It is interesting to note that, for a given number density, the steady-state, stable surface temperature does not vary significantly with the current density over a wide range (see Fig. 3). This is because in this region the ion current primarily determines the sheath voltage drop, which is then to a very good approximation a constant since the number density is fixed. Heating due to ion bombardment is then balanced by the external cooling. Therefore, inspection of Eq. (11) reveals that the surface temperature should not depend significantly on j_∞ in this region. By contrast, changes in n_∞ at a fixed j_∞ affect the stable operation drastically via increased electron and/or ion bombardment. This is reflected in Fig. 4. The variation of the surface temperatures with electrode work function is shown in Fig. 5 for $T_{cool} = 500$ K, $j_\infty = 10^6$ A/m², and $n_\infty = 8 \times 10^{21}$ m⁻³. The previously discussed stable and unstable regimes are again found to exist. The

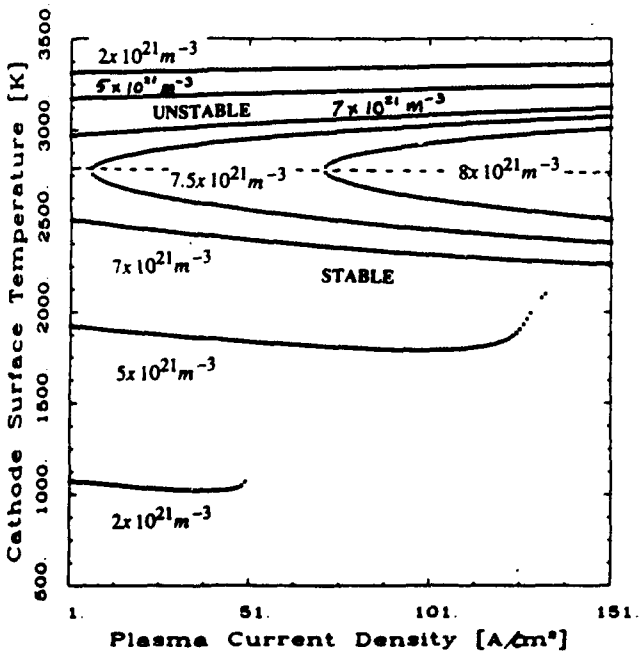

Fig. 3 Steady-state surface temperature as predicted by Eqs. (10) and (11) vs net plasma current density j_∞ for various values of n_∞: h = 20 kW/m²/K; ϕ = 2.63 V; T_{cool} = 500 K; $A = 3 \times 10^4$ A/m²/K²; T_∞ = 12000 K.

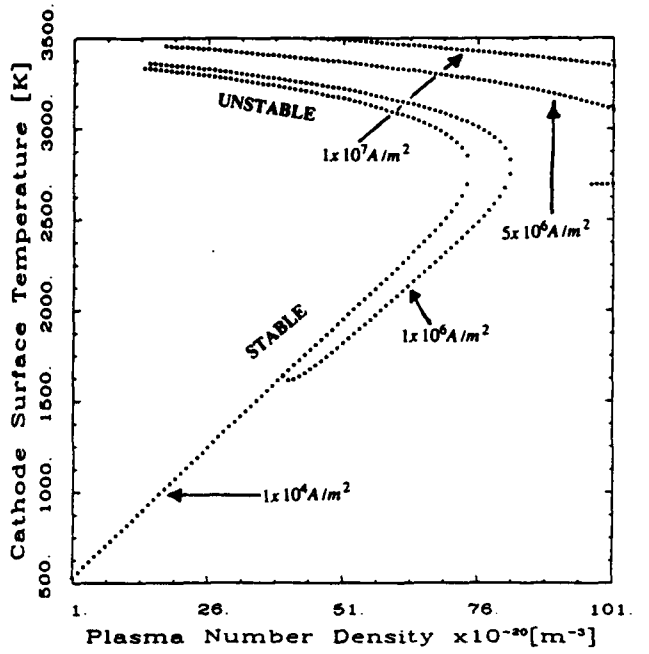

Fig. 4 Steady-state surface temperature as predicted by Eqs. (10) and (11) vs net plasma current density n_∞ for various values of j_∞: h = 20 kW/m²/K; ϕ = 2.63 V; T_{cool} = 500 K; $A = 3 \times 10^4$ A/m²/K²; T_∞ = 12000 K.

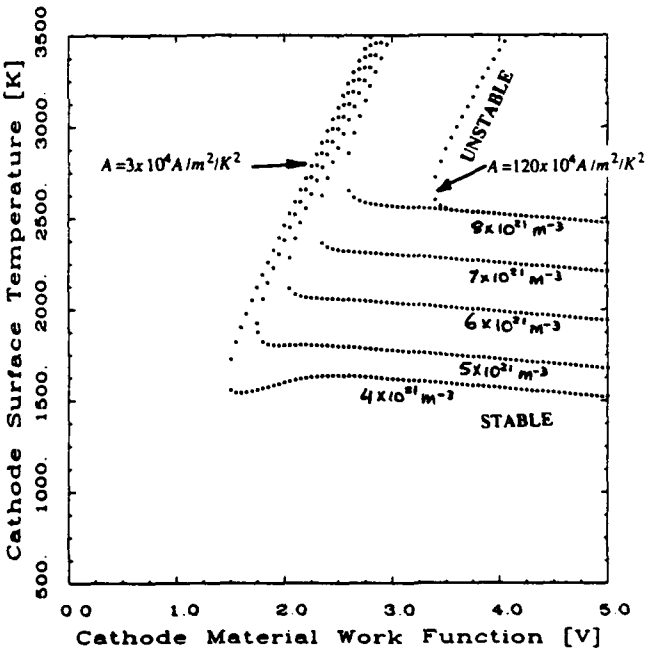

Fig. 5 Steady-state surface temperature as predicted by Eqs. (10) and (11) vs electrode work function for $j_\infty = 10^6$ A/m², $n_\infty = 8 \times 10^{21}$ m⁻³, T_{cool} = 500 K, h = 20 kW/m²/K, and T_∞ = 12000 K.

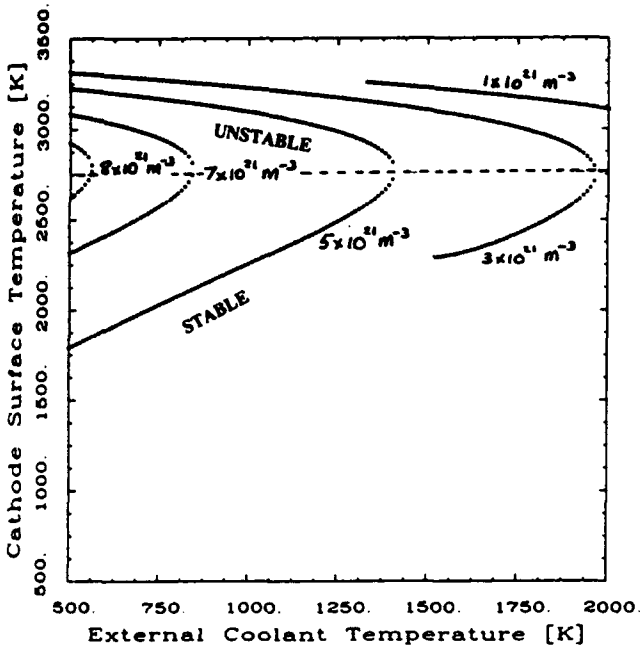

Fig. 6 Steady-state surface temperature as predicted by Eqs. (10) and (11) vs external coolant temperature T_{cool} for ϕ = 2.63 V, j_∞ = 10^6 A/m², h = 20 kW/m²/K, A = 3 × 10^4 A/m²/K², and T_∞ = 12000 K.

stable, steady-state surface temperature is almost invariant with respect to ϕ in this regime, again because the ion current principally determines the sheath drop and ion bombardment dominates. Also shown in this figure is the solution for a different value of the thermionic emission constant (A = 120 × 10^4 A/m²/K²). The effect of a higher value of A is simply to shift the turning point (i.e., the point where stable and unstable solutions merge and then disappear) toward the higher work function side. Otherwise, the stable, steady-state surface temperature is practically the same as for a lower value of A since ion bombardment is still the dominant mechanism. Figure 6 displays the surface temperatures vs the external coolant temperature for ϕ = 2.63 V, j_∞ = 10^6 A/m², n_∞ = 5 × 10^{21} m^{-3}, and h = 20 kW/m²/K. Both stable and unstable regimes are seen to exist and exhibit the features that have just been discussed.

This section has focused on results for a thermionically emitting cathode operating under typical MPD conditions. Stable and unstable regimes as well as limits on steady-state operation have been found. These limits are found to be influenced strongly by both discharge and electrode parameters. The next section will focus on a detailed discussion of the operating limits that have been found.

IV. Limits on the Steady Diffuse Mode

In this section, two different mechanisms that lead to local melting of the cathode surface are discussed. The first mechanism is an excessive heating due to electron bombardment that occurs when the sheath voltage drop falls below a critical value. A positive feedback between electron bombardment and surface electron emission results in this thermal runaway. The second mechanism is heating due to ion bombardment, which dominates as the sheath voltage drop increases sharply for a relatively small increase in the plasma current density. A steady state can no longer be maintained unless plasma discharge parameters change dramatically.

We consider the thermal runaway mechanism first. The value of the critical voltage drop at which the thermal runaway due to electron bombardment occurs can be obtained quite readily for the case of pure thermionic emission. For a given plasma current density and plasma number density at the sheath edge, Eq. (10) may be substituted into Eq. (11) and the resulting expression differentiated with respect to T to yield

$$\frac{\partial Q}{\partial T} = -h + \frac{2kj_E}{e}\left(-\frac{e\phi}{kT} - 3\right) + \frac{2kT_\infty j_E}{eT}\left(2 + \frac{e\phi}{kT}\right)\left(1 - \frac{j_i}{2j_e}\right) \tag{13}$$

For stability (in the Lyapunov sense), we require that $\partial Q/\partial T$ be less than zero. A *sufficient* condition for stability from Eq. (13) is

$$\frac{j_i}{j_e} \geq 2 \tag{14}$$

which, by using Eqs. (7) and (8), gives a condition on the sheath voltage drop V_c:

$$V_c \geq \frac{kT_\infty}{2e} \ln\left[\frac{2m_i}{\pi m_e}\right] \tag{15}$$

For argon and an electron temperature of 12,000 K, this yields an approximate value of 5.5 V for the critical sheath voltage drop. It is important to note that this is only a *sufficient* condition for stability. From Eq. (13), it can be seen that the exact value of the critical voltage drop depends on the electrode properties (work function and emission current), surface temperature, and external cooling h. This more general criterion on the total sheath voltage drop necessary to ensure stability of a given steady state is

$$V_c \geq \frac{kT_\infty}{2e} \ln\left[\left(\frac{m_i}{2\pi m_e}\right)^{1/2}\left(2 - \frac{T(3 + e\phi/kT)}{T_\infty(2 + e\phi/kT)} - \frac{ehT}{kj_E T_\infty(2 + e\phi/kT)}\right)\right] \tag{16}$$

Above the value given by the critical voltage drop, a steady state defined by Eqs. (10) and (11) (with Q = 0) can be maintained indefinitely, even for small fluctuations in n_∞ and j_∞. Below this value, the positive feedback between electron bombardment and surface electron emission leads to thermal runaway, and a stable steady state cannot be maintained. The surface subsequently melts locally. Alternatively, the condition $\partial Q/\partial T < 0$ may be interpreted as providing a constraint on the amount of cooling (i.e., the value of h) necessary for steady and stable operation. Equation (14) along with Eq. (9) may be rewritten, therefore, in the following form, yielding an important upper limit on the local surface temperature for diffuse operation:

$$j_E(T) = AT^2 \exp(-e\phi/kT) \leq j_\infty - j_e \tag{17}$$

Under MPD conditions, the critical temperatures predicted by Eq. (17) are well below the material melting temperature.

A second mechanism exists that can cause local melting of the cathode surface. For high j_∞ (given an n_∞) or low n_∞ (given a j_∞), it is possible that $j_\infty \to j_i + j_E$. When this occurs, the total sheath voltage drop increases sharply. This can be seen from Eq. (10), where $V_c \to \infty$ as $j_\infty \to j_i + j_E$. This has two important consequences. First, emitted electrons cause increased ionization outside the sheath since they gain large amounts of energy after traversing the sheath. Second, the ions gain substantial amounts of energy while falling through the sheath. These cause a rapid increase in ion bombardment with subsequent heating of the surface. This temperature rise necessarily results in increased surface electron emission.

Consequently, there arises a conflict between the emission current necessary for cooling the cathode surface (i.e., to balance heating by ion bombardment) and the emission current necessary to preserve overall current conservation at steady state. The increasing sheath drop also drastically reduces the electron current from the plasma necessary to counteract an increasing emission current and, hence, maintain a steady state. This leads to unsteady behavior in the sheath, thereby forcing the surface and the plasma to also become unsteady. In the meanwhile, the local surface temperature can rise due to ion bombardment until the surface has locally melted. Although the present theory becomes inapplicable at this point, it is capable of predicting this limit. An important phenomenon associated with this second mechanism, but not with the first, is the triggering of plasma oscillations.[30] When the sheath voltage drop rises and approaches energies equal to or greater than that of the first excited states of the propellant atoms, ionization levels can be enhanced in the presheath region. Also, while the thermionically emitted electrons relax their momenta relatively quickly due to elastic collisions with neutrals, their energy relaxation times are much longer due to infrequent collisions with plasma electrons. When the number density of thermionically emitted (beam) electrons approaches the local number density of plasma electrons, longitudinal oscillations can result.[30] This condition may be expressed quantitatively within the context of the present work as

$$n_e << 2.563 \times 10^{13} j_E^{2/5} V_C^{8/5} \tag{18}$$

where n_e is the number density of plasma electrons immediately adjacent to the sheath. This second mechanism, which is related to a high back-EMF (Electro Motor Force), may explain the onset phenomenon observed in the MPD thrusters.[31,32]

The two aforementioned mechanisms responsible for limiting the diffuse mode also cause local melting of the cathode surface. Local surface melting may be a precursor to spot formation. However, it must be pointed out that an intermediate stable state may exist where molten regions that are submicron in size (microspots[1]) are scattered over the cathode surface while most of the discharge appears diffuse. It is therefore possible that the two mechanisms found and discussed here correspond to transitions from diffuse to spot mode or another intermediate mode with microspots.

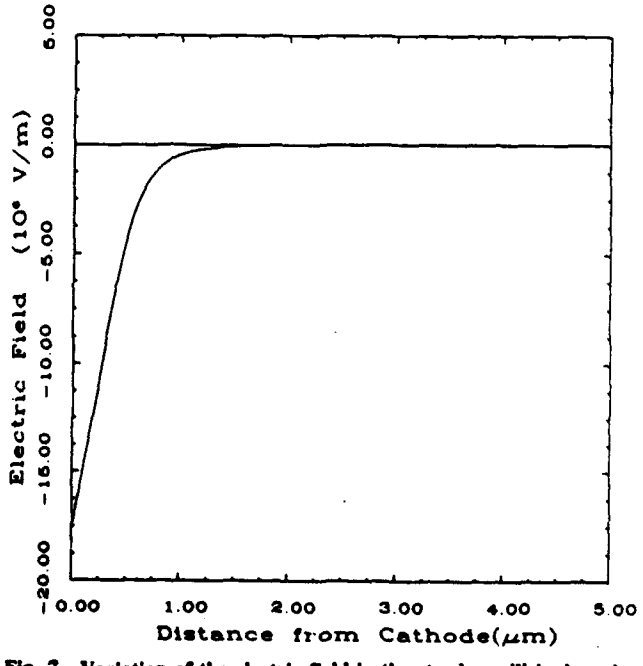

Fig. 7 Variation of the electric field in the steady, collisionless electrode-adjacent sheath vs vertical distance from the cathode surface: $j_\infty = 10^6$ A/m²; $n_\infty = 5 \times 10^{21}$ m⁻³; $T_\infty = 12000$ K; $T_{cool} = 500$ K; $\phi = 2.63$ V; $h = 20$ kW/m²/K²; the calculated surface temperature is 1824 K; the value of the electric field at the cathode surface is 1.76×10^7 V/m. (Note that the electric field is negative because of the convention used here. The actual field is positive, i.e., pointing toward the surface.)

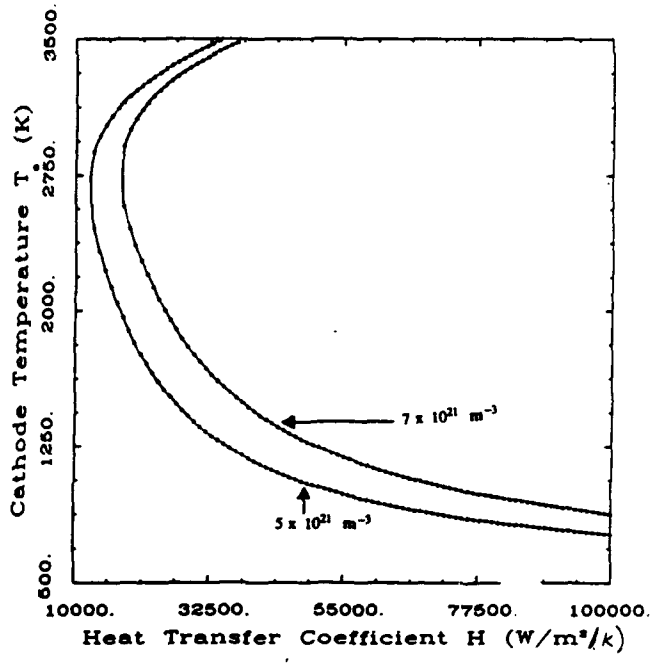

Fig. 8 Variation of the cathode surface temperature as predicted by Eqs. (10) and (11) vs the heat transfer coefficient h for a net current density of $j_\infty = 10^6$ A/m² and for two different number densities: $T_\infty = 12{,}000$ K; $\phi = 2.63$ V; $T_{cool} = 500$ K.

V. Effects of Field-Enhanced and Temperature-Field Emission

Thus far, we have considered a purely thermionically emitting cathode. In general, however, the emission current density depends both on the surface temperature and on the surface electric field.[33] In this section, the influence of this field-enhanced (also known as Schottky emission) and temperature-field (T-F) emission is evaluated and discussed.

The governing equations for the sheath and the cathode surface are described by the surface energy balance [Eq. (1)] and overall current conservation [Eq. (9)]. These equations are still applicable in the presence of an electric field at the surface of the cathode. However, a simple analytic solution cannot be obtained because the sheath voltage drop cannot be determined explicitly in terms of the surface temperature. This is because the emission current density in Eq. (9) depends on T and E_c, and E_c, in turn, depends on V_c. The required additional equation for E_c may be obtained from a solution of Poisson's equation in the sheath. An outline of this procedure is given by Prewett and Allen[25] for the case of a constant surface emission current density. Extension of their solution for the potential distribution in the sheath, for the case where the emission current density depends on both T and E_c, is straightforward and will not be discussed here. The additional equation for E_c for monoenergetic ions is the following implicit equation:

$$\frac{\varepsilon_0}{2}(E_c^2 - E_\infty^2) = n_\infty kT_\infty \left[\left(1 + \frac{2eV_c}{kT_\infty}\right)^{1/2} - 2 + \exp[-eV_c/kT_\infty]\right] - j_E(2m_e V_c/e)^{1/2} \tag{19}$$

where E_w is the electric field at the sheath edge where $V = 0$. In general, E_w is much smaller than E_c and may be ignored, and the emission current density j_E may be calculated from quantum-mechanical considerations. A general integral expression for j_E as a function of T and E_c is given by Murphy and Good.[33] For low values of E_c, j_E may be simply expressed by the well-known Schottky formula.[33] For the higher values of E_c, the emission is influenced by both E_c and T and is known as T-F emission. Thus, Eqs. (1), with $Q = 0$, (9), and (19) represent three coupled and nonlinear equations for the three unknowns T, V_c, and E_c. This system has been solved numerically. It is also possible to numerically integrate Poisson's equation to determine the variation of the potential and the electric field in the sheath. Figure 7 displays the computed variation of the electric field vs vertical distance from the surface for a particular value of j_∞ and n_∞. However, it must be pointed out that the resulting profiles represent the solution within the sheath only. A uniformly valid solution for the sheath, transition region, and the plasma beyond has to be obtained through matched asymptotic expansions.[26-28] Consequently, the solution of Poisson's equation given here represents only the inner solution. For the range of parameters considered in this paper, computed values of E_c are of the order of 10^7 V/m or less. Such values of the electric field produce a negligible increase in current emission at surface temperatures of interest to the MPD thruster. Consequently, the stable diffuse mode is well represented by pure thermionic emission.

VI. Discussion and Conclusions

The thermal response of the cathode in an MPD thruster has been studied under steady-state diffuse conditions. The electrode-adjacent sheath has been included for monoenergetic ions. The solution of Poisson's equation in the sheath, together with overall current conservation and an energy balance at the electrode surface, serve to determine the electric field at the surface, the surface temperature, and the total sheath voltage drop simultaneously and self-consistently. Two operating regimes are found. One is stable, while the other is an unstable thermal runaway caused by excessive *electron bombardment*. The thermal runaway leads to eventual local melting of the cathode surface and may be a precursor to spot formation. The stable steady state, on the other hand, is influenced strongly by discharge and electrode parameters. The values of n_∞, j_∞, and T_∞ used here have been obtained from an approximate nonequilibrium model of the electrode-adjacent flow.[22] The rate of cooling is found also to be extremely important. Varying values of h result in two operating regimes, similar to the results displayed in Fig. 6. Furthermore, the dependence of the surface temperature on h is quite significant. For $n_\infty = 5 \times 10^{21}$ m^{-3}, $j_\infty = 10^6$ A/m^2, $T_{cool} = 500$ K, and $\phi = 2.63$ V, a 1% decrease in h results in about a 10% increase in the local surface temperature (see Fig. 8). Of course, for h larger ($\approx 10^5$ W/m^2/K) than the value used here, the variation is less dramatic but still non-negligible.

Two mechanisms are found to be responsible for destabilizing the stable, steady, diffuse mode. The first occurs at values of the sheath voltage drop *below* a critical value. Small sheath voltage drops lead to increased electron bombardment and subsequent thermal runaway if the cooling is insufficient. Such a condition can occur in the MPD thruster operating at near-onset total currents. Near onset, the current density is sharply peaked and large near the inlet and the exit regions while going through a minimum in the middle region (in the axial direction) of the thruster. The current density in the middle region of the thruster becomes smaller with increasing total current to the thruster, due to a high back-EMF,[31,32] which then leads to smaller sheath voltage drops. The second mechanism, due to excessive ion bombardment and accompanied by plasma oscillations, occurs at high values of the current density (for a given plasma number density) or for low values of the plasma number density (for a given current density). Here, high sheath voltage drops result in increased ion bombardment leading to increased surface electron emission. Since plasma electrons are repelled at high sheath potentials, overall current conservation given by Eq. (9) cannot be satisfied at steady state. The sheath is then no longer steady. The second mechanism may be inhibited if an increase in the sheath edge charged particle number density n_∞ occurs via increased ionization due to electrons emitted from the cathode surface. Clearly, this requires overall sheath voltage drops of the order of the propellant ionization potential. The occurrence of both mechanisms is strongly influenced by discharge parameters.

The simple model discussed in this paper represents a first attempt at relating the plasma discharge, the sheath, and the electrode. Although this model has revealed some important underlying physics, there are several deficiencies. First, the presheath has not been considered in detail. The presheath is important not only for determining the ion velocity distribution function, but also for asymptotically determining a uniformly valid potential distribution. This potential distribution will then yield the correct variation in the sheath when considered on the scale of the Debye length and will also yield the correct variation in the plasma when viewed on the macroscopic length scale in the problem. Such presheath solutions exist, as mentioned previously in Sec. 2, but only for charge-exchange reactions or in the absence of surface electron emission. For the plasma in the MPD thruster, additional ionization by electrons emitted from the surface is important under some conditions. Second, radiative heating of the electrode surface by the plasma has been neglected. This not only contributes to direct heating, but also to increased heating by particle bombardment via increased charged particle number densities at the sheath edge. Radiative transfer in the MPD plasma is a topic for detailed study. Although these two deficiencies can affect the quantitative predictions of the surface temperature, they will not affect the existence of the thermal runaway mechanism and unstable operating regimes found here. The theory presented in this paper together with models of the flowing plasma[22,31,32] provide the designer with a number of tools. In addition to the prediction of erosion rates under a variety of possible operating conditions, the proper cathode length, diameter, material, external cooling conditions, and choice of propellant can be systematically evaluated.

Experimental verification of the predictions of the theory presented in this paper requires simultaneous measurement of the plasma current density, plasma charged particle number density near the electrode, amount of external cooling, and the local surface temperature. Although temperature measurements in low-power steady-state MPD thrusters have been made,[34] lack of knowledge with regard to the local current and number densities makes comparison between this theory and existing measurements unreliable. The measured steady-state cathode surface temperatures in a subscale device for thoriated tungsten range from 2087 to 2281 K for a range of total currents from 500 to 1200 A and mass flows from 46.4 to 150.8 mg/s.[34] This is comparable to the parameter range considered in this paper. Despite the difficulties encountered in nonintrusively measuring plasma number densities and current densities, efforts to measure these variables along with the local surface temperature would be desirable and invaluable. Such local surface temperature measurements, if based on optical pyrometry, must also account for reflection from the radiating MPD plasma. As a final point, it must be mentioned that scanning electron micrographs of used cathodes *always* display evidences of craters from spots and microspots in some regions. These spots can be formed easily during the startup transient or the shutdown transient of the arc. Therefore, future experiments aimed at understanding the diffuse mode limits must exercise great caution to make sure that spots are not formed during arc initiation or shutdown.

Acknowledgment

This work was supported by the Air Force Office of Scientific Research Grant AFOSR-87-0360 and in part by a DuPont Young Faculty Award.

References

[1]Schrade, H. O., Auweter-Kurtz, M., and Kurtz, H. L., "Cathode Erosion Studies on MPD Thrusters," *AIAA Journal*, Vol. 25, No. 8, 1987, pp. 1105–1112.

[2]Ecker, G., "The Vacuum Arc Cathode—A Phenomenon Of Many Aspects," *IEEE Transactions on Plasma Science*, Vol. PS-4, No. 4, 1976, pp. 218–227.

[3]Harstad, K., "Electrode Processes in MPD Thrusters," Jet Propulsion Laboratory, Pasadena, California. Publication 81-114, March 1982.

[4]Guile, A. E., and Juttner, B., "Basic Erosion Processes of Oxidized and Clean Metal Cathodes by Electric Arcs," *IEEE Transactions on Plasma Science*, Vol. PS-8, No. 3, 1980, pp. 259–269.

[5]Schrade, H. O., Auweter-Kurtz, M., and Kurtz, H. L., "Analysis of the Cathode Spot of Metal Vapor Arcs," *IEEE Transactions on Plasma Science*, Vol. PS-11, No. 3, 1983, pp. 103–110.

[6]Guile, A. E., and Hitchcock, A. H., "Oxide Films on Arc Cathodes and Their Emission and Erosion," *Journal of Physics D: Applied Physics*, Vol. 8, 1975, pp. 663–669.

[7]Cheng, D. Y., "Dynamics of Arc Ignition and Cathode Spot Movement of Thermionically Emitting Cathode Surfaces," *Journal of Applied Physics*, Vol. 41, No. 9, 1970, pp. 3626–3633.

[8]Rakhovsky, V. I., "Current Density per Cathode Spot in Vacuum Arcs," *IEEE Transactions on Plasma Science*, Vol. PS-12, No. 3, 1984, pp. 199–203.

[9]Prock, J., "Time-Dependent Description of Cathode Crater Formation in Vacuum Arcs," *IEEE Transactions on Plasma Science*, Vol. PS-14, No. 4, 1986, pp. 482–491.

[10]Ecker, G., "Theoretical Aspects of the Vacuum Arc," *Vacuum Arcs*, edited by J. M. Lafferty, Wiley, New York, 1980, pp. 228–320.

[11]Moizhes, B. Ya., and Rybakov, A. B., "Transition from Distributed Emission to a Cathode Spot in an Arc," *Soviet Physics—Technical Physics*, Vol. 15, No. 9, 1971, pp. 1574–1576.

[12]Hantzsche, E., "Thermal Runaway Prevention in Arc Spots," *IEEE Transactions on Plasma Science*, Vol. PS-11, No. 3, 1983, pp. 115–122.

[13]Miller, H. C., "Vacuum Arc Anode Phenomena," *IEEE Transactions on Plasma Science*, Vol. PS-11, No. 2, 1983, pp. 76–89.

[14]Lafferty, J. M., "Triggered Vacuum Gaps," *Proceedings of the IEEE*, Vol. 54, 1966, pp. 23–32.

[15]Jolly, D. C., "Anode Surface Temperature and Spot Formation Model for the Vacuum Arc," *Journal of Applied Physics*, Vol. 53, 1982, pp. 6121–6126.

[16]Ecker, G., "Anode Spot Instability. I. The Homogeneous Short Gap Instability," *IEEE Transactions on Plasma Science*, Vol. PS-2, 1974, pp. 130–146.

[17]Schuocker, D., "Improved Model for Anode Spot Formation in Vacuum Arcs," *IEEE Transactions on Plasma Science*, Vol. PS-7, 1979, pp. 209–216.

[18]Boxman, R. L., "Magnetic Constriction Effects in High-Current Vacuum Arcs Prior to the Release of Anode Vapor," *Journal of Applied Physics*, Vol. 48, 1977, pp. 2338–2345.

[19]Kimblin, C. W., "Anode Voltage Drop and Anode Spot Formation in DC Vacuum Arcs," *Journal of Applied Physics*, Vol. 40, 1969, pp. 1744–1752.

[20]Subramaniam, V. V., and Lawless, J. L., "Thermal Instability of the Anode in a Magnetoplasmadynamic Thruster," *Journal of Propulsion and Power*, Vol. 6, No. 2, 1990, pp. 221–224.

[21]Hugel, H., "Effect of Self-Magnetic Forces on the Anode Mechanism of a High Current Discharge," *IEEE Transactions on Plasma Science*, Vol. PS-8, No. 4, 1980, pp. 437–442.

[22]Subramaniam, V. V., and Lawless, J. L., "Electrode-Adjacent Boundary Layer Flow in Magnetoplasmadynamic Thrusters," *Physics of Fluids*, Vol. 31, No. 1, 1988, pp. 201–209.

[23]King, D. Q., private communication, June 1988.

[24]Bohm, D., "Minimum Ionic Kinetic Energy for a Stable Sheath," *Characteristics of Electrical Discharges in Magnetic Fields*, edited by A. Guthrie and R. Wakerling, McGraw-Hill, New York, 1949, pp. 77–86.

[25]Prewett, P. D., and Allen, J. E., "The Double Sheath Associated with a Hot Cathode," *Proceedings of the Royal Society of London, Section A*, Vol. 348, 1976, pp. 435–446.

[26]Riemann, K.-U., "Kinetic Theory of the Plasma Sheath Transition in a Weakly Ionized Plasma," *Physics of Fluids*, Vol. 24, No 12, 1981, pp. 2163–2172.

[27]Emmert, G. A., Wieland, R. M., Mense, A. T., and Davidson J. N., "Electric Sheath and Presheath in a Collisionless, Finite Ion Temperature Plasma," *Physics of Fluids*, Vol. 23, No. 4, 1980, pp. 803–812.

[28]Main, G., "Asymptotically Correct Collisional Presheaths," *Physics of Fluids*, Vol. 30, No. 6, 1987, pp. 1800–1809.

[29]Crawford, F. W., and Cannara, A. B., "Structure of the Double Sheath in a Hot Cathode Plasma," *Journal of Applied Physics*, Vol. 36, No. 10, 1965, pp. 3135–3141.

[30]Alexandrov, A. F., Bogdankevich, L. S., and Rukhadze, A. A., *Principles of Plasma Electrodynamics*, Springer-Verlag, New York, 1984.

[31]Lawless, J.L., and Subramaniam, V. V., "Theory of Onset in Magnetoplasmadynamic Thrusters," *Journal of Propulsion and Power*, Vol. 3, No. 2, 1987, pp. 121–127.

[32]Subramaniam, V. V., and Lawless, J. L., "Onset in Magnetoplasmadynamic Thrusters with Finite Rate Ionization," *Journal of Propulsion and Power*, Vol. 4, No. 6, 1988, pp. 526–532.

[33]Murphy, E. L., and Good, R. H., Jr., "Thermionic Emission, Field Emission, and the Transition Region," *Physical Review*, Vol. 102, No. 6, 1956, pp. 1464–1473.

[34]King, D. Q., private communication, Sept. 1988.

Appendix E

Thermal Instabilities of the Anode in a Magnetoplasmadynamic Thruster

V. V. Subramaniam and J. L. Lawless

Reprinted from

Journal of Propulsion and Power

Volume 6, Number 2, March–April 1990, Pages 221–224

AMERICAN INSTITUTE OF AERONAUTICS AND ASTRONAUTICS, INC.
370 L'ENFANT PROMENADE, SW • WASHINGTON, DC 20024

Thermal Instabilities of the Anode in a Magnetoplasmadynamic Thruster

V. V. Subramaniam*
Ohio State University, Columbus, Ohio
and
J. L. Lawless†
Space Power Inc., San Jose, California

Nomenclature

A = thermionic emission coefficient
d = anode thickness
e = electronic charge
J = total current
j = current density passing through the anode
j_e = electron current density from the plasma (Its sense is positive away from the anode.)
j_E = current density of thermionically emitted electrons (Its sense is positive into the anode.)
j_∞ = average net current density through the plasma, taken positive away from the anode
k = Boltzmann's constant
L = anode length
m_e = electron mass
n_e = electron number density at the plasma-sheath boundary
$O(\ )$ = order of magnitude of the quantity in parenthesis
q_0 = heat flux on the anode inner surface (Its sense is positive into the anode surface.)
T = temperature
T_0 = anode inner surface temperature
T_{0c} = critical value of T_0 where $\partial j_\infty/\partial T_0 = 0$
T_d = anode outer surface temperature
T_e = plasma electron temperature
V_A = anode sheath voltage drop, defined as the potential at the plasma-sheath edge minus the anode potential
W = anode width
x = outward coordinate taken to be 0 at the anode inner surface, and d at the anode outer surface
ϵ = emissivity of outer anode surface
λ = thermal conductivity of anode material
σ_{SB} = Stefan-Boltzmann constant
σ = electrical conductivity of anode material
ϕ_A = anode material work function

I. Introduction

An important consideration in the use of magnetoplasmadynamic (MPD) thrusters operating at steady state for space missions is electrode erosion. Erosion in MPD thrusters has been studied experimentally and has focused mainly on the cathode.[1-3] There are also ongoing experiments in cathode erosion.[4] However, in this article, we present a simple analysis of the energy balance on the anode in an effort to predict anode surface temperatures. This can subsequently be used to predict erosion rates by evaporation. As will be shown, even such a simple model reveals subtle physical phenomena.

Electrode erosion is connected with the modes of current conduction through the electrode surface. Two modes are known to exist: spot and diffuse. The diffuse mode at subonset conditions is the focus of this article. Vainberg et al.[5] have considered anode behavior at onset conditions and beyond. Their explanation of anode melting rests on the anode sheath reversal mechanism, which has also been observed by Hugel.[6] In constrast to these earlier works, it is shown in this article that a thermal runaway may occur well *before* the sheath reversal. This work supports earlier conjectures that local surface melting of the anode precedes spot formation.[7] Two operating modes are predicted by the theory presented here. One of these yields a stable steady-state temperature for the anode, whereas the other results in a thermal runaway in which the anode regeneratively heats itself until it melts. The total current, anode geometry, and material work function are shown to strongly influence the steady-state anode temperature for the stable operating regime.

In the following section, the governing equations describing anode heat transfer will be derived. The solutions to these equations under some conditions of interest are given and discussed in Sec. III, followed by the summary and conclusions in Sec. IV.

II. Anode Energy Balance

Consider the hollow cylindrical anode geometry of the MPD thruster modeled as a long thin slab of length L, width W, and thickness d (shown in Fig. 1). At steady state, the energy balance gives

$$\lambda \frac{d^2T}{dx^2} = -\frac{j^2}{\sigma} \tag{1}$$

Equation (1) is subjected to the following boundary conditions:

$$-\lambda \frac{dT}{dx}\Big|_{x=0} = q_0 \tag{2}$$

$$-\lambda \frac{dT}{dx}\Big|_{x=d} = \epsilon \sigma_{SB} T_d^4 \tag{3}$$

For the case of constant properties, the system of Eqs. (1-3) may be readily integrated to give

$$\epsilon \sigma_{SB} T_d^4 = \frac{j^2 d}{\sigma} + q_0 \tag{4}$$

and

$$\lambda T_d = -\frac{j^2 d^2}{2\sigma} - q_0 d + \lambda T_0 \tag{5}$$

Received Feb. 22, 1988; revision received Oct. 3, 1988.

*Assistant Professor. Member AIAA.
†Senior Scientist and Manager of Advanced Concepts. Member AIAA.

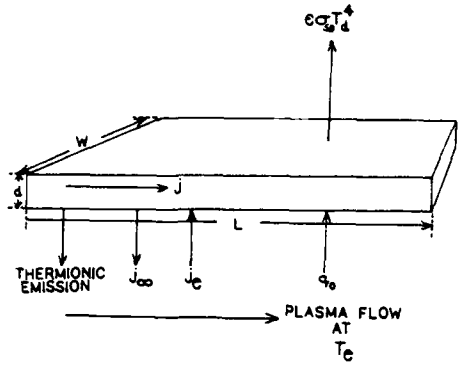

Fig. 1 The hollow cylindrical anode is shown in this idealization as a long thin slab of length L, width W, and thickness d.

Now, if q_0 is known and j is given, Eqs. (4) and (5) represent two equations for the two unknowns T_0 and T_d.

The heat flux on the anode inner surface q_0 must be found by considering particle bombardment from the plasma through the sheath. Consider, therefore, a power balance per unit area on the anode inner surface. The focus here is on conditions prior to sheath reversal; therefore, the anode is at a lower potential with respect to the plasma potential at the sheath edge. The power balance, then, mainly consists of a balance between electron bombardment and thermionic emission cooling. It can be shown that under these operating conditions evaporative cooling is a relatively small effect. Ion bombardment may be easily included in our analysis, but we neglect it for simplicity. Although this is expected to influence final results quantitatively, the conclusions regarding the mechanisms responsible for a thermal runaway will not be altered. We then have

$$q_0 = j_e(\phi_A + 2kT_e/e) - AT_0^2 \times (\phi_A + 2kT_0/e) \exp\{-e\phi_A/kT_0\} \tag{6}$$

The electron current density from the plasma j_e can be determined from overall current conservation

$$j_e = j_\infty + AT_0^2 \exp\{-e\phi_A/kT_0\} \tag{7}$$

Inclusion of ion bombardment would involve additional terms on the right hand side of Eqs. (6) and (7). The anode sheath drop may be determined from Eq. (7) to be

$$V_A = -\frac{kT_e}{e} \ln[(j_\infty + j_E)/j_r] \tag{8}$$

where $j_r = en_e(kT_e/2\pi m_e)^{1/2}$ and $j_E = AT_0^2 \exp\{-e\phi_A/kT_0\}$. The anode is at a potential of $-V_A$ with respect to the plasma-sheath edge (taken as the $V=0$ datum) in the regime under consideration. Combining Eqs. (6) and (7) gives

$$q_0 = j_\infty\left(\phi_A + \frac{2kT_e}{e}\right) + \frac{2AkT_0^2(T_e - T_0)}{e} \exp\{-e\phi_A/kT_0\} \tag{9}$$

Finally, combining Eqs. (4) and (5), we get an implicit equation for T_0

$$F(T_0) = \frac{j^2 d}{\sigma} + q_0 - \epsilon\sigma_{SB}\left(T_0 - \frac{q_0 d}{\lambda} - \frac{j^2 d^2}{2\lambda\sigma}\right)^4 = 0 \tag{10}$$

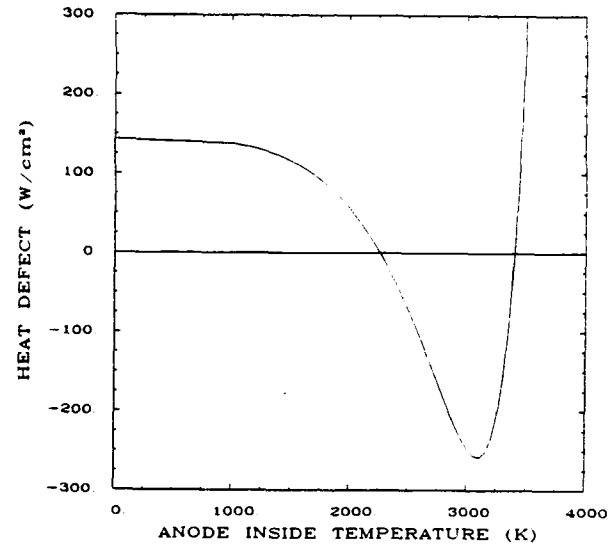

Fig. 2 A typical variation of the heat defect (defined as the net heat flux into the anode minus the net heat flux out) is shown here vs the anode inside surface temperature T_0.

where q_0 is given by Eq. (9). Given d, L, W, T_e, and J, the axial current density throught the anode ranges up to $j = J/Wd$, and the average current density through the plasma at the anode surface is $j_\infty = J/WL$. Although this simplification is unnecessary (since j and j_∞ can be treated as separate pointwise parameters), it allows the thermal steady state to be related directly to the total current (a more tangible quantity) rather than the current densities. With these quantities, Eq. (10) may be solved for T_0. Once T_0 is determined, T_d may be readily obtained from Eqs. (4) or (5). Equations (9) and (10) have been solved in this manner for representative conditions in the MPD thruster. These results are discussed in the following section.

III. Analysis and Results

In the previous section, it was shown that an energy balance on the anode at steady state yields an implicit equation for the anode inside the surface temperature T_0. This equation [Eq. (10)] is nonlinear in T_0 and must be solved numerically. This section will focus on the solution of this implicit equation, resulting in the discovery of a thermal runaway mode and culminating in a discussion of various operating limits.

For illustrative purposes, let us consider a tungsten anode of width 30 cm and length 10 cm. Let the electron temperature T_e be fixed at 15,000 K. The typical variation of the implicit function $F(T_0)$ vs T_0, given by Eq. (10), is displayed in Fig. 2. The function $F(T_0)$ represents the net heat into the anode per unit area per unit time. It is immediately evident from Fig. 2 that two steady-state solutions exist. Without performing a stability analysis, one can conclude on the basis of physical reasoning that the lower temperature is a stable root and the higher one is an unstable root. Consider the smaller temperature first. Any perturbation to the left of this root (i.e., on the lower temperature side) results in a net heat flux into the anode. To counter this, the surface temperature must increase in order to maintain a steady state. Similarly, any small perturbation to the right (i.e., on the higher temperature side) results in a net heat flux out of the anode. To counter this, the surface temperature must decrease. Thus, we see that the tendency of the thermal response is to drive the temperature toward this root. Using this physical argument on the second root (i.e., higher temperature), we may conclude that it is unstable. If the surface temperature increases just above the value given by the second root, the steady-state energy balance indicates a further increase in temperature in order to maintain a steady state. This is because the only possible way of losing energy is through radiation and by thermionic emission,

both of which increase with increasing temperature. This results in a thermal runaway with eventual melting of the anode.

A physical interpretation of the two aforementioned solutions will now be discussed. Examination of Eq. (8) indicates that the anode sheath drop decreases as the net plasma current density increases. This results in increased electron bombardment, as can be seen from Eqs. (6) and (7), causing heating of the anode surface. Two possible scenarios may ensue. The resulting increase in the surface temperature leads to an increase in the emission current density, which further lowers the anode sheath voltage drop. This positive feedback may repeat itself until thermal runaway leads to local melting of the surface. The second scenario is stable, steady operation arising from the fact that sufficient cooling of the anode prevents the thermal runaway by excessive electron bombardment. The two solutions found to Eq. (10) represent these two situations.

The anode surface temperature T_0 for stable operation is found to be strongly dependent on the total current, anode geometry, and the anode work function. Figure 3 shows the anode thickness for various total currents, and Fig. 4 shows the anode inside surface temperature vs total current for various anode thicknesses. From these results, it is evident that for a given total current, there exists an optimum thickness for achieving a minimum anode temperature. An interesting feature of the pair of solutions found to the steady-state heat balance equation is that the stable and unstable roots start moving toward each other as the current is increased. This continues until a critical value of the current is reached, beyond which no steady solution can be found below the melting point of the material. Also, for a fixed total current, these roots approach each other as the thickness is increased. It is possible that the analytical behavior of this unstable thermal runaway point will yield insight into electrode material breakdown.

Some interesting limits may be readily obtained by analyzing the equations presented in Sec. II. For instance, from Eq. (5) it is clear that

$$j^2d^2/2\sigma < kT_0 \quad \text{or} \quad j < j_c = (2k\sigma T_0)^{1/2}/d \tag{11}$$

which is very similar (within a proportionality constant) to the thermal runaway condition obtained by Hantzsche[8] for cathode spots. However, it must be pointed out that Eq. (11) is obtained here for an anode of constant electrical conductivity, operating in the diffuse mode. This sharply differs from Hantzsche's consideration of a cathode spot with an electrical conductivity that varies according to the Wiedemann-Franz law (i.e., $\sigma \propto 1/T$). Furthermore, in constrast to Hantzsche's work, surface cooling due to thermionic emission *does not* prevent thermal runaway. This thermal runaway can occur under the steady, diffuse mode operation of the anode.

An important stability criterion may be derived by requiring that $\delta F/\delta T_0 < 0$ for stable diffuse operation. Using Eq. 7, we find

$$V_A \geq \frac{-kT_e}{e} \ln \left[\frac{j_\infty + 0\left(\frac{4\epsilon J_{SB} T_d^3 T_0^2}{2\phi_A T_e}\right)}{j_r} \right] \tag{12}$$

For V_A below the value given by the right-hand side of Eq. (12), excessive electron bombardment will cause a thermal runaway. Thus, local surface melting can occur prior to sheath reversal.

A limit may also be found for the plasma current density j_∞. Considering thin anodes (i.e., $T \approx T_0$ throughout the anode), neglecting ohmic heating and any external cooling except for radiation, we may write the energy balance at steady state as

$$\epsilon\sigma_{SB}T_0^4 = j_\infty\left(\phi_A + \frac{2kT_e}{e}\right) + \frac{2kAT_0^2}{e}(T_e - T_0)\exp(-e\phi_A/kT_0) \tag{13}$$

Using the fact that $T_e \gg T_0$, differentiating with respect to T_0, and setting $\partial j_\infty/\partial T_0 = 0$, we obtain

$$(j_\infty)_{max} \approx \frac{[1-(4kT_{0c}/e\phi_A)]}{[\phi_A + (2kT_e/e)]}\epsilon\sigma_{SB}T_{0c}^4 \tag{14}$$

where $(j_\infty)_{max}$ is the extremum plasma current density, and T_{0c} is the critical value of T_0 where $\partial j_\infty/\partial T_0 = 0$. Additional heat transfer to an external coolant results only in a slight modification of Eq. (14):

$$(j_\infty)_{max} \approx \frac{[1-(4kT_{0c}/e\phi_A)]}{[\phi_A + (2kT_e/e)]}\epsilon\sigma_{SB}T_{0c}^4 + \frac{[1-(kT_{0c}/e\phi_A)]}{[\phi_A + (2kT_e/e)]}hT_{0c} \tag{15}$$

where h is the heat transfer coefficient between the anode (at T_0) and an external coolant (at $T_c \ll T_0$). For $T_e = 20{,}000$ K, Eq. (14) approximately yields 47.6 A/cm^2 for a tungsten anode ($\phi_A = 4.52$ V) and 5.4 A/cm^2 for a thoriated tungsten anode ($\phi_A = 2.63$ V). The lower work function yields a lower maximum plasma current density because of a lower value of T_{0c}. Since these limiting current densities are far lower than

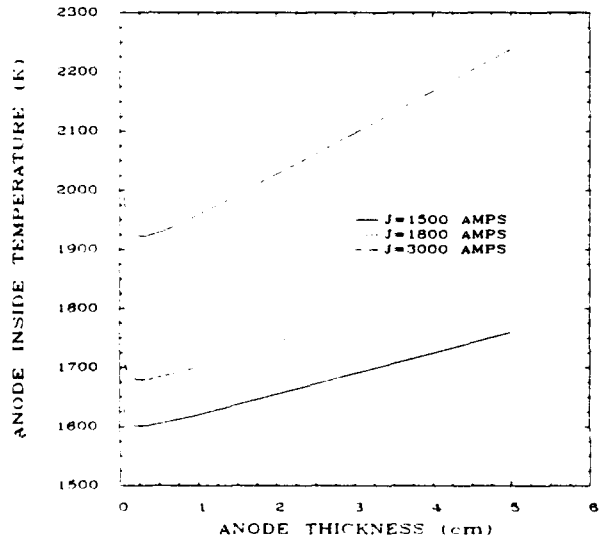

Fig. 3 The anode inside surface temperature is plotted here vs anode thickness, for various total currents.

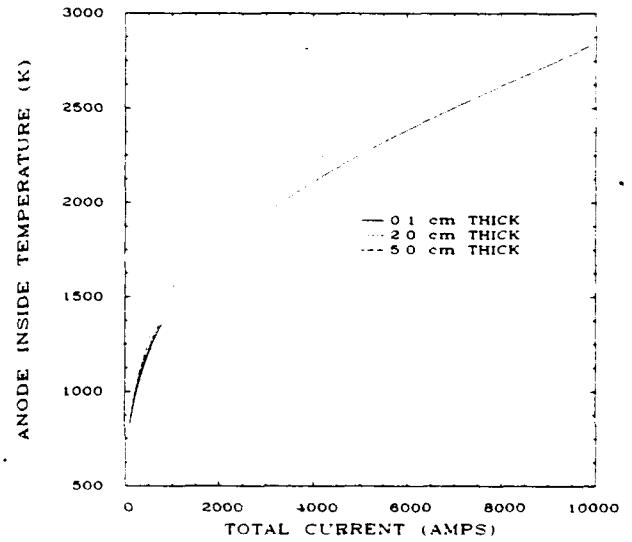

Fig. 4 The anode inside surface temperature is shown here vs total current, for various anode thicknesses.

those required for a steady MPD discharge, it is clear that the anode must be cooled externally. This is done in practice.[1,4]

IV. Summary and Conclusions

An anode energy balance has been performed that includes the effects of the anode sheath. Results show that under many conditions, two steady-state solutions can be found. One of these corresponds to a stable operating point, the other to a thermal runaway. The stable root that gives the anode inside surface temperature at steady state was found to be strongly dependent on the total current, anode geometry, and the material work function. A stability condition in the form of a minimum anode sheath voltage drop [Eq. (12)] has also been given.

Several conclusions can be derived from the anode thermal analysis:

1) There exists, for a given current density, an optimum thickness for achieving a minimum anode temperature.

2) Under many conditions, there exists a pair of steady-state solutions to the heat balance, one of which is a stable operating point, the other of which is an unstable thermal runaway point.

3) There exists a maximum steady operating current density for a given electrode geometry based on melting temperature and cooling considerations.

The thermal runaway mode discovered for the anode may explain anode spots under MPD conditions. Although some limits have been found, anode heat transfer effects need to be explored further in order to learn more about what controls the limits of stable operation. Since external cooling is seen to be extremely important, detailed experimental results quantifying cooling rates for various operating conditions and geometries would be valuable. Radiative heat transfer from the plasma, which has been neglected here, is another important area for further research.

Acknowledgments

This work was supported by AFOSR-83-0033 and by AFOSR-87-0360. The authors acknowledge helpful discussions with D. Q. King.

References

[1]Kurtz, H. L., Auweter-Kurtz, M., and Schrade, H. O., "Self-Field MPD Thruster Design—Experimental and Theoretical Investigations," AIAA Paper 85-2002, Alexandria, VA, Sept.-Oct. 1985.

[2]Schrade, H. O., Auweter-Kurtz, M., and Kurtz, H. L., "Cathode Erosion Studies on MPD Thrusters," *AIAA Journal*, Vol. 25, Aug. 1987, pp. 1105-1112.

[3]Harstad, K., "Electrode Processes in MPD Thrusters," Jet Propulsion Laboratory Publication 81-114, March 1982.

[4]King, D. Q., private communication, Nov. 18, 1987.

[5]Vainberg, L. I., Lyubimov, G. A., and Smolin, G. G., "High-current Discharge Effects and Anode Damage in an End-Fire Plasma Accelerator," *Soviet Physics Technical Physics*, Vol. 23, April 1978, pp. 439-443.

[6]Hugel, H., "Effect of Self-Magnetic Forces on the Anode Mechanism of a High Current Discharge," *IEEE Transactions on Plasma Science*, Vol. PS-8, No. 4, Dec. 1980.

[7]Miller, H. C., "Vacuum Arc Anode Phenomena," *IEEE Transactions on Plasma Science*, Vol. PS-11, No. 2, June 1983.

[8]Hantzsche, E., "Thermal Runaway Prevention in Arc Spots," *IEEE Transactions on Plasma Science*, Vol. PS-11, No. 3, Sept. 1983.